The Encapsulation of an *E. coli* TXTL in Cell-sized Compartments Towards Prototyping Synthetic Cells

A Dissertation
Submitted to the Faculty of the Graduate School
of the University of Minnesota
By

Jonathan T. Garamella

In Partial Fulfillment for the Requirements
For the Degree of:
Doctor of Philosophy

May 2019

Abstract

The bottom-up assembly of synthetic cell systems capable of recapitulating biological functions has become a means to understand living matter through construction. Cell-free protein synthesis platforms, which allow for the rapid prototyping of biological systems by reducing the design-build-test cycle relative to *in vivo* experiments, have emerged as a tool to achieve this goal. In this dissertation, I report on the most recent iteration of an all *E. coli* TXTL and its use towards the realization of a bottom-up synthetic cell. TXTL offers robust protein synthesis with access to the full complement of regulatory parts available in *E. coli*. I detail efforts to encapsulate TXTL into cell-sized liposomes, providing researchers a platform to carry out complex reactions in containers in which the local environment and membrane composition can be altered. While a functional *E. coli* divisome was not reconstructed, the FtsZ and MreB family of proteins were expressed in liposomes, with MreB showing significant deformation. Finally, I developed synthetic cell prototypes programmed to be mechanosensitive, coupling this function to create multiple synthetic cell prototypes that are biosensing or adaptive based on the local environment.

Contents

List of Tables

List of Figures

Abbreviations

TXTL:	Transcription-translation
RNA:	Ribonucleic acid
DNA:	Deoxyribonucleic acid
CFR:	Cell-free reaction
CFPS:	Cell-free protein synthesis
AH:	Alpha-hemolysin; α-hemolysin
MscL:	Mechanosensitive channel of large conductance
PC:	Phosphatidylcholine
RBS:	Ribosome binding site
RNAP:	RNA polymerase
σ 70:	Sigma factor 70
P70a:	The promoter corresponding to sigma factor 70
UTR:	Untranslated region
eGFP:	Enhanced green fluorescent protein
deGFP:	Mutated version of eGFP with improved TL
Crispr:	Clustered regularly interspaced short palindromic repeats
3-PGA	3-phosphoglycerate
IPTG	Isopropyl β-D-1-thiogalactopyranoside
AA or aa:	Amino acids

Chapter 1

Introduction

1.1 An Overview of Cell-free Synthetic Biology

The field of synthetic biology is less of a singular area of study and more of an amalgamation of many disciplines, from biology to physics to biochemistry to engineering. Unlike pure physics, which is well defined as the study of matter and energy, there is no consensus definition for synthetic biology. Put most broadly, it uses principles and approaches from engineering to channel tools and techniques from molecular biology in order to forward-engineer biochemical processes and cellular behavior. While conventional genetic engineering attempts to solve complex problems by focusing on one or two genes, synthetic biology aims to fundamentally alter the genetic architecture or build something from scratch. Synthetic biology has transformative potential, with applications ranging from the creation of organisms able to process hazardous waste, produce clean fuels, or battle cancer [1]–[4]. While these modern day applications are incredible, the field had to start somewhere and, indeed, has a rich history [5].

This history begins with Jacob and Monod's breakthrough work in 1961 [6]. The insight they gained studying the *lac* operon in *E. coli* allowed them to postulate that a cell's response to environmental stimuli is controlled by genetic regulatory elements [7]. Naturally, they soon imagined assembling new regulatory elements guided by the same principles and constructed from the same molecular components [8]. The design of regulatory elements became accessible in the 1970s and 80s with advances in molecular cloning. In 1978, Nathans, Arber, and Smith received the Nobel Prize in Physiology or Medicine for their work in discovering restriction enzymes and their application to restriction mapping [9]. The polymerase chain reaction (PCR) technique was patented by Kary Mullis a few years later and it's combination with restriction site cloning allowed the design and creation of genetic regulatory elements to become widespread [10]. Building on this work, in the mid 1990's, automated DNA sequencing and computational techniques allowed for the sequencing of complete microbial genomes. Simultaneously, high-throughput techniques were developed to assay biochemical indicators – nucleotides,

proteins, lipids, and metabolites – allowing researchers to catalogue a vast array of cellular processes and interactions. This incredible influx of information led to the field of systems biology, as biologists and computer scientists joined forces to computationally analyze and reverse engineer cellular networks [11]. Materializing from this work was the idea that genetic networks and processes could be understood as discreet, interacting, modules, much in the same manner as mechanical systems. At this point, the confluence of biologists, computer scientists, physicists, and engineers had the nascent field of synthetic biology ready to explode.

Given the synthetic biology's nominal tie to the field of biology, it is somewhat surprising that some of the foundational works were undertaken by physicists. However, given the scope of the projects, it becomes clear why this is the case. In the same volume of Letters to Nature, both Elowitz and Leibler and James Collins and his colleagues published seminal papers. Elowitz and Leibler designed and constructed what they termed a repressilator in *E. coli* [12]. They used three transcriptional repressors, LacI, tetR, and lambda cI, to create an oscillating synthetic network with a period on the order of hours, much longer than a typical cell cycle. This work showed the possibility to build an artificial genetic network from naturally occurring genetic components with new properties. Collins et al. used *E. coli* to construct a genetic toggle switch from two constitutive promoters and two repressors [13]. This bistable gene-regulatory network, which can be flipped both chemically and thermally, demonstrated a synthetic memory unit made not from protein engineering, but from network engineering. Notably, both works are foundational not only for their results, but for the blueprint they provided for the field: constructive (genetic networks not found in natured), predictable (mathematical modeling and simulation) and quantitative (measureable, well-defined outputs). The work described thus far, and much of the work in the field in general, was and is carried out in vivo as cells, especially *E. coli*, have been extensively studied [12]–[18].

As the work described in this thesis is in vitro synthetic biology developed from a cell-free protein synthesis platform, let us consider the development of in vitro synthetic biology from that perspective [19]. Strangely enough, cell-free protein synthesis (CFPS) technology first appeared in the same year that Jacob and Monod published their

groundbreaking work, 1961. Matthaei and Nirenberg landmark research used an *E. coli* extract to express polypeptide sequences from natural and synthetic mRNA, thus deciphering the genetic code [20]. Zubay and colleagues expanded on this work by beginning with a DNA template to express mRNA in order to study gene regulation in vitro [21], [22]. At that juncture, the low yield of mRNA produced limited the questions that could be investigated. This led to the development of coupled transcription-translation systems, where stronger phage promoters and more efficient RNA polymerases (T7 or SP6) were used [23]–[25]. These coupled systems benefited from not only the strong promoters and polymerases, but also by continuing to sue the more stable DNA template and avoiding the introduction of loads of synthetic mRNA. Around this same time, Spirin and others developed the concept of a continuous CFPS, where reagents are cycled into the reaction and by-products are cycled out [26]. This increased protein yields from the order of μg/ml to mg/ml, greatly enhancing the capabilities of cell-free extracts [27], [28]. Modern cell-free synthesis platforms are generated in two distinct ways: a top-down approach and a bottom-up approach. The PURE (protein synthesis using recombinant elements) system represents the bottom up approach and entails purifying the molecular components responsible for protein synthesis and combining them to form a mixture capable of expressing protein from a DNA template [29], [30]. Crude extracts, representing the top-down approach, are semi-purified cell-lysates that do not contain endogenous DNA, insoluble biological elements, and unlysed cells. These extracts, generated from a wide range of organisms, do contain the necessary components for transcription, translation, and energy regeneration [31]–[37]. Both of these approaches have become powerful tools for synthetic biology, especially in regards to their flexibility relative to an in vivo approach, with applications in biosynthesis, enzyme evolution, high-throughput prototyping, and foundational biophysics, such as artificial life [38]–[44].

The question of artificial life is one that has been debated by philosophers and scientists for hundreds of years. Though the goal of such work is to craft artificial life de novo, such a project requires and drives the development of new technologies. This work also encourages biologists, chemists, and physicists to tackle the question of “what is

life?" i.e. what do we mean when we say that an organism is alive [45]? While the answer to this question is not settled, cellular life is generally considered to be a synthesis of metabolism (the ability to collect chemical and/or physical energy to synthesize the necessary molecular building blocks), information (the ability to process molecular instructions stored in polymers), and self-organization (the ability to assemble molecules into active machines) -- the three of which are necessary for replication and evolution [46]. The field of artificial life, at least experimentally, grew from Miller and Urey's attempts to spark life from a prebiotic soup [47]. This led to the first of three approaches to the creation of unicellular analogs: protocells. The construction of protocells looks back to go forward, exploring the origin of life using prebiotic components to assemble simple compartments. They are often based on primitive metabolic or self-assembly schemes and lack a critical information component [48], [49]. Artificial cells attempt to generate what some have termed "orthogonal life" due to the combination of synthetic and natural components [50], [51].

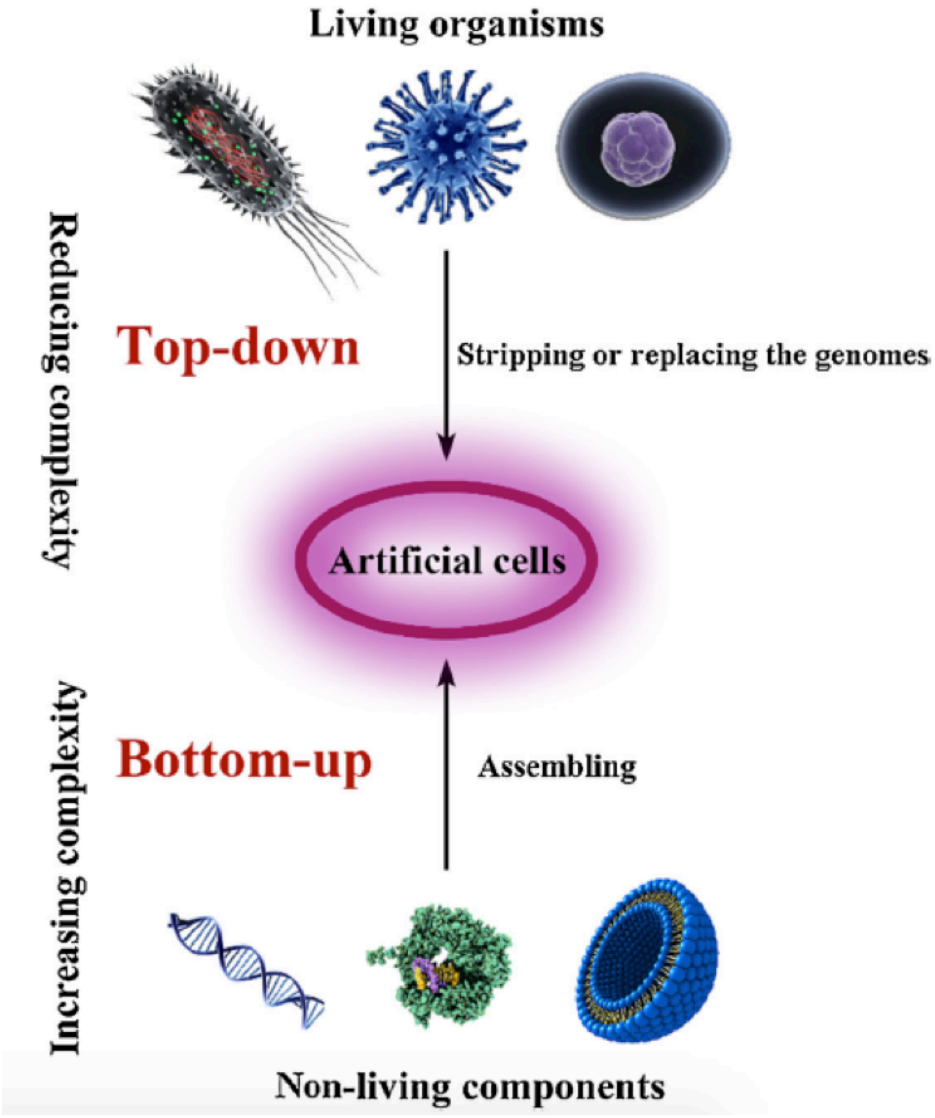

Figure 1.1 Depiction of the two approaches to form synthetic cells. The top-down construction strips living organisms of unnecessary components to create the simplest form of life. The bottom-up approach combines a set of non-living components to create a novel living organism. This figure is reprinted from the open access article: 10.1016/j.mattod.2016.02.020. [52]

The minimal cell approach consists of synthesizing a cell using natural molecular components and containing the minimum set of genes for self-maintenance and self-reproduction. This approach is itself further split into top-down and bottom-up construction as seen in Figure 1.1. Top-down construction seeks to create a minimal cell by taking a living organism and reducing the genome to a base set of genes responsible for life, stripping away those that are non-essential [52]. Computational and experimental techniques has given an estimation of the number of genes necessary to sustain life as

high as 250 or as low as 150, though these low estimates spur a debate around the supposed cell's reliance on it's environment [53], [54]. In 2016, Venter and others were able to design and grow an organism with 473 genes, the smallest of any living organism. This result, while a landmark achievement for the field, is still a ways away from the final goal as almost a third of genes in Syn 3.0 have unknown functions, leaving a complete definition of life unclear [55]. The other approach, and the one I will be working towards in this paper, is the bottom-up approach to a minimal cell. While the top-down approach looks to tear down existing life, bottom-up construction attempts to build a living organism from disparate components. It is arguably a more difficult approach, as all three components – information, metabolism and compartmentalization – need to be designed sui generis. It is now technically possible to synthesize and clone entire genomes, though a specific set of genes to sustain life, as we have seen, is not known. On top of that, the DNA would need to be replicated for progeny of the minimal cell to function. Likewise, compartmentalization and self-organization would require not a complete cytoskeleton of structure and division, but also robust lipid synthesis such that growth and budding could occur. The execution of such a complex scheme of proteins and lipids would require an incredibly robust metabolism. Nutrients would need to be taken up from the environment in a systematic way and then recycled or excreted. There is progress in all of these areas, though much work remains to be done. TXTL and its encapsulation underlies much of this work, motivating the results presented in this dissertation.

1.2 Brief Summary of Results

To prepare the reader for what to expect in this dissertation, I will briefly describe the major results described herein. As of April 2019, these data have led to the publication of one application note and four peer-reviewed journal articles, with one more in submission. With colleagues in the Noireaux lab, I developed and optimized an *E. coli* TXTL system that can serve as a platform for synthetic biology and biophysics [44]. This TXTL, miniaturized for the purposes of high-throughput synthetic biology, can produce over 2 mg/ml protein in bulk reactions, execute complex gene circuits, and synthesize entire bacteriophages, all while being compatible across various setups from test tubes, to microfluidics, to liposomes [56]. I then characterized the behavior of TXTL when it is

encapsulated in liposomes using the emulsion transfer method in order to develop a platform to prototype synthetic cells [57]. Methods to alter the exterior solution and membrane composition of these liposomes are discussed, as well as the encapsulation efficiency of various components related to TXTL. Using these techniques, I describe the difficulties encountered when attempting to recapitulate the *E. coli* cytoskeleton of structure and division, and a potential work around to these obstacles in the form of DNA nanotubes engineered with increased robustness in TXTL [58]. Finally, I describe multiple mechanosensitive synthetic cell prototypes based upon MscL. The first of these uses TXTL to express DNA programs to create a biosensing compartment, able to rapidly sense changes in the chemical environment using the calcium sensitive reporter G-GECO [59]. Next, I describe the construction of a synthetic cell equipped with an inducible genetic circuit. Liposomes loaded with TXTL are induced with IPTG when exposed to hypo-osmotic solution, resulting in the expression of a bacterial cytoskeletal protein, MreB, which associates with the membrane to generate a cortex-like structure. This work provides the first example of molecular integration that couples mechanosensitivity, gene expression, and self-assembly (*In submission*).

Chapter 2

The All *E. coli* Transcription-Translation System

2.1 TXTL System

While the field of synthetic biology is relatively young, there is already an incredible amount of diversity and variation among cell-free protein synthesis platforms (Fig. 2.1) [33]. The PURE system represents the bottom-up approach to TXTL, as components are synthesized, purified, and optimally mixed. This approach omits any nucleases or proteases present in crude extracts but is unable to activate endogenous metabolism. It is one of the most flexible and modular platforms, but is also typically more expensive than others. Top-down extract preparations, so-called crude extracts, differentiate in their abilities and the organism they are derived from. These extract preparations can be simple (Saccharomyces cerevisiae, tobacco BY-2) or labor intensive (wheat germ), ranging in protein yield from a 10s of µg/ml (insect cell, HeLa extracts, Saccharomyces cerevisiae) to nearly 104 µg/ml (*E. coli*, wheat germ). As many eukaryotic proteins require post-translation modification, HeLa or insect cell extracts have been formulated for this purpose.

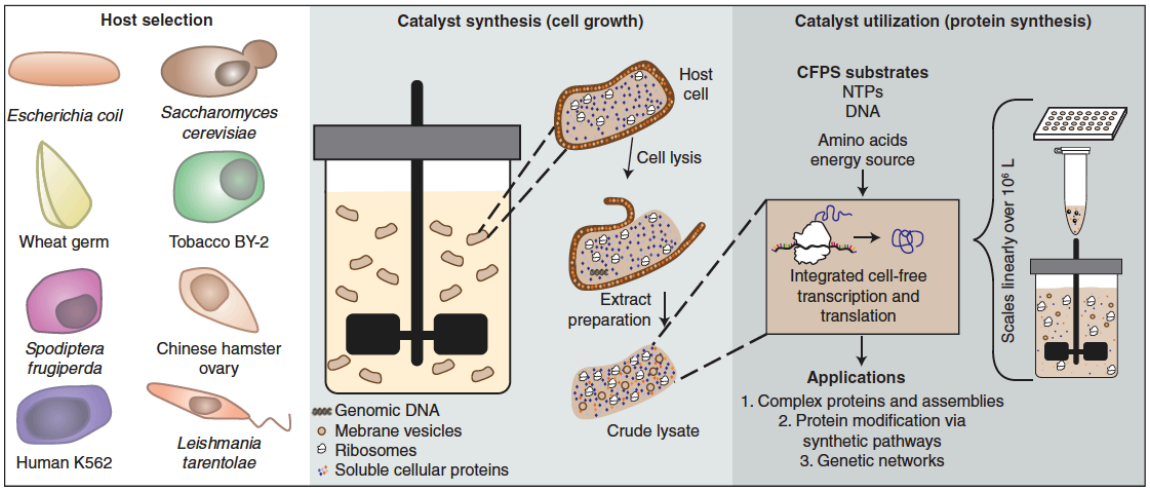

Figure 2.1 Cell-free protein synthesis platforms allow for rapid prototyping and decreased development time. Multiple organisms can be used as the extract base, grown and broken down to be used as a functional lysate. This is then mixed with a cocktail of DNA substrates, amino acids, NTP's, energy buffers, and other salts. This figure is reprinted from **Cold Spring Harb. Perspect. Biol.** 2016 Dec 1;8(12). Copyright 2016 Cold Spring Harbor Laboratory Press. [33]

The all *E. coli* TXTL system we use in our lab boots up transcription from the *E. coli* RNA polymerase (RNAP) holoenzyme formed with sigma factor 70 (σ70) [44]. Although σ70 is not quite as strong as the T7 bacteriophage promoter used in hybrid cell-free extracts, basing a TXTL system on *E. coli* RNAP allows in vitro transcription to be as close as possible to in vivo conditions while having an even greater advantage of being able to use the entire repertoire of transcriptional regulation present in *E. coli* [60]. There are seven transcription factors native to *E. coli*: σ19, σ24, σ28, σ32, σ38, σ54, and σ70. Each sigma factor is expressed in *E. coli* in response to different conditions. For example, σ28 is known as the flagellar sigma factor and actives genes responsible for motility in *E. coli* while σ38 is activated when the environment is nutrient poor. σ70 is the primary sigma factor in *E. coli*, often called the housekeeping sigma factor, and is responsible for expressing most genes in *E. coli* [61]. Our extract is made in such a way that the only sigma factor present in the lysate is σ70, meaning promoters corresponding to the other sigma factors are completely silent. This gives an incredible degree of control to study extant gene networks and to build synthetic networks in vitro.

The extract for the TXTL system is derived from the competent cells BL21 Rosetta2, which contains the pRARE2 plasmid encoding seven rare tRNAs [62]. These cells are grown in nutrient rich 2xYT medium and dutifully kept at 37 ºC for the entire growth process. Combining this temperature control with both a cascading growth cycle and also collecting the cells in the log phase of their growth ensures that only σ70 is present in the extract as all of these measures ensure the cells are as healthy as possible. Since they do not need to move to find nutrients and are never exposed to temperature shocks, the other sigma factors are not expressed. Three liters of cell culture at OD 600 2-2.5 is collected to produce ~30 mL of lysate, which in turn can be used for ~90 mL of TXTL reactions. After collection the cells are washed before being lysed by a French press at 10-13000 psi. This crude lysate is then incubated with PEG to encourage precipitation of endogenous cellular information and degradation products. Dialysis is then done to standardize the ionic concentrations and remove small molecules under 10 kDa. Finally, it is flash frozen in liquid nitrogen and stored at -80 °C. It is stable at this temperature for over a year, ready to be thawed and used in TXTL reactions.

2.2 Cell-Free Reaction

2.2.1 Components

Cell-free reactions (CFR) are composed of a multitude of different components that carry information, create a mimetic cellular environment, or alter the chemical composition of the solution in order to optimize protein synthesis. The crude *E. coli* lysate comprises about one third of the entire 90 µl reaction volume and contains the cellular machinery required for transcription (RNA polymerase) and translation (ribosomes), along with other enzymes not removed during the preparation of the extract. The optimal protein concentration in a CFR is 9-10 mg/ml while the protein concentration in *E. coli* is between 250-300 mg/ml. Although ~10 mg/ml protein in a reaction is not unique to this extract, it is unknown precisely why this concentration of crude extract is optimal in a reaction. The next third of the reaction is made up of an energy buffer and an amino acid buffer. The energy buffer is an ATP regeneration platform based on 3-phosphoglyceric acid (3PGA) and the amino acid buffer is an equimolar mixture of the 20 canonical amino acids [63], [64]. The final third of the reaction is completed with information carrying DNA or mRNA, enzymes and proteins of interest, and miscellaneous molecules like dyes or small molecules not present in the energy mix. For an experienced user of TXTL, the system is typically compiled by adding each component separately. However, it is possible to prepack TXTL reactions, making it more accessible as a platform for collaboration or education [42], [65]. The prepack system retains the same qualities of a high-expression yield and is stable for over a year at -80 °C. While this technique affords less control over the composition of a reaction, it is ideal for experiments where the reaction conditions are the same or for experimenters unskilled at micropipetting.

A typical cell-free reaction, optimized for expression of deGFP from the P70a promoter, also contains 2-5 mM magnesium-glutamate, 60-120 mM potassium-glutamate, 25-40 mM maltodextrin and 0.5-2.5% w/v polyethylene glycol, molecular weight 8000 Da (PEG8000). Magnesium and potassium are ions critical for the function of transcription and translation. Maltodextrin is involved in the ATP regeneration pathway [63]. PEG is a polymer that acts to increase molecular crowding and thus greatly affects

reaction rates. The effect of increasing potassium, magnesium, maltodextrin, and PEG can be seen in Figure 2.2.

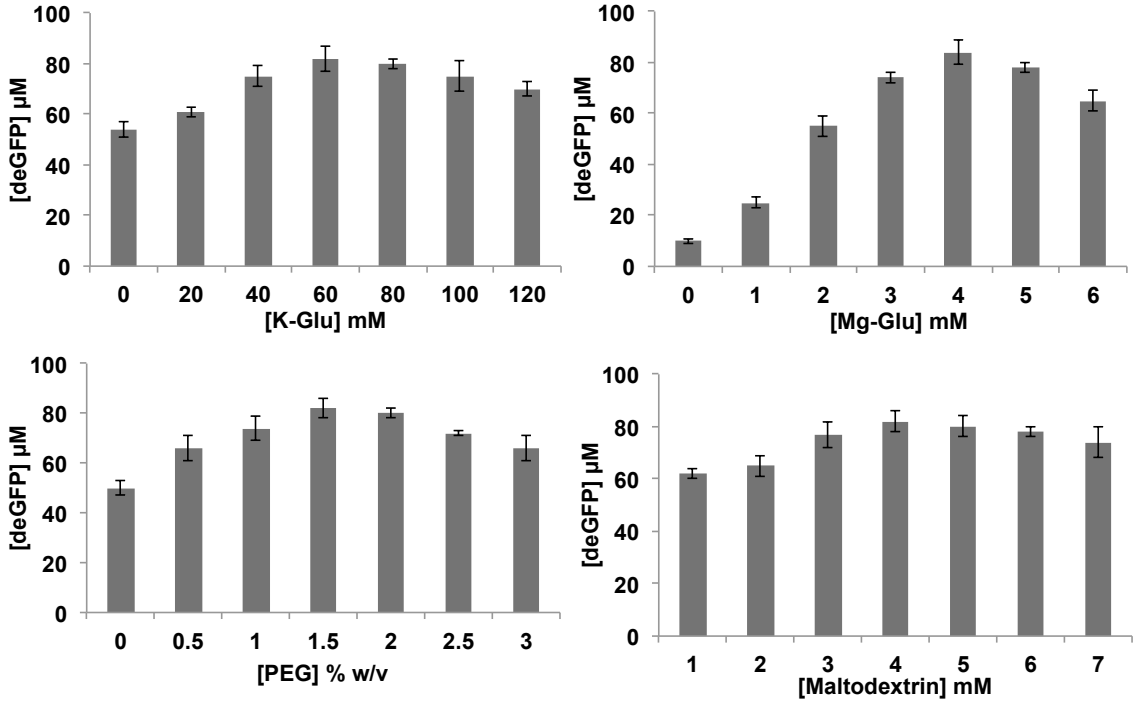

Figure 2.2 Endpoint deGFP protein expression against varying concentrations of potassium glutamate, magnesium glutamate, PEG 8000, and maltodextrin. 5 nM P70a-deGFP plasmid was incubated in TXTL in test tubes at 12 µl over 12 h at 29 °C. Error bars represent the standard deviation from 3 trials.

The energy buffer is composed of many different components. The concentration of each component in a TXTL reaction, along with their function, is given below:

- 50 mM Hepes pH 8, maintains physiological pH
- 1.5 mM ATP and GTP, energy sources and mRNA units
- 0.9 mM CTP and UTP, mRNA units
- 0.2 mg/mL tRNA, connects mRNA codons to amino acids
- 0.26 mM coenzyme A, oxidator in ATP regeneration pathway
- 0.33 mM NAD, redox electron carrier
- 0.75 mM cAMP, signaling molecule for catabolite activator protein, a transcriptional activator
- 0.068 mM folinic acid, aids in transcription

- 1 mM spermidine, aids in transcription, DNA binding, and pH control
- 30 mM 3-PGA, phosphate donor in ATP regeneration pathway

These components are dissolved individually in either water or potassium hydroxide as described previously [62]. They are then mixed, aliquoted, flash frozen in LN2, and stored at -80 °C. This energy buffer is stable for several years at -80 °C without significant loss of activity.

As the name implies, the amino acid buffer supplies TXTL reactions with amino acids, the building blocks of polypeptide chains and thus, proteins. The mix is prepared by dissolving the 20 canonical amino acids in potassium hydroxide, mixing them in equimolar proportions, and finally adjusting the pH with glacial acetic acid. The pH is adjusted to physiological conditions, with the optimum being between pH 7 – 8. Like the energy buffer and cell-free lysate, the amino acid buffer is aliquoted, flash frozen in liquid nitrogen, and stored it -80 °C. It is stable at that temperature for at least three years. The final concentration of each amino acid in a TXTL reaction is 3 mM. This mixture is highly concentrated for two reasons: 1) to minimize the amount of KOH added to a reaction and 2) to minimize the amount of acetic acid added to a reaction. For this reason, the mixture can precipitate when thawed, though it is readily mixed by vortexing or pipetting with no loss of activity.

2.2.2 Conditions

Protein synthesis in TXTL reactions is highly dependent on the reactions conditions in the same way TXTL is sensitive to the concentrations of certain critical components. Conditions, in this context, encompass the local environment the reaction takes place in. Protein synthesis is at a maximum when the reaction is incubated at 29°C. We speculate that this temperature is ideal to balance the synthesis and degradation of mRNA, as well as translation rates. Protein synthesis obviously requires transcription, but there is a negative value in producing so much mRNA that the ribosomes present in the lysate are saturated as mRNA consumes energy. At temperatures other than 29°C, protein synthesis still occurs, though the overall output is lower and the rates of production are slower. *E. coli* itself grows at 37 °C, so it is conceivable that there could be experiments where carrying out reactions at 37 ºC might be necessary e.g. there is an enzyme of interest that

only functions at 37°C. Furthermore, since varying the temperature has an effect of synthesis rates, the temperature could be introduced as a variable when studying genetic circuits, much in the same way that plasmid stoichiometry is varied.

Cell-free reactions are also extremely sensitive to oxygen, with endpoint protein concentration being dramatically diminished in oxygen poor conditions. Oxygen is especially relevant to the optimization of TXTL as we typically optimize with deGFP fluorescence acting as a proxy for extract activity and protein synthesis. GFP is known to require high amounts of oxygen for chromophore maturation [66]. Since we carry out reactions at atmospheric pressure and gas concentration, we can alter the oxygenation of a given reaction by increases the amount of contact a reaction droplet or volume has with the air. In bulk reactions carried out in test tubes, the optimal volume is 10-12 µl in a 1.7 mL Eppendorf tube. Larger volumes can be used, though endpoint synthesis is depressed. Using smaller volumes does not increase gene expression. Many experiments are monitored kinetically on a plate reader, however, and we therefore have tested several different reactions volumes in 96-well plates. 2 µl reaction volumes are the optimum, maintaining the greatest deGFP synthesis rate for the longest period of time. Theoretically, spreading a TXTL reaction out thinly would increase the surface-area-to-volume ratio. Practically, this is impossible, as the fluorescence measurement requires reproducibility in droplet shape and location between wells (data not shown).

TXTL reactions are active in many other environments, not being limited to test tubes or well plates. They can be encapsulated in emulsion droplets, liposomes and microfluidic droplets [44], [59], [67]. This gives researchers the opportunity to investigate, among other things, proteins that require a membrane to fold, such as MscL. It also greatly reduces the volume of reactions while increasing the number of reaction vessels, allowing researchers to probe areas where large data is required. The miniaturization of TXTL is also desirable as it reduces the number of reagents used, in turn reducing cost. The Labcyte Echo 550 Liquid Handler is an incredibly powerful tool to not only miniaturize TXTL, but also to rapidly assemble reactions. The Echo 550 works by using acoustic energy to transfer droplets 2.5 nl in volume from a source plate into a destination plate i.e. the 96 well plate we use in the plate readers. We have used the

Echo to scale down TXTL reactions to 0.5 µL, though 2 µl remains the optimum for overall endpoint synthesis.

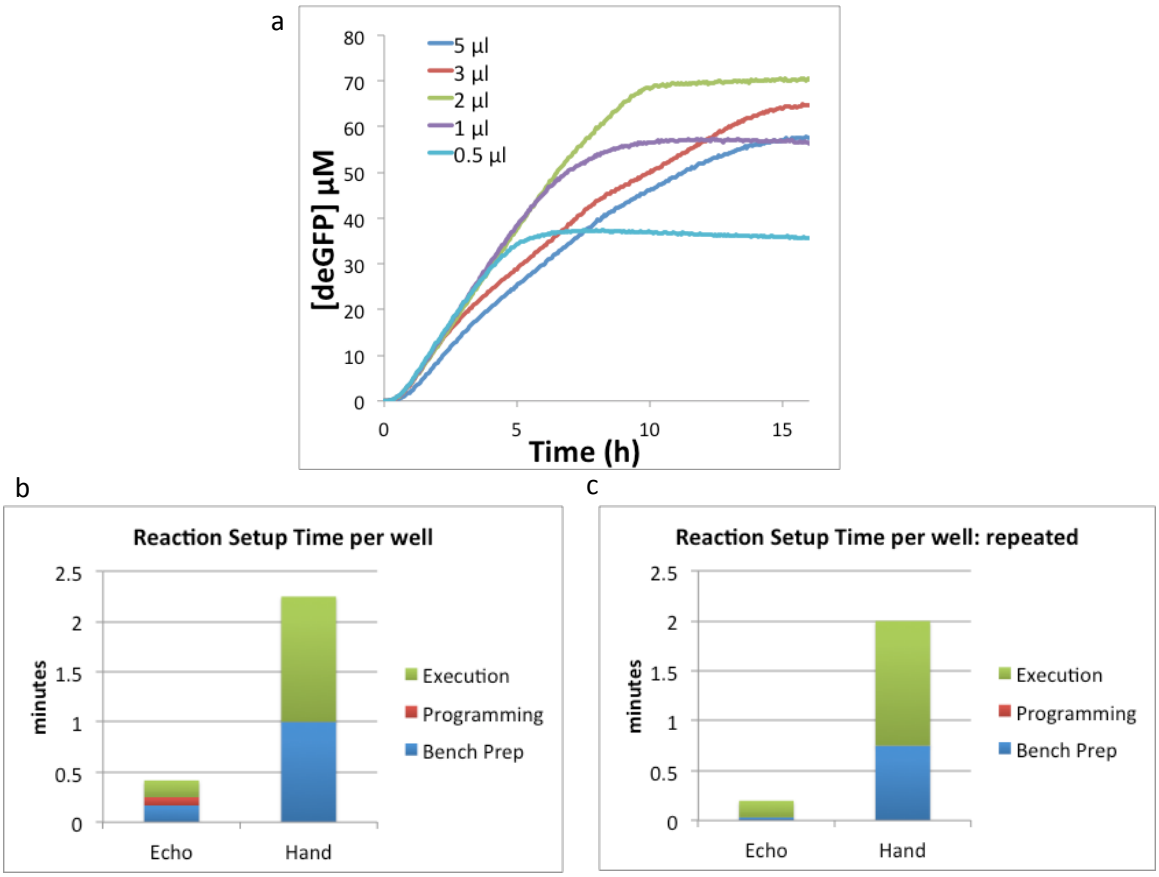

Figure 2.3 a) deGFP expression kinetics for varying TXTL reaction volumes expressing 5 nM P70a-deGFP compiled with the Labcyte Echo 550. b) Time necessary to assemble a TXTL reaction by hand versus the Labcyte Echo 550. c) Time necessary to assemble a repeated TXTL reaction by hand versus the Labcyte Echo 550 [68].

The Echo dispenses hundreds of droplets every second, greatly reducing the time it takes to assemble a reaction (Fig. 2.3). A full, 96 well plate can be assembled in roughly 16 minutes once the source plate is loaded, decreasing the experimental time by a factor of five. It is not entirely clear why volumes of 0.5 and 1 µl are not as well-suited for TXTL reactions as 2 µL, though this may just require a new optimization of reagents. The Echo provides an even another advantage as it reduces the stress and fatigue on the experimenter.

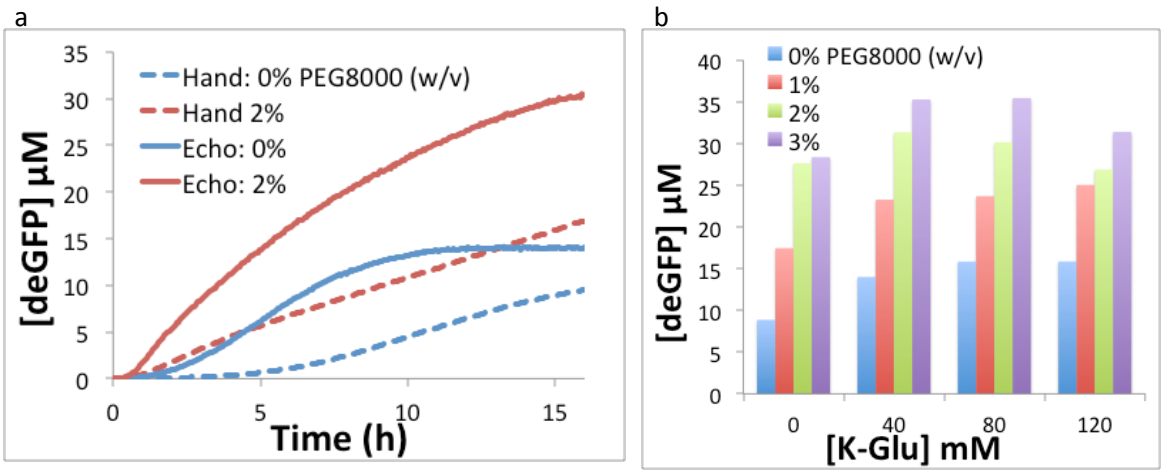

Figure 2.4 a) deGFP expression kinetics for TXTL reactions at 0 and 2 % PEG weight by volume assembled by hand versus the Labcyte Echo 550. 2 nM P70a-deGFP was expressed. b) Endpoint deGFP expression for TXTL reactions at various concentrations of potassium glutamate and PEG8000. 2 nM P70a-deGFP was expressed [68].

Prior to having the Echo in our lab, it would take a new student hundreds of hours of practice micropipetting to reliable assemble TXTL reactions in a reproducible manner (Fig. 2.4). With the Echo, a complete novice can be up and running with TXTL in a matter of days.

2.2.3 Plasmids

DNA is the main source of information in TXTL reactions and the most effective way to deliver this DNA is via plasmids. The plasmids for toolbox 2.0 consist of an origin of replication, antibiotic resistance, a (often regulated) promoter site, untranslated region (UTR), gene of interest, and terminator. The gene sequence to be expressed is most commonly the fluorescent protein deGFP. However, we also often express other transcription factors to build genetic circuits or membrane proteins to be studied in liposomes, both of which will be discussed in later chapters. Toolbox 2.0 was initially optimized using the P70a promoter, recognized by the holoenzyme formed by *E. coli* RNAP and σ70. The P70a promoter is the strongest *E. coli* σ70 reported, originating from the bacteriophage lambda. The regulatory sequence consists of the strong, σ70 specific, Cro promoter "Pr" with two operator sites, OR1 and OR2, overlapping the -10 and -35 sequences, both of which correspond to the repressor cI [31]. Unless it is otherwise

specified, the untranslated region between the promoter and gene is UTR1 from the bacteriophage T7. This UTR is commonly used in recombinant protein expression, as it is one of the strongest bacterial untranslated regions and contains a very strong ribosome-binding site. All plasmids transcribed by *E. coli* RNAP contain the terminator T500 unless otherwise specified. The purpose of the terminator is to prevent RNAP from transcribing superfluous mRNA, as this both wastes of energy and sequesters the RNAP. Using P70a-deGFP, cell-free expression lasts 8-10 hours and produces roughly 2 mg/ml of active fluorescent protein. Protein synthesis as a function of plasmid concentration is linear up to 2-3 nM and protein production linearly increases over the first 4-5 hours of expression (Fig. 2.5).

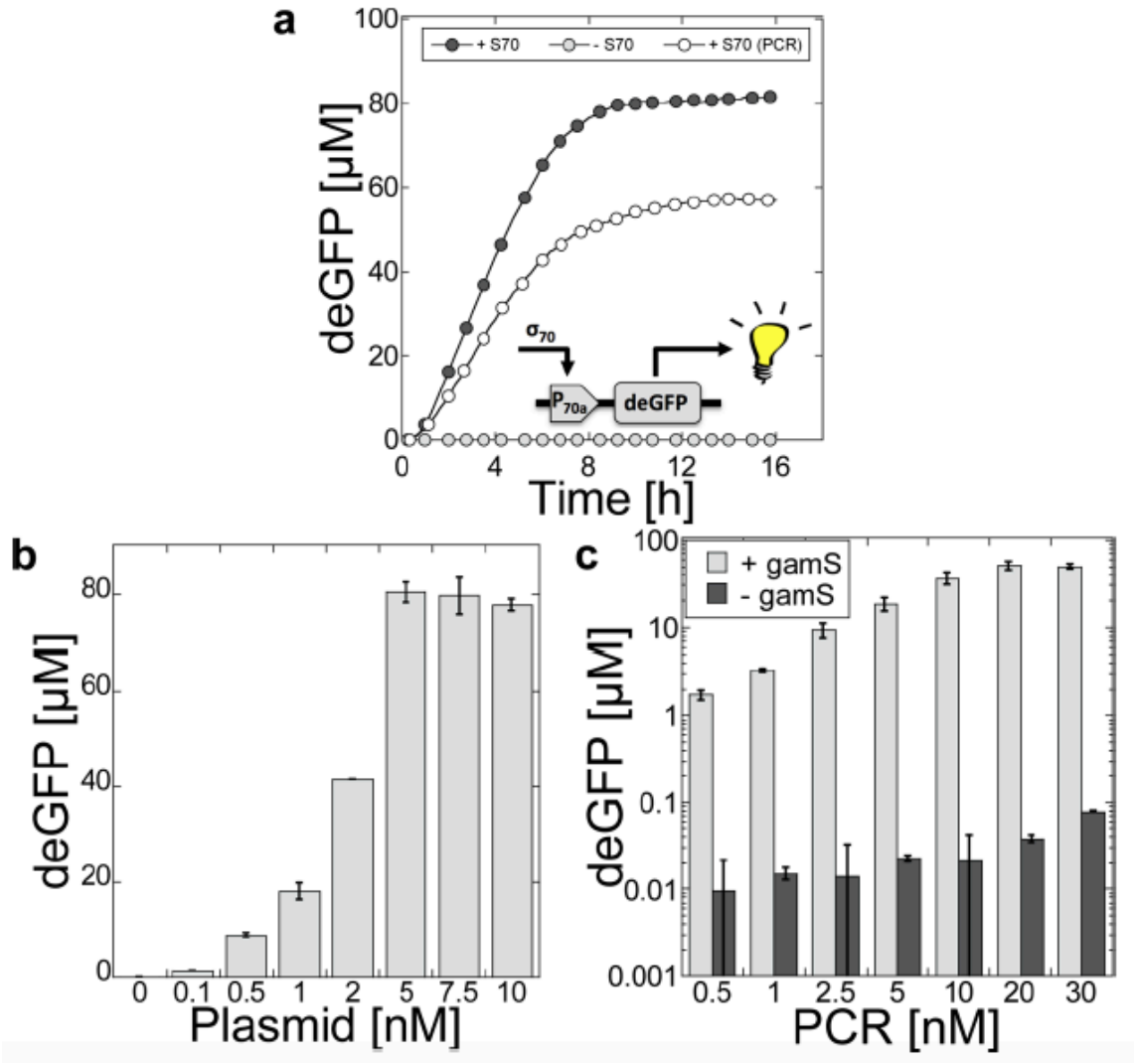

Figure 2.5 P70a-deGFP expression in TXTL a) Expression kinetics of deGFP from plasmid and linear P70a-deGFP b) Endpoint deGFP expression using plasmid P70a-deGFP c) Endpoint deGFP expression using linear P70a-deGFP in the presence or absence of gamS. Reprinted with permission from *ACS Synth. Biol.*, **2016**, *5* (4), pp. 344–355. Copyright 2016 American Chemical Society.

TXTL reactions also respond positively to active mixing with a semi-continuous mode of expression. To increase reaction lifetime and synthesis yield, a dialysis membrane can be used to feed the reaction and remove byproducts [26], [31], [69]. We demonstrate the synthesis of 207 µM and 247 µM deGFP produced using the P70a-deGFP and P70a-T7RNAP/T7p14-deGFP plasmids, respectively, after 24 hours of incubation (Fig. 2.6). 20 µl of TXTL reaction were pipetted onto a dialysis membrane with a 10 kDa cut-off. The other side of the membrane contained 200 µl feeding solution, which is equivalent to a cell-free reaction except that a buffer acts in the place of the lysate. The 96-well plate from Harvard Apparatus wherein these reactions are contained was rotated on axis over the entire 24-hour period.

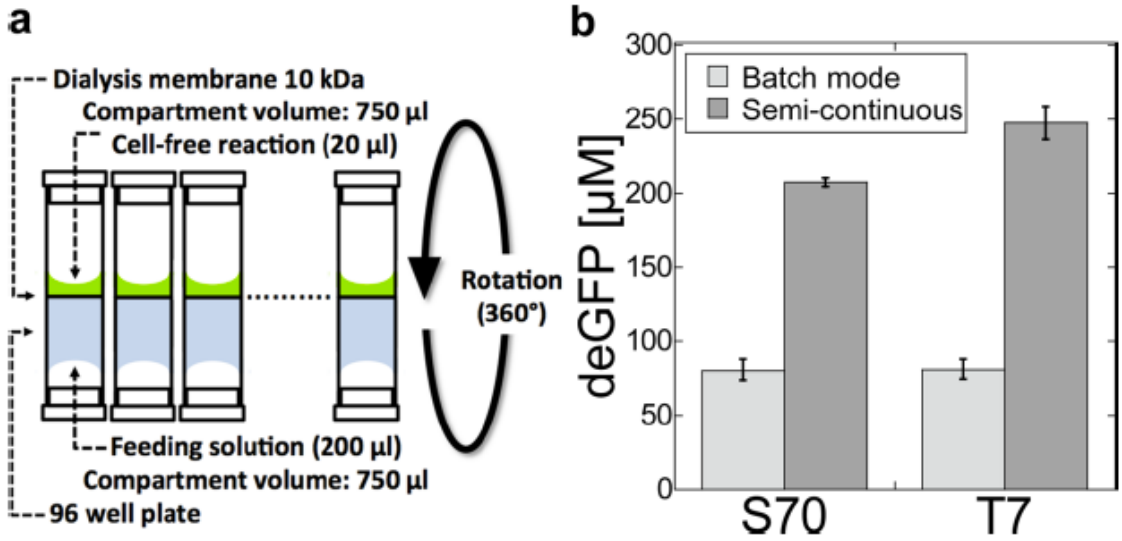

Figure 2.6 Semi-continuous deGFP expression in TXTL. a) Schematic of the plate used in the semi-continuous reaction. b) Endpoint deGFP expression of P70a-deGFP and T7p14-deGFP at optimal conditions in batch and semi-continuous mode. Reprinted with permission from *ACS Synth. Biol.*, **2016**, *5* (4), pp. 344–355. Copyright 2016 American Chemical Society.

Of course, to use plasmids in TXTL reactions, we need to amplify them. As there are an incredible number of parameters to test whether they be cofactors, plasmid stoichiometries, energy or amino acid buffer concentration, or extract dilution, it sometimes requires a large volume of highly concentrated plasmid DNA stock to optimize a given plasmid or circuit. Standard transformation and amplification techniques work for most plasmids, but many can be toxic to *E. coli*, especially membrane proteins and transcription factors. To overcome these obstacles, we can alter the origin of replication, the promoter, or the competent cell strain we grow the plasmids in. We use colE1 (several hundred copies per cell) for high copy plasmids and p15A (~10 copies per cell) for low copy plasmids. The logic here is simple: if a protein is toxic to a cell, reduce the concentration of that protein in each cell by reducing the number of plasmids encoding it. As σ70 is the housekeeping transcription factor, it is the main sigma factor expressed in ideal conditions, like those a cell would experience when being used for plasmid amplification. Therefore, toxic proteins can be difficult to clone under the P70a promoter. However, during healthy cell growth, the other sigma factors are hardly expressed and toxic genes can be cloned under promoters corresponding to the other *E. coli* sigma factors. Perhaps even more obvious is to use the promoter T7p14 from bacteriophage T7. Since there is no endogenous T7 RNAP in *E. coli* and the core RNAP does not interact with this promoter, T7p14 will be almost completely silent during amplification [65]. These promoters and their transcription cascades will be discussed in greater detail in Chapter 2.2.4.

We use two main competent cell strains to amplify plasmids: JM109 and KL740. JM109 overexpresses the lacI repressor, repressing the promoter PL-lacO1 [70]. This strain is used to amplify plasmids not containing genes under the P70a promoter. If our experimental design dictates that we need a protein, which happens to be toxic, controlled by the P70a promoter, KL740 can be used as it overexpresses the cI repressor from lambda phage. This cI repressor acts to bind to the two operator sites, OR1 and OR2, that overlap the -10 and -35 sequences in the promoter. Standard bacterial cultures can be made in LB medium at volumes of 5 mL (miniculture), 50 mL (midiculture), or 200 mL (maxiculture). KL740 is grown at 29 °C while JM109 grows at the normal *E. coli*

temperature of 37 °C. The competent cells are grown in liquid culture overnight and then plasmid amplification kits (Sigma, Zymo) are used to isolate the desired plasmid. After the plasmid is isolated, it is often necessary to clean the DNA using a PCR purification kit, like Purelink from Invitrogen. At this point, the plasmid is quantified via Nanodrop and stored at -20 °C. It depends on the plasmid, but typically we want stocks of at least 50 nM.

2.2.4 Linear DNA

Although plasmid DNA is the most common information carrier in TXTL reactions, sometimes it is simply not possible to use them. There are some genes that are toxic to *E. coli* such that it is not feasible to clone them into plasmids and amplify them. For example, while it is relatively simple to insert the mechanosensitive channel of large conductance (MscL) into a plasmid, there are mutant versions of MscL that cause the pore to open more easily. In cases such as these, we use linear DNA as the TXTL template, in the form of PCR products or dsDNA fragments purchasable from companies like IDT. This ability greatly accelerates the design/build/test cycle in TXTL reactions, a cycle that is already much faster than in vivo experiments. Linear DNA is also cheaper and more accessible to novice experimentalists, as no knowledge of molecular cloning is necessary. However, it is not as simple as adding PCR products to TXTL reactions. As the all *E. coli* cell-free expression system uses a crude lysate, there are enzymes leftover from *E. coli*, specifically, endonucleases and exonucleases. These act in living cells to repair DNA or degrade DNA of outside origin, but in a cell-free extract simply act to degrade linear DNA.

The main nuclease responsible for degradation of linear DNA in *E. coli* TXTL systems is exonuclease V, also known as the RecBCD complex [71]. The RecD subunit of this complex degrades DNA templates by ~500 bp/s, starting from the 3’ end of a linear strand [72]. Although it is possible to prepare a lysate without this complex, this strain has not been optimized for cell-free protein expression and is limited in that transcription must be booted up from the T7 promoter [73]. Initially, we used purified gamS protein from lambda phage, as it is known to bind and inhibit RecBCD [71]. Using this method, we are able to express over 50 μM of deGFP from the linear template P70a-

deGFP, with 200 – 300 bases present on either side of the promoter-gene region (Fig. 2.7). When using linear DNA, it is necessary to use much more DNA template in order to reach peak expression; in this case, 20 nM PCR product was used.

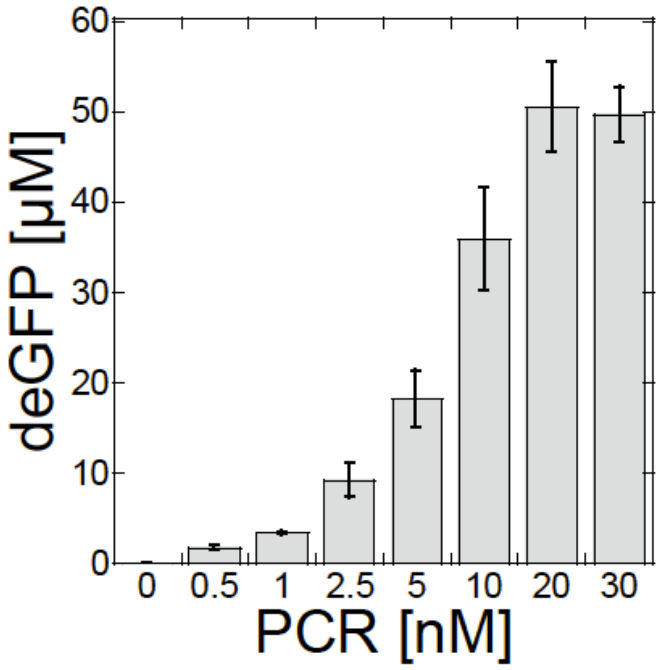

Figure 2.7 Endpoint deGFP expression of linear P70a-deGFP at various DNA concentrations. Reprinted with permission from *ACS Synth. Biol.*, **2016**, *5* (4), pp. 344–355. Copyright 2016 American Chemical Society.

There is another technique that allows the use the linear DNA in TXTL reactions that was realized after we had a better understanding of the mechanism of RecBCD. In *E. coli*, RecBCD is the main pathway for double-strand break repair [74]. This activity is regulated by the χ sequence (5'-GCTGGTGG-3') in *E. coli* and is therefore repeated roughly 1000 times in the genome [72]. During homologous recombination, RecBCD stalls on χ sites. It was shown by my colleagues that the introduction of an annealed χ sequence does stabilize linear DNA in TXTL and only slight hinders expression from plasmid DNA. Using linear and plasmid P70a-deGFP templates, they tested three different double stranded χ sequences: Chi4, Chi6, and Chi9. The numbers denote the amount of times the χ sequence is repeated in the strand. A five base spacer separates each χ site. Chi6 and Chi9 allow TXTL reactions to proceed more efficiently than GamS in concentrations as low as 2 μM of χ DNA, while Chi4 is not as effective as GamS until it is introduced at 4 μM. They also tested a scrambled version of Chi6 (Scr), as well as a single stranded version of Chi6 (ssChi6) and it's scrambled counterpart (ssScr). These

scrambled and single stranded inhibitors are not as effective as the double stranded equivalents. During my research, we decided to use this Chi6 sequence as opposed to Chi9. This is because it is much cheaper and faster to order, being 85-nt as opposed to 125-nt oligonucleotides. We order Chi6 sequences, forward and reverse, from Integrated DNA Technologies (IDT) and anneal them in a thermocycler. The Chi6 sequences are resuspended in water at 1 mM and then mixed to a 30 µl volume (15 µl of each oligonucleotide). This solution is then heated to 95 °C, cooled 1 °C per minute until room temperature is reached. This 500 µM solution of active Chi6 is then aliquoted by 2.5 µl. In TXTL reactions, we use Chi6 at 2 µM.

2.2.5 Gene Circuits

While expressing proteins using the σ70 cascade is useful and certainly simple, it is necessary to use transcription cascades to introduce gene regulation. The simplest and most common way we do this is by making use of the P28a or T7 promoter. For years, plasmid amplification has relied on using the T7 promoter, as it is silent in *E. coli* [75]. Likewise, the *E. coli* promoter P28a, specific to the flagellar sigma factor, σ28, is also silent in *E. coli* grown under optimal conditions [76]. Since neither transcription factor is produced in *E. coli*, both of these promoters can be used to amplify toxic genes using either JM109 (Promega) or DH5alpha (NEB) competent cells. To express proteins using the T7 or P28a promoters, T7 RNAP or σ28 must first be expressed using the plasmids P70a-T7RNAP or P70a-S28, respectively. Using these cascades allows a brief delay in gene expression, though overall protein production is similar to using P70a alone (Fig. 2.8).

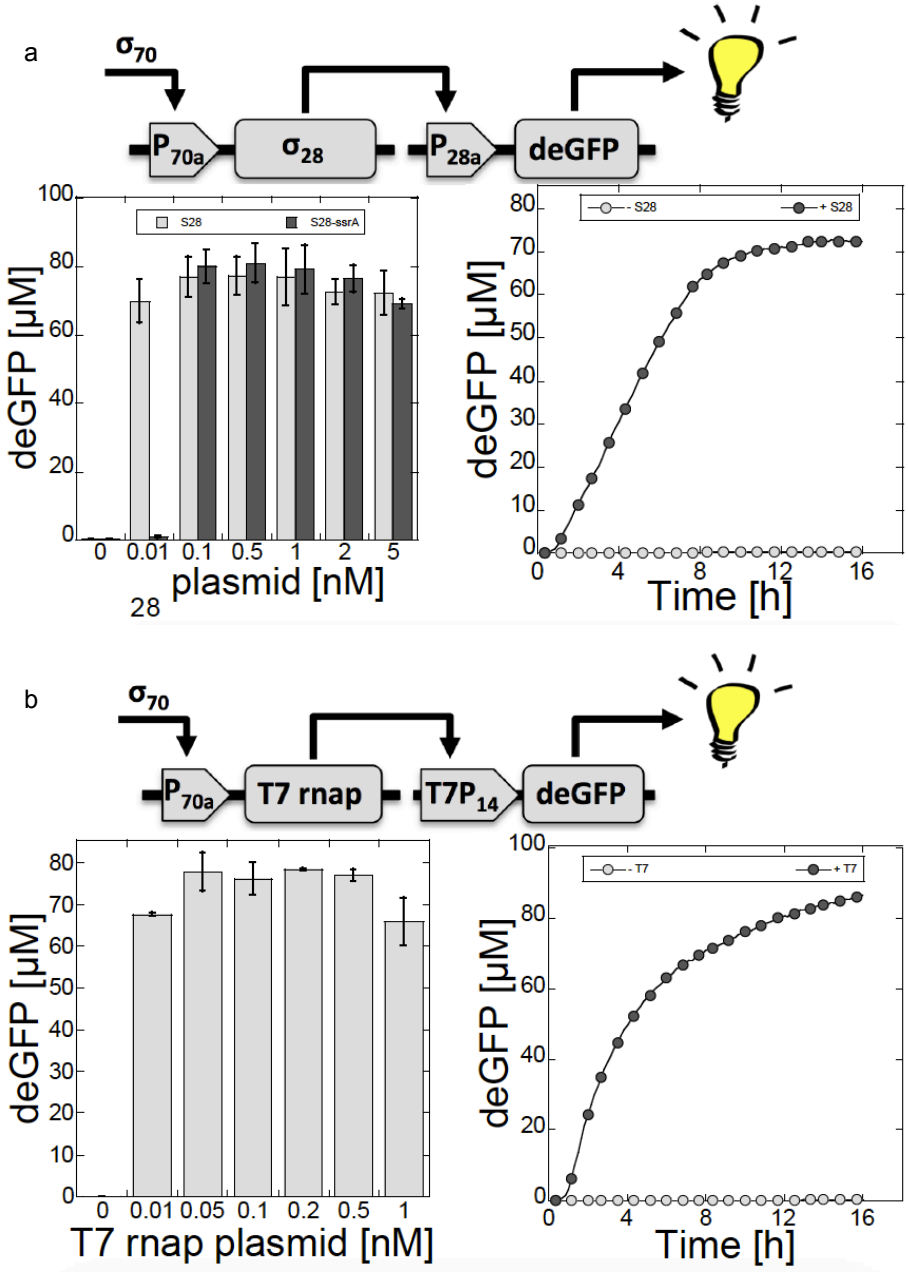

Figure 2.8 a) Endpoint and kinetics of protein expression from the σ28 cascade. b) Endpoint and kinetics of protein expression from the T7 cascade. Reprinted with permission from *ACS Synth. Biol.*, **2016**, *5* (4), pp. 344–355. Copyright 2016 American Chemical Society.

Though these are the most common and most powerful transcription cascades I used, we also optimized expression from the other five sigma factors from *E. coli* and from the strongest promoter from the bacteriophage T3.

To increase complexity slightly further, degradation tags can be applied to any of the proteins in the pathway. The AAA+ protease clpXP from *E. coli* is present in the extract, which readily acts on the degrons ssrA or ompA [77], [78]. My colleagues previously showed that protein degradation using the endogenous ClpXP in the extract is a zeroth-order reaction, proceeding at a rate of about 5-15 nM/min of His-eGFP-ssrA (Fig. 2.9). Though this information is useful in characterizing the extract, this rate is too low to create efficient protein degradation in TXTL reactions since the maximum protein synthesis rate is roughly 150 nM/min [44], [79]. To achieve powerful protein degradation using ClpXP, we cloned the tandem clpP-clpX genes in a plasmid under the P70a promoter. This plasmid was then added to a reaction and the concentration of His-eGFP-ssrA was monitored. The addition of the P70a-clpXP was done in three ways: i) added as a pre-expressed protein; ii) added at the outset of the reaction at the same time as eGFP; iii) added to the reaction and allowed to incubate one hour before the addition of His-eGFP-ssrA. The third technique is the most effective, delivering protein degradation up to 250 nM/min at 6 nM of plasmid P70a-clpXP used.

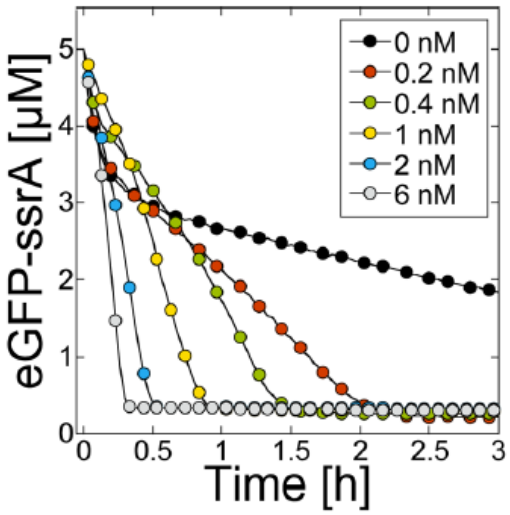

clpXP [nM]	eGFP degradation rate (nM/min)
0	6.51 ± 1.25
0.2	28.04 ± 3.87
0.4	48.24 ± 8.06
1	88.32 ± 17.71
2	159.13 ± 21.92
6	256.07 ± 38.24

Figure 2.9 Degradation of the protein eGFP-ssrA in TXTL at various concentrations of clpXP. Reprinted with permission from *ACS Synth. Biol.*, **2016**, *5* (4), pp. 344–355. Copyright 2016 American Chemical Society.

At lower plasmid concentrations of 0 or 0.2 nM, we see a fast initial degradation rate that slows after 15 minutes, indicating the endogenous ClpXP machinery is quickly saturated.

While transcriptional activator cascades with protein degradation surely can be thought of as simple circuits, they allow very little control over gene regulation. We constructed two longer transcriptional cascades of five and six gene, assembling them in series like circuits that begin with an AND gate composed of NtrC and σ54.

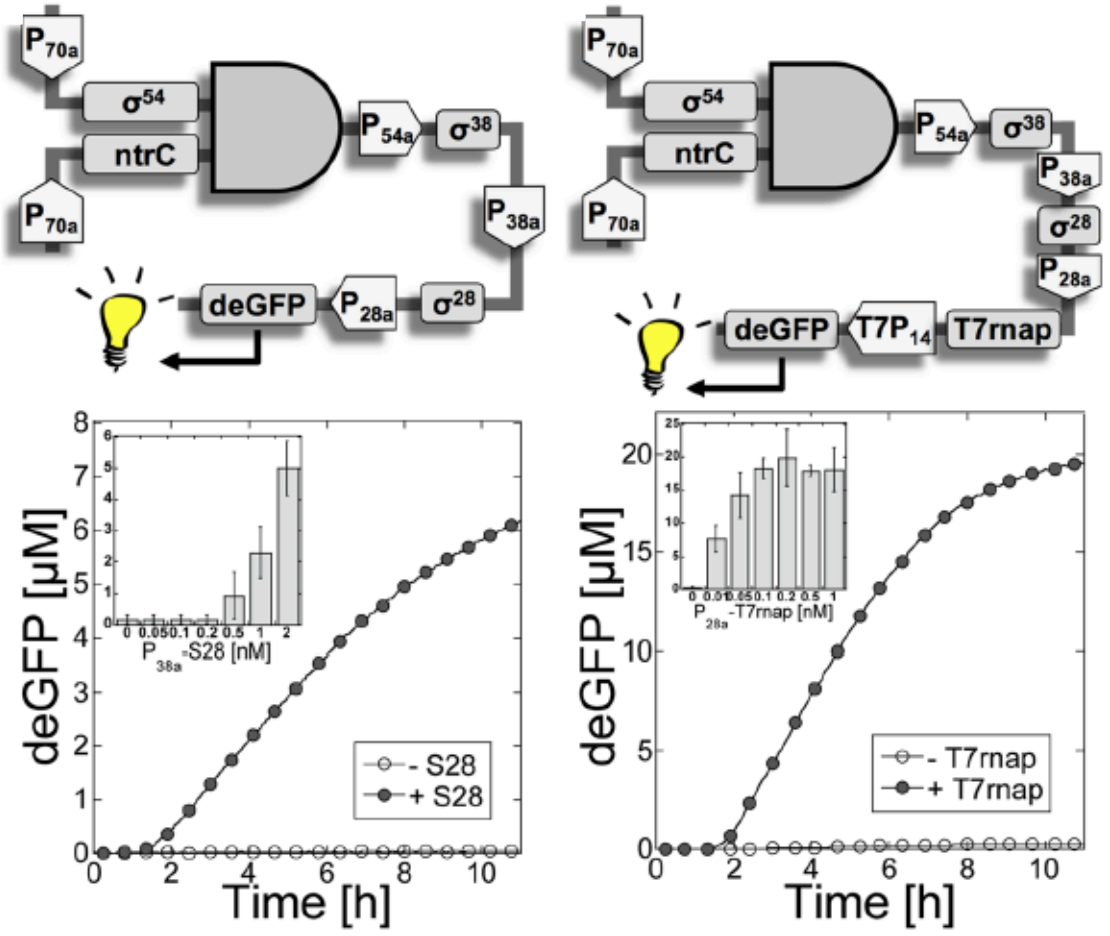

Figure 2.10 Schematics and expression kinetics of 5 (left) and 6 (right) gene cascades in TXTL. Inset in each plot shows ranges of the second to last plasmid in the cascade. Reprinted with permission from *ACS Synth. Biol.*, **2016**, *5* (4), pp. 344–355. Copyright 2016 American Chemical Society.

The sigma factors are arranged based on both their strength and competition between the sigma factor and the core RNAP. We began with the weakest sigma factors and weakest competitors, ending with the strongest and most competitive. This was done to get a

strong, specific output signal from an input from five or six plasmids that is not the result of a leak on non-specific transcriptional activators. The competition between sigma factors and the corresponding promoters can be seen in Table 2.1.

σ factor / promoter	σ_{70}	σ_{19}	σ_{24}	σ_{28}	σ_{32}	σ_{38}	σ_{54}/NtrC
P_{70a}	7.65	7.47	7.24	5.95	6.73	7.09	5.99
P_{19a}	0.04	0.27	0.02	0.02	0.01	0.02	0.05
P_{24a}	0.04	0.03	0.21	0.02	0.02	0.03	0.02
P_{28a}	0.01	0.02	0.01	5.69	0.02	0.01	0.02
P_{32a}	0.41	0.44	0.40	0.31	3.65	0.40	0.27
P_{38a}	0.02	0.04	0.05	0.01	0.02	0.40	0.01
P_{54a}	0.02	0.02	0.02	0.01	0.00	0.01	0.15

Table 2.1 Crosstalk between transcriptional activation units in the linear regime of plasmid concentration (0.1 nM and 1 nM of the sigma factor encoding plasmid and the reporter protein encoding plasmid, respectively). Reprinted with permission from *ACS Synth. Biol.*, **2016**, *5* (4), pp. 344–355. Copyright 2016 American Chemical Society.

Both cascades begin with the aforementioned AND gate, followed by a weak (σ38) and then strong (σ28) competitor. The six-gene cascade ends with the T7 cascade. Each gene was cloned into a separate plasmid and the cascade was optimized sequentially such that the leak is of the order of the background when the second to last stage is omitted. We also created a pulse by adding a repressor to the σ28 cascade and using a degradable deGFP as our reporter (Fig 2.11).

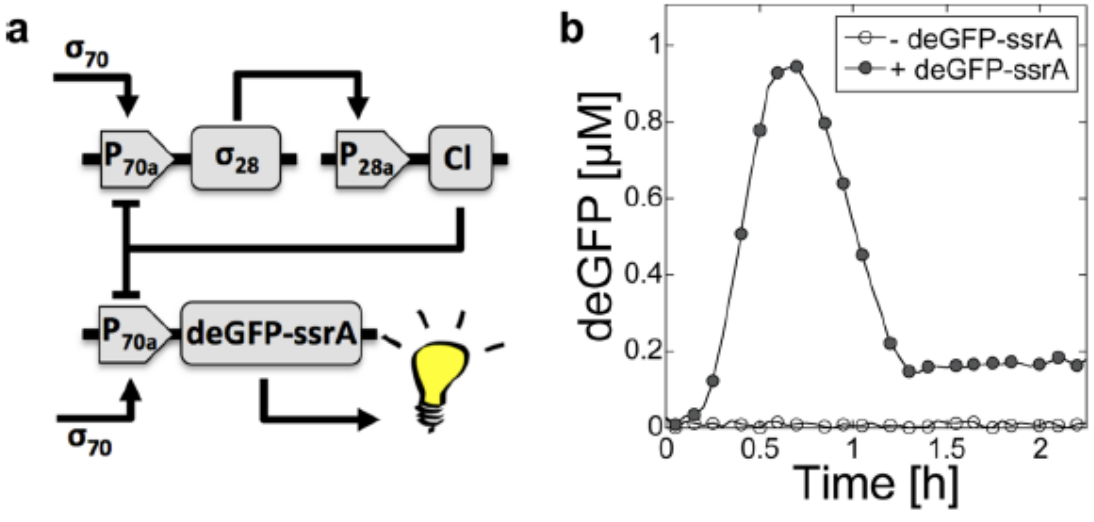

Figure 2.11 Schematic (a) and expression kinetics (b) of a pulse circuit in TXTL. Reprinted with

deGFP-ssrA and S28 were immediately expressed using the core *E. coli* RNAP and σ70, while the cI repressor from lambda phage was expressed in a delay using the P28a promoter. Since cI binds to the operator sites around the P70a promoter, it blocks transcription of both S28 and deGFP-ssrA. Thus, after being initially expressed, the fluorescent signal decreases over time as the ClpXP complex degrades the tagged deGFP and P70a is shut off after cI is expressed.

2.3 Quantitative Synthetic Biology

2.3.1 Fluorescence Readouts

The majority of the data presented in this thesis was gathered by measuring the fluorescence output of reporter proteins, either on plate readers or fluorescence microscopes. Thus far, we have looked at purely plate reader data, as we will discuss microscopy data later on in the context of a minimal cell system. To measure fluorescence in plate readers, TXTL reactions are incubated in test tubes for endpoint reactions and then pipetted into the well plate. To measure kinetics, the reactions are immediately pipetted into the well plate or transfer into the plate with the Echo before being put into the plate reader. We use two plate readers in the lab: the BioTek Synergy H1 and the BioTek Neo2. The software, Gen5, runs both readers and we primarily use both as monochrometers, which allows us to select specific excitation and emission wavelengths. The entire purpose of TXTL reactions is to express produce in a cell free environment, of course, but without an output signal we would have no way of understanding what is taking place. There are two things we can measure in terms of TXTL productivity: mRNA produced via transcription and protein produced during translation. During my thesis, I did not spend significant time monitoring mRNA synthesis, though it is easily done with RNA aptamers such as malachite green, Broccoli, Spinach, or Mango [80]. We mainly use fluorescent proteins to monitor the behavior of a circuit as they produce a stronger signal than RNA aptamers and are more readily accessible. We prefer to reporter proteins over luciferase as they do not require the addition of a chemical such as luciferase to monitor fluorescence and can be tracked in

time. Therefore, reporter proteins, many of them derived from the green fluorescent protein (GFP) from jellyfish, are the primary output signal in TXTL reactions.

As seen in Fig. 2.5, a reporter protein like GFP is expressed to concentrations greater than 50 μM in TXTL reactions, an amplification of 104 relative to the DNA input. The proteins are incredibly stable, lasting for weeks in TXTL reactions unless they are tagged to degrade. We use a truncated version of GFP, what we call deGFP, which is more translatable in TXTL [81]. In the wild-type GFP, there is a DNA sequence resembling a ribosome binding site (RBS) downstream from the desired start codon, and shortly after this pseudo-RBS there is a start codon. In deGFP, this sequence has been removed. Upon folding, deGFP emits a well-defined spectrum if it is excited by the proper wavelength. We have characterized a library of reporter proteins using TXTL to span the visible spectra (Fig. 2.11).

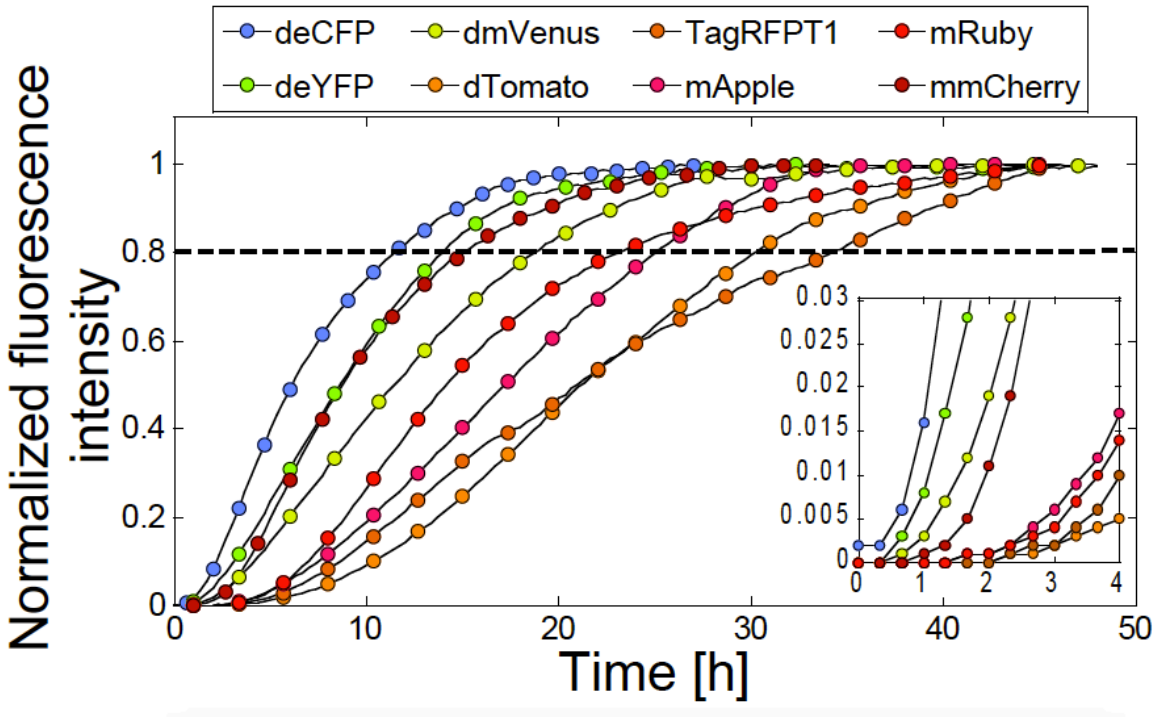

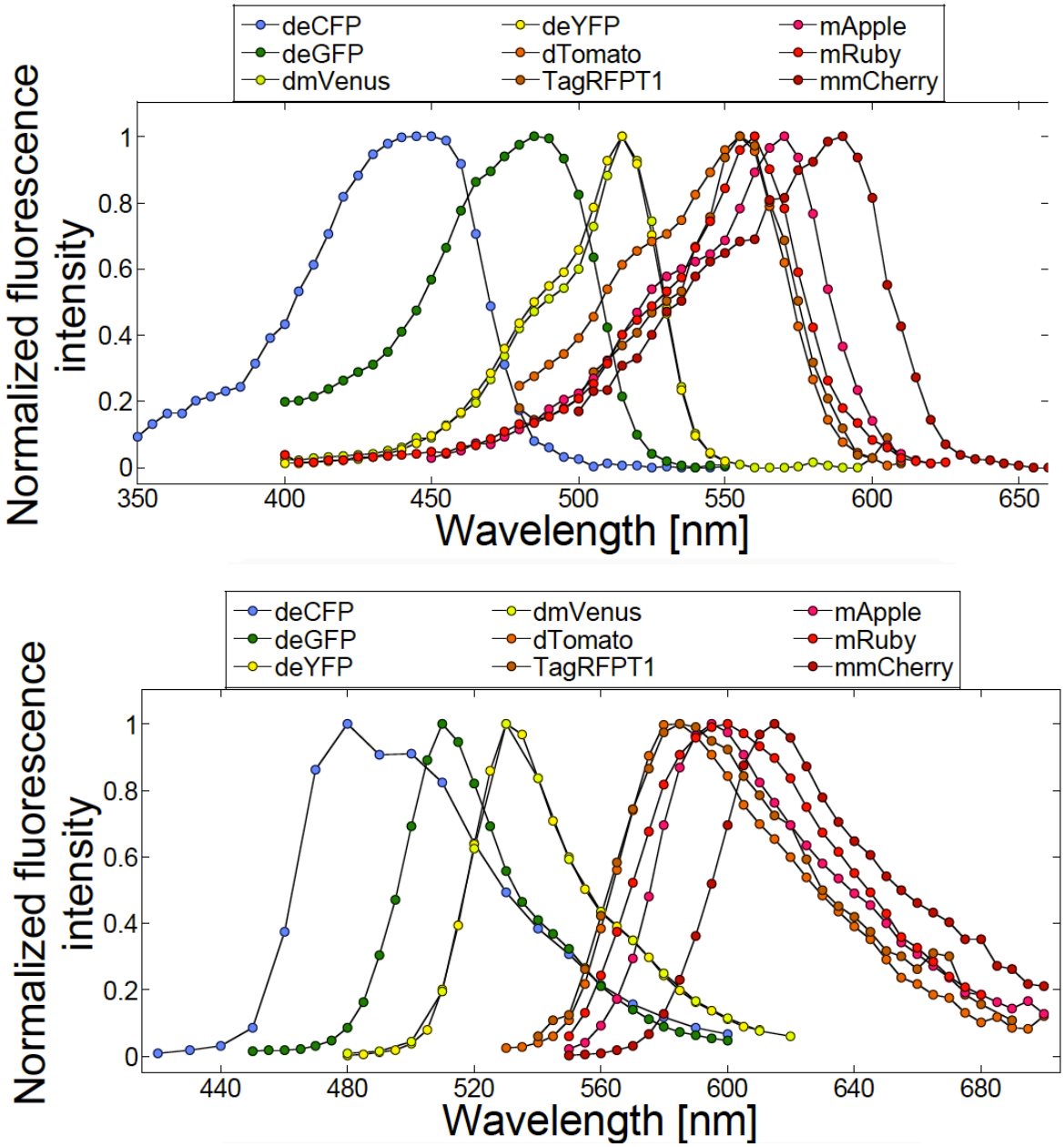

Figure 2.12 Maturation (top), excitation (middle), and emission (bottom) spectra for various reporter proteins characterized in TXTL. Reprinted with permission from *ACS Synth. Biol.*, **2016**, *5* (4), pp. 344–355. Copyright 2016 American Chemical Society.

It is useful to have a number of reporter proteins to use in case an experiment requires the monitoring of more than one circuit, for example. With deGFP and mmCherry, it would be simple to measure the production of two transcription cascades simultaneously.

Reporter proteins are also commonly used in Förster resonance energy transfer experiments [82], [83].

For experiments using GFP as the output, our plate readers our calibrated using recombinant GFP (reGFP) from Cell Biolabs, Inc. and a separate stock of His-eGFP that we prepare. The reGFP from Cell Biolabs is sold at 1 mg/ml and we verify this again by absorption at 488 nM with an extinction coefficient of 55000 M-1 cm-1. This stock is then diluted in water to make a standard curve between 0 and 30 μM at various gains (typically between 40 and 60). To measure concentrations above 30 μM deGFP, we prepare our own recombinant GFP and purify it to a concentration of ~150 μM. Our stock is quantified using the standard curve prepared by the reGFP from Cell Biolabs and by absorption. We then make a standard curve using the 150 μM stock between 0 and 100 μM. It is important to note that the intensity vs. concentration curves are not linear between 0 and 100 μM, but taper off beginning at ~50 μM. For this reason, we fit our standard curves with 2nd order polynomials. Nevertheless, the fitting of the data points is extremely accurate using this method ($R2 > 0.995$). The plate readers are optically stable with the calibration curves remaining accurate for 1-2 years. However, we verify them every three months using the reGFP from Cell Biolabs.

Another type of fluorescence measurement we utilize on the plate reader is a technique known as fluorescence anisotropy. Fluorescence anisotropy makes use of the simple physical principle that different sized molecules in the same solution will have different coefficients of rotational diffusion. By exciting the molecule with polarized light and then measuring the polarization of the light emitted, we can infer the relative rotational diffusion between molecules. Larger molecules will rotate more slowly such that the light emitted will be more aligned with the exciting light. The opposite is true of smaller molecules. For a rapidly rotating molecule, the emitted light will be polarized more or less randomly relative to the incident light. The anisotropy can be calculated as $r = (I_{parallel} - I_{perpendicular})/(I_{total})$, where I is the intensity of the emitted light measured. Fluorescence anisotropy is potentially an incredible powerful tool for TXTL, as it can show the binding of molecules together and give insight into filamentation or polymerization. We use the Neo2 to measure fluorescence anisotropy on reactions carried

out in 96-well plates. The filter cube has a 540 nm excitation filter and a 590 nm emission mirror with a 550 nm cut-off dichroic mirror.

2.3.2 Fluorescence Microscopy

The rest of the quantitative data presented in this thesis was gathered using fluorescence microscopy. We use an Olympus IX-81 microscope to perform epifluorescence microscopy. To capture bright-field images of semi-transparent objects (liposomes or emulsions), we use phase contrast microscopy, a technique to convert phase shifts in transparent media to changes in image brightness. Our microscope is equipped with a Prior Scientific automated stage, which can be programmed to move automatically in three dimensions. This stage is controlled with Metamorph Advanced Imaging Software. Image analysis is also done with this software. We have multiple Tokai Hit heated stages, one of which acts as a chamber to prevent evaporation by control humidity. The IX-81 is equipped with filter sets that function with long pass filters or dichroic mirrors. It is set up with filters to measure CFP (438 nm excitation, 483 nm emission), GFP (473 nm excitation, 520 nm emission), YFP (500 nm excitation, 542 nm emission), TRITC (525 nm excitation, 585 nm emission), Texas Red (556 nm excitation, 617 nm emission), and DAPI (387 nm excitation, 435 nm emission). We primarily use a 40X air objective and a 100X oil objective, though we also have 10 and 20X air objectives as well as 40 and 60X oil objectives.

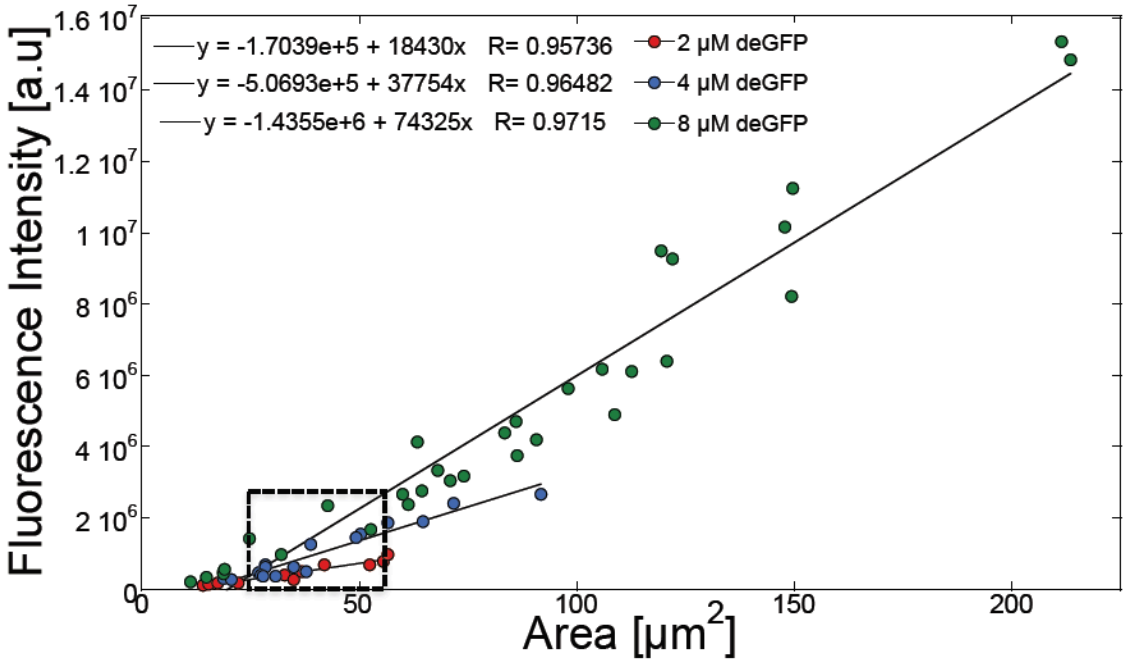

Figure 2.13 Fluorescence intensity versus area curves for different concentrations of GFP encapsulated in liposomes composed of Egg PC. Reprinted with permission from *ACS Synth. Biol.*, **2016**, *5* (4), pp. 344–355. Copyright 2016 American Chemical Society.

Using reporter proteins, we are able to quantify the protein concentration inside a liposome or emulsion droplet or localize a protein of interest. We quantify the protein concentration in liposomes much in the same way that we quantify plate reader data: by building a standard curve. Unlike in a 96-well plate, however, liposomes have variable volumes and we therefore need to control for this. First, we expressed deGFP in a TXTL reaction overnight and then cut the remaining DNA using a restriction enzyme (XhoI). The protein concentration of this treated reaction was quantified on the plate reader. This stock of deGFP was then diluted to 2, 4 and 8 μM in a blank TXTL reaction and encapsulated in liposomes. Three separate calibration curves were prepared to verify that protein concentration scales linearly with intensity (Fig. 2.12). The liposomes were analyzed and intensity vs. area curves were generated. The curves were linearly fit and their leading coefficients compared. Since protein expression in liposomes is similar to that of bulk reactions, we also verified that the intensity scaled linearly with the exposure time (data not shown). Often we study proteins that are not aqueous or do not distribute

in the vesicle uniformly, interacting in some way with the lipid container or assembling into polymers. In this case, it is useful to attach a fluorescent fusion protein to either the C or N-terminus of the protein to be studied [84]. We attach this by way of a flexible linker that ideally does not interfere with protein function. In doing so, we are able to localize non-fluorescent proteins in the lumen or at the membrane. For the case of membrane proteins, we can further characterize their location by performing a line scan on the object. This allows us to see the fluorescent intensity at a given location.

Chapter 3

The Bottom-up Approach to Synthetic Cells using TXTL

3.1 Encapsulation of TXTL

As described in the first chapter of this thesis, while there are many approaches to the formulation of a synthetic cell, I will focus on a bottom-up approach, as TXTL is a nearly ideal platform for this work. Of course, much work in the field of minimal cells is driven by the overarching and astounding goal of simulating life in the laboratory. However, some of the motivation for a functioning synthetic cell derives from the behavior of protein expression in TXTL. When measuring protein expression by fluorescence, there is an initial lag phase for 10 to 15 minutes as the DNA is transcribed and the first transcripts are translated and folded. There is then a brief period of exponential growth before a linear steady-state phase is reached. Finally, protein expression begins to slow as a saturation phase is reached before expression completely plateaus. This is not a balance of protein expression against degradation as the fluorophore are extremely stable unless tagged with degrons. This indicates that the cell-free system is only a limitless reservoir for the first 1-1.5 hours of incubation, though the machinery likely is able to work after several days [26]. These data suggest that cell-free synthesis could persist for days if an unlimited energy buffer was supplied and the dilution of toxic byproducts was carried out. Indeed, large scale, long-lived bioreactors have been tested for protein production [85].

By encapsulating TXTL in some sort of compartment, whether it be block copolymers, phospholipids, or some other amphiphile, allows for the potential to place a femtoliter scale cell-free reaction in a relatively infinite bath of resources, assuming the membrane allows some sort of permeability. In a sense, a cell-sized bioreactor is the most primitive concept of an artificial cell [86]. Encapsulation of TXTL also allows for the study of the interplay between information, metabolism, and self-organization at scales from 1-50 μm [46], [86]–[88]. Furthermore, by changing the membrane composition or the environment, we can attempt to understand how membrane specific proteins incorporate into the artificial membrane or study how particular membrane pores allow

for transport of small molecules. Even still, this does not begin to describe the excitement in undertaking such a task as building what would be deemed a living organism in the laboratory.

3.2 Introduction to the Emulsion Transfer Method

Having now detailed the capabilities and applications of the TXTL system, we can begin to discuss the actual encapsulation in a lipid bilayer. There are many different methods of encapsulation and these different methods lead to a wide size distribution. Therefore, Vesicles, used here to describe aqueous compartments bound by layers amphiphilic polymers (membranes) created in vitro, can range in diameter from a few tens of nanometers to a few tens of microns. The former are referred to as large unilamellar vesicles (LUV), while the later are known as giant unilamellar vesicles (GUV). I work almost exclusively with GUVs as the diameters correspond to those of living cells, making GUVs ideal cell-mimicking compartments to further advance fields involving their applications, specifically the artificial cell. GUVs have several advantages over LUVs. There are six orders of magnitude more molecules in a given volume so there is a smaller degree of stochastic fluctuation present in chemical reactions. They are also large enough to be analyzed via optical microscopy, useful for real time monitoring of topological changes and of reaction conditions inside. Although vesicles are a broad term, it is useful to define the nomenclature of the different types. Liposomes are formed from naturally occurring lipids, polymerosomes are composed of polymers, and surfactant vesicles are comprised of synthetic surfactants chemically different than natural lipids [89].

The first method utilized that led to the formation of GUVs was pioneer by Reeves and Dowben [90]. They deposited egg PC dissolved in a methanol/chloroform mixture via evaporation and then hydrated the lipid film with water in the presence of nitrogen. This method is known as lipid film hydration or swelling. A variation of this method applies an electric field as swelling occurs, a process known as electroswelling [5]. Neither of these processes offer encapsulation efficiencies viable to implement their use in concert with the TX-TL system. Lipid-coated ice droplet hydration, lipid-stabilized water/oil/water emulsions, small vesicle fusion, planar bilayers, and micellar solutions all

have advantages and disadvantages for specific applications but will not be discussed in this work [91]. Microfluidics have also become popular due to the control over the size distribution and the ability to rapidly generate a large number of objects [92]. As phospholipids are the main component of natural membranes, we utilize a technique that allows one to readily vary the membrane composition, a technique known as the emulsion transfer method.

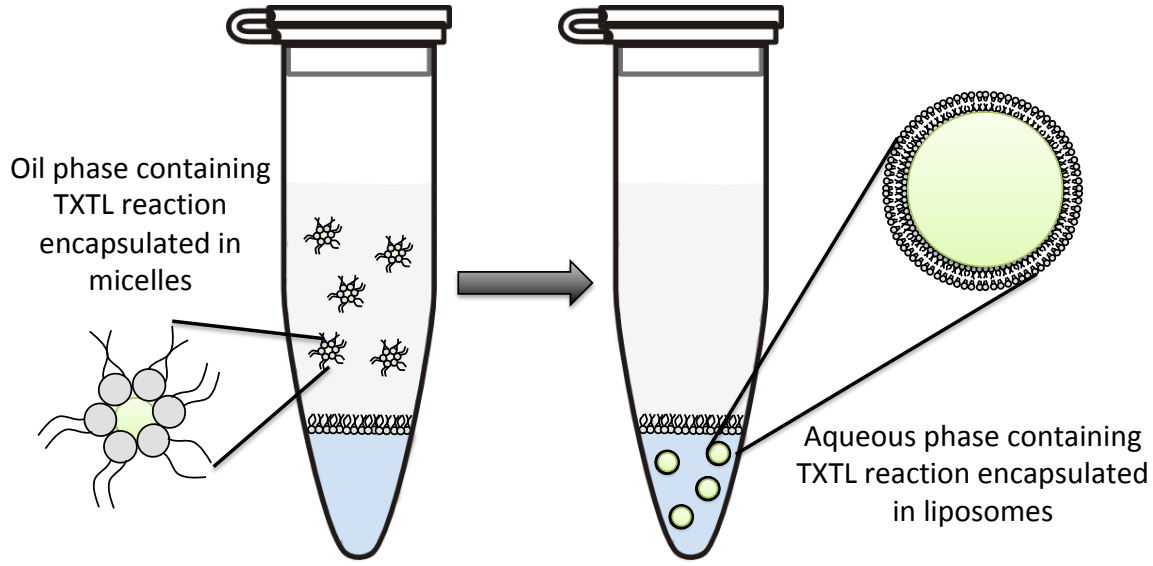

Figure 3.1 Illustration of the emulsion transfer method. Reprinted from **Methods Enzymol.** 2019; 617:217-239 with permission from Elsevier.

The emulsion transfer method for preparing phospholipid vesicles [93], shown in Figure 3.1, has been known to be a viable method to encapsulate TXTL reactions for over a decade [39]. Unlike the other methods described, it does not offer a tightly controlled size distribution, though this can be useful for studying the behavior of proteins responsible for structure or division, especially considering these proteins may function differently in vitro as opposed to in vivo. The process is conceptually simple: a water-in-oil emulsion is prepared using phospholipids as the surfactant and this solution is centrifuged into an aqueous phase [57]. The composition of the membrane and of the aqueous phase can be varied based upon the goals of the experiment. This ability will be described later on in this chapter. Below, I describe the simplest version of the protocol using

phosphatidylcholine (PC) lipids, consisting of primarily 16 and 18 length carbon chains, and a feeding solution of 300 mM glucose dissolved in a 1X PBS solution.

1) Preparation of the emulsion
    a) Dissolve dried Egg PC (Avanti #840051) in chloroform at 50 mg/ml. Store at -20 ºC for up to 3 months.
    b) To a 1.5 ml microcentrifuge tube, add 500 ml liquid paraffin.
    c) To this same microcentrifuge tube, add 15 µl of the lipid/chloroform solution, previously prepared, and vortex at max speed until the oil and lipid solution is well mixed, about 10 seconds.
    d) Evaporate the chloroform from the oil/lipid mixture by placing the microcentrifuge tube on a heat block at 50 ºC for 30 minutes.
    e) To a 7 ml flat-bottom, cylindrical vial, add 350 µl of the lipid/oil suspension. To this, add six µl of a TXTL reaction and vortex at maximum speed for five seconds to obtain the emulsion
2) Obtain the liposomes via centrifugation
    a) Add 200 µl of the emulsion atop 20 µl of a feeding solution in a 1.7 ml microcentrifuge tube.
    b) Let the biphasic solution settle such that the interface stabilizes.
    c) Centrifuge the sample at 1500 g for 10 minutes. At this point, the liposomes containing the cell-free reaction will be in the aqueous feeding solution.
    d) Remove the oil from the tube using a pipette. Once this is done, remove the aqueous phase, avoiding contaminating it with any oil.
3) This solution is ready to be incubated or observed immediately.

3.3 Membrane and Feeding Solution Composition

There are a nearly innumerable number of environments in which lift exists on earth, excluding any potentially viable environments residing in the expanse of the universe. Cellular organisms can of course exist in what we would consider optimal conditions and, indeed, humanity does mostly exist in optimal environments, though life has evolved to survive in even the most extreme environments [94]. Acidophiles and Alkaphiles span the pH range, preferring conditions with pH < 3 or > 9, respectively [95]. Thermophiles

can function in extreme temperatures, solving the issue of protein denaturation by incorporating more disulfide bonding forming cysteine amino acids [96]. There are even radioresistant extremophiles able to withstand large amounts of ionizing radiation being investigated for potential in anti-cancer drugs and sunscreen [97]. Given this incredible diversity for living systems, it is imperative that when designing a synthetic cell, it is critical that we are able to adjust the environment that we introduce our synthetic cell to. With the emulsion transfer method, we are able to readily alter both the interior solution as well as the exterior solution the cell resides. Furthermore, the composition of the phospholipid membrane can also be altered to provide functionality that the environment may demand. Since developing a synthetic cell is as much an engineering problem as it is a biology problem, we need to have precise control as the local environment dictates the function that the cell requires. For example, if our synthetic cell is introduced into a non-toxic, nutrient rich solution, it would be best to add permeability to the membrane by adding a non-specific pore such as alpha-hemolysin (AH). If the synthetic cell is intended for use in an environment that may undergo osmotic shock, it would make more sense to add a way for compartment to respond to osmotic pressure by encoding for a mechanosensitive pore like MscL. Likewise, if the environment is not conducive to stability, we would a more rigid composition of the membrane, by adding cholesterol, for example, or the cytoskeleton, by adding a protein such as MreB.

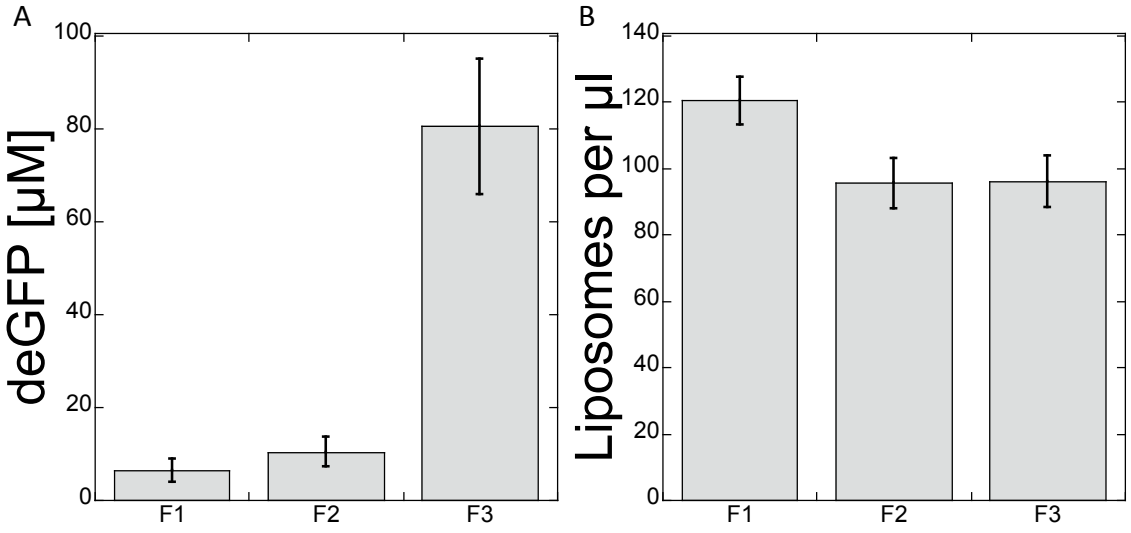

Figure 3.2 Endpoint protein expression (A) and the number of liposomes produced per μl (B) as

a function of the type of feeding solution used. 5 nM P70a-deGFP was expressed in Egg PC liposomes. Reprinted from **Methods Enzymol.** 2019; 617:217-239 with permission from Elsevier.

During the course of my thesis, I developed three unique exterior, or feeding solutions, in which to incubate liposomes [57]. Each has its own purpose and thus the use of each is dependent on the goals of the experiment as each has a significant effect on gene expression (Figure 3.3). The simplest of the three, F1, is a solution of glucose dissolved in 1X phosphate buffered saline (PBS). The PBS simulates physiological conditions where TXTL operates effectively (pH 7 -8) while the glucose can be used to balance the osmotic pressure with the interior reaction solution. The next feeding solution, F2, increases in complexity. It consists of a Tris-buffered aqueous solution of many of the reagents that make up a TXTL reaction: potassium glutamate, magnesium glutamate, maltodextrin, and polyethylene glycol. This more complex solution allows for the transfer of ions across the membrane and begins to replenish the reaction with nutrients. Lastly, the most complex solution, F3, is a mirror of a TXTL reaction with one minor difference: a buffered solution replaces the lysate. Thus, F3 includes the amino acid mixture as well as the energy buffer. It is therefore a true feeding solution, as F3 is able to provide an essentially infinite bath of amino acids and energy. In these conditions, the interior reaction efficacy is mostly limited by the buildup of toxic byproducts. Figure 3.2 shows the protein expression (A) and number of liposomes present per μl (B) for Egg PC liposomes expressing deGFP via P70a. While the greatest number of liposomes are generated using F1, there is significantly less deGFP produced relative to F3. This is due to the fact that F3 contains both the energy and amino acid mixture. The membrane is slightly permeable, as I will describe later in this chapter, and therefore some of the exterior components are able to enter the liposomes, increasing expression. This figure does show the immense benefits of having a complete feeding solution, though it is worth noting that F1 and F2 are much simpler to compile. This fact is not to be lost when considering the obstacles to entry in the field of synthetic biology. The energy and amino acid buffers can be prohibitively expensive relative to the other components but simple experiments can still be performed using only glucose and PBS.

As we control the composition of the local environment, we must also consider the interaction the synthetic cell has with that environment. Utilizing an emulsion transfer preparation, this can be done either by controlling the composition of the bilayer itself, both the lipids and the embedded proteins. Later we will consider how the proteins expressed and inserted into the bilayer effect the behavior of the synthetic cell prototype, though here we will restrict the scope to the lipid composition. As the lipid bilayer acts as the physical boundary for our synthetic cell, thus acting as the basis for self-organization, it controls the organism's ability to exchange nutrients with the cellular exterior. There is literature to suggest soluble and membrane proteins interact or respond to specific lipids, domains, or global bilayer properties [98]. Furthermore, it is well known that different lipids have different spontaneous curvatures, affecting structure, stability, and rigidity [99]. Both of these facts likely play a part in the behavior or MreB and FtsZ as these proteins anchor into the membrane or apply force to it. Other membrane proteins, and proteins with hydrophobic regions in general, require specific lipids or lipid environments to correctly fold. Likewise, particular lipids could affect transmembrane proteins by providing structural or functional support. The gating properties of MscL, for example, are affected by the bilayer composition [100]. Nearly all cells also extensively regulate the surface charge potential of the lipid bilayer as this influences headgroup packing and thus protein function [101]. Membrane fluidity, responsible for protein packing and localization, can also be influenced by simple molecules such as cholesterol [102]. This makes the makeup of the bilayer crucial.

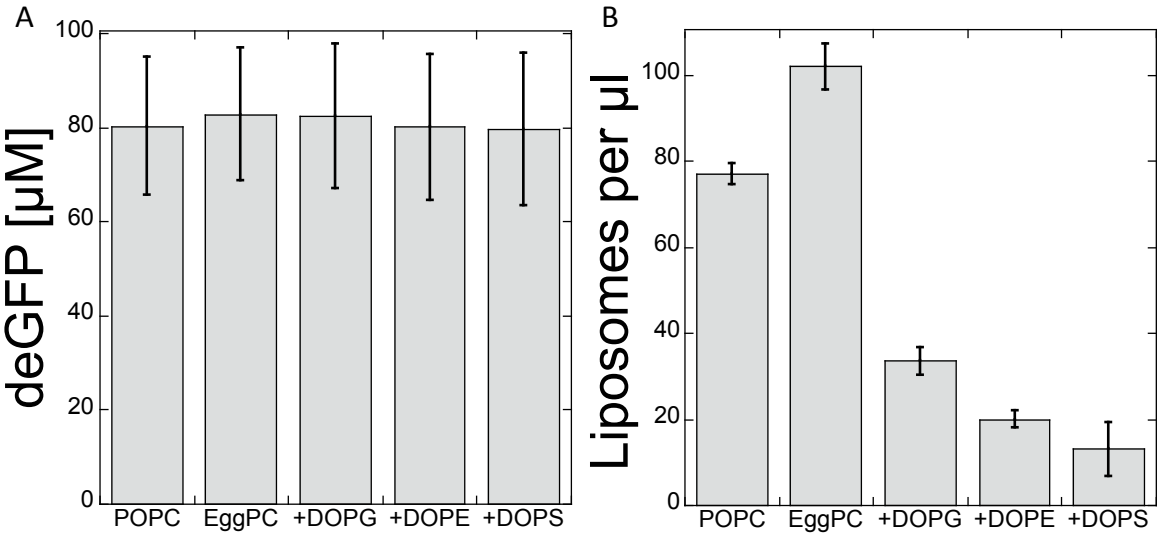

Figure 3.3 Endpoint protein expression (A) and the number of liposomes produced per μl (B) as a function of the type of lipids used. 5 nM P70a-deGFP was expressed. The mixtures are 9:1 Egg PC : DOPG, DOPE, or DOPS. Reprinted from **Methods Enzymol.** 2019; 617:217-239 with permission from Elsevier.

By using the emulsion transfer method, we have a incredible degree of control over the bilayer composition [57]. Figure 3.4 shows the amount of protein produced in liposomes (A) and the number of liposomes per μl (B) when encapsulating a TXTL reaction programmed to produce deGFP in liposomes comprised of variable lipids. The 1-palmitoyl-2-oleoyl-sn-glycero-3-phosphocholine (POPC) liposomes are composed of only POPC, while the others are mixtures of Egg PC and another pure lipid e.g. DOPG+ is 9:1 Egg PC:DOPG by molarity. The Egg PC lipids used were purchased from Avanti and are a mixture of different chain length PC lipids, though the majority chain length is 16 or 18 hydrocarbons. These lipid mixtures were chosen based upon their physiological significance. Expression of soluble proteins typically does not vary based upon membrane composition, suggesting the TXTL reaction does not interact greatly with the membrane (Fig. 3.4A). This is to be expected, as we seek to retain only cytosolic components of *E. coli* in preparation of the cell-free extract. However, the membrane composition does have a large effect on the yield of liposomes produced using this technique (Fig. 3.4B). This is to be expected as the lipid head groups vary in charge and size, causing them to pack differently, thus affecting stability. In these experiments,

nothing is done to limit non-specific protein adsorption, another factor influencing membrane stability [103]. The only change in the above protocol for preparing these liposomes is to mix in another lipid, dissolved in chloroform or another organic solvent, into the liquid paraffin. It is necessary to keep the temperature above the transition temperature of the lipid with the highest transition temperature, ensuring the lipids can randomly distribute in the oil/lipid solution. The ease of incorporating these lipid mixtures into the membrane is significant, as membranes in nature are extremely diverse [104].

While the achievement of a minimal cell with a variable membrane is a fantastical goal to aspire to, it is important to ground grand ideas such as these with real world applications. As synthetic cells have applications for drug or particle delivery, this is where we began. To do so, I tested a variety of PEGylated lipids in liposomes to see the effect on gene expression and liposome yield using the emulsion transfer method. PEG is considered the "gold standard" surface coating used to inhibit non-specific protein absorption [105], [106]. For this reason, PEGylated nanoparticles are known to improve drug or gene delivery by reducing aggregation, opsonization, and phagocytosis [107]. An excluded volume effect drive this, as PEG sterically impedes molecules from interacting, with the excluded volume effect increasing with the size of the PEG monomer [108]. We hypothesized that the introduction of PEG to the membranes of our liposomes would decrease non-specific protein absorption, increasing stability. Since the interior and exterior solutions are rich in biomolecules and proteins that have the potential to interact with the lipid head groups, we PEGylated the membrane to attempt to block this interaction.

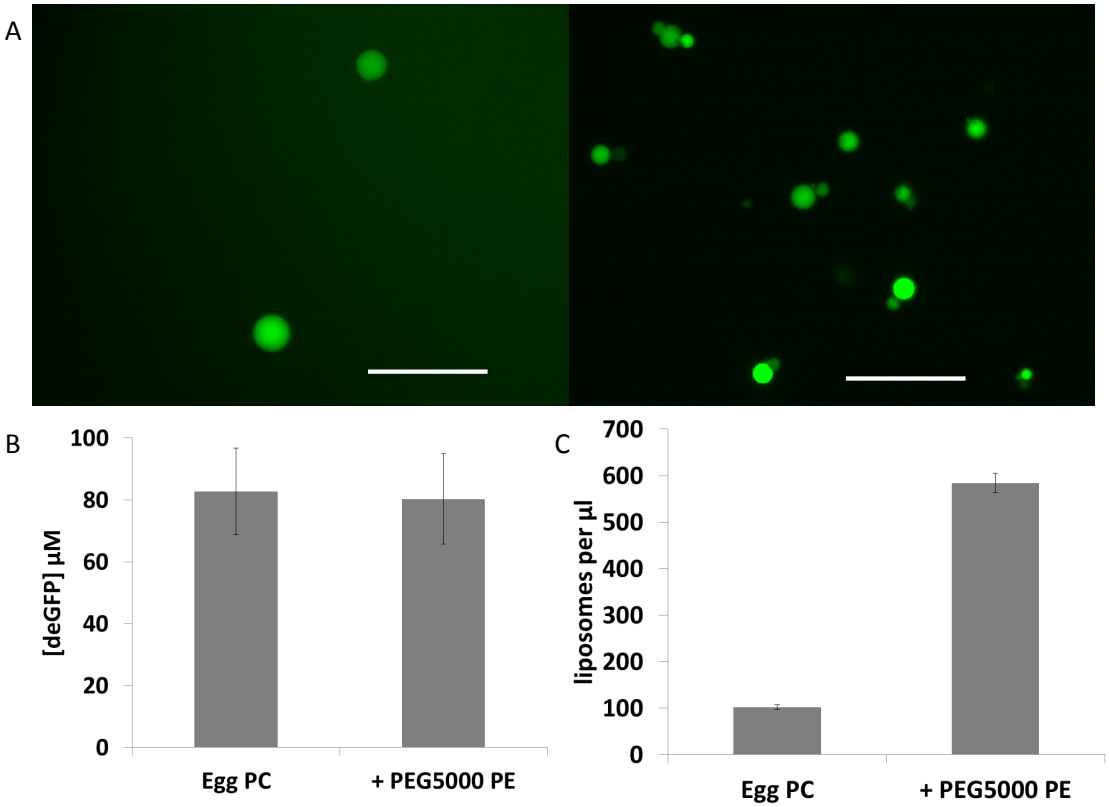

Figure 3.4 Effect of the addition of PEGylated lipids to Egg PC liposomes A) Typical 40X field of view for liposomes prepared using Egg PC (left) and Egg PC with 5% PEG5000 PE (right) expression 5 nM P70a-deGFP. B) Endpoint deGFP expression via P70a-deGFP in liposomes composed of pure Egg PC and Egg PC with 5% PEG5000 PE. Number of liposomes per µl observed for liposomes composed of pure Egg PC and Egg PC with 5% PEG5000 PE. Scale bars: 50 µm.

To test this phenomenon, I choose physiologically relevant, PEGylated lipids, 16:0 PEGn PE, where 16:0 is the length of each chain, n is the number of monomers is the PEG oligomer, and PE is the head group, phosphatidylethanolamine. By adding only 5% 16:0 PEG5000 PE to Egg PC liposomes, I found that we could dramatically increase the number of liposomes produced in a single preparation while maintaining the same level of protein expression (Fig. 3.4). Figure 3.4A shows the visual representation of a typical field of view using a 40X lens, while this is quantified in Figure 3.4C. Incredibly, by PEGylating the membrane, I was able to increase the yield of the emulsion transfer method nearly 8-fold. While PEGylated lipids with monomer chains of 550, 1000, 2000, and 5000 were tested, only PEG5000 had such a significant effect on liposome yield.

However, none of these lipids affected gene expression (Fig. 3.4B). These data suggest membrane composition plays a critical role in membrane-protein interaction in vitro, and that PEGylation can be used in a synthetic cell environment to achieve similar effects as those seen in vivo. This discovery also bridges the gap between the emulsion transfer method and microfluidics in the sense that it allows one to prepare a population large enough for meaningful statistical analysis. Furthermore, this development creates a liposome volume density large enough sufficient to begin to study synthetic cell communication. Consider two populations of liposomes, one of which is coated with an agonist and the other with the associated receptor. The solutions containing these populations could be mixed and the PEGylated liposomes, having sufficient volume density, would regularly come in contact. Figure 3.5 below is a simple proof of concept of such an experiment. Two separate TXTL reactions, one expressing mmCherry and the other deCFP, were encapsulated in liposomes composed of 19:1 Egg PC: 16:0 PEG5000 PE. These two populations were then mixed by gently pipetting them before being observed via fluorescence microscopy. As can be seen, the two populations spontaneously come into contact, providing a simple experimental platform to investigate intracellular communication, molecular diffusion, or surface protein binding.

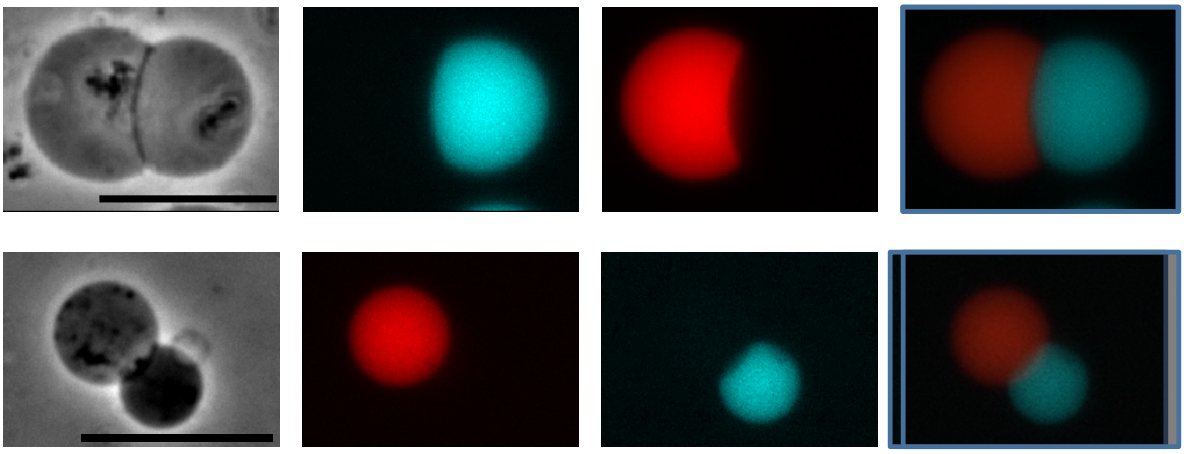

Figure 3.5 Liposomes expressing deCFP and mmCherry in contact with one another after mixing two distinct solutions. Scale bars: 10 μm

3.4 Encapsulation of Non-genetic Components

The encapsulation of components is an aspect of synthetic cells that is largely driven by drug delivery applications [109], [110]. In the simplest sense, if treatment by a specific

chemical requires a critical concentration of that chemical to be effective, as all drug treatments require, then the technique to deliver that drug to a localized region must be able to ensure that it is hitting that critical concentration. If that delivery method relies on the encapsulation of a chemical inside liposomes, it is imperative to understand how effective the encapsulation technique is. More fundamentally for the purposes of a synthetic cell, we need to know if bulk conditions can be translated into a lipid container when conceptualizing a functional synthetic cell. I studied the encapsulation efficiency of the emulsion transfer technique with respect to the components most critical to TXTL: small molecules, larger proteins, and DNA. The energy and amino acid buffers contain many small cofactors and substrates necessary for transcription and translation. To study this encapsulation, I used a fluorescently tagged version of the nucleoside UTP. The lysate itself supplies the larger TXTL machinery, such as the RNA polymerase and ribosomes, and we simulate the encapsulation of these components using varying sizes of TRITC-Dextran. To look at the encapsulation of genetic material, I used a DNA labeling kit to prepare fluorescent plasmid DNA.

To assess the emulsion transfer technique's ability to encapsulate complex reactions, I compared the fluorescence intensity of the liposomes against its area. Since the size of the population is not uniform, this allows us to ascertain how the concentration of the chemical scales with the size of the object. If the intensity versus area curves scale linearly, we can conclude that the concentration is uniform across all sizes. Further, by comparing the intensity versus area curves of varying concentrations, we can investigate how the intensity scales with concentration.

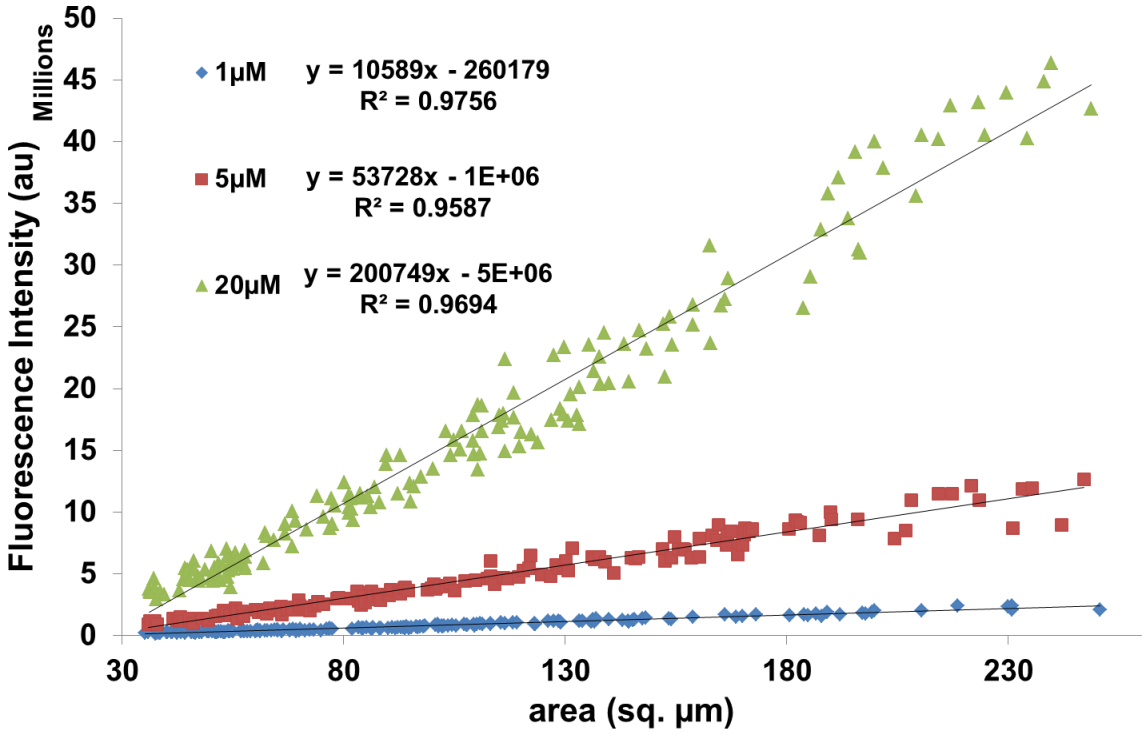

Figure 3.6 Intensity versus area curves for liposomes containing varying concentrations of UTP-FITC. Fit equations represent a linear fit.

Figure 3.6 shows the total intensity versus liposome area curves for 1, 5, and 20 μM UTP-FITC encapsulated into liposomes prepared using 19:1 Egg PC: PEG5000 PE. The data was fit linearly, with the fit equation and R-squared value given on the plot. A regression analysis was performed on the data, where the R-squared value represents the percentage of the variation in the data that can be explained by the linear model. The R-squared > 0.95 indicate the encapsulation of the nucleoside scales linearly with the area of the liposome. In other words, the concentration of the molecule inside the liposome is independent of its size. Examining the leading coefficients of the trend lines, we see an increase in intensity that is expected based upon the increase in concentration i.e. we would expect the total intensity to increase by a factor of five from 1 μM to 5 μM, and the data yields an increase of ~5.3. The same scaling can be seen between 1 and 20 μM as well as 5 and 20 μM. This suggests that when using the emulsion transfer technique, the concentration inside the liposomes is directly proportional to that which is encapsulated.

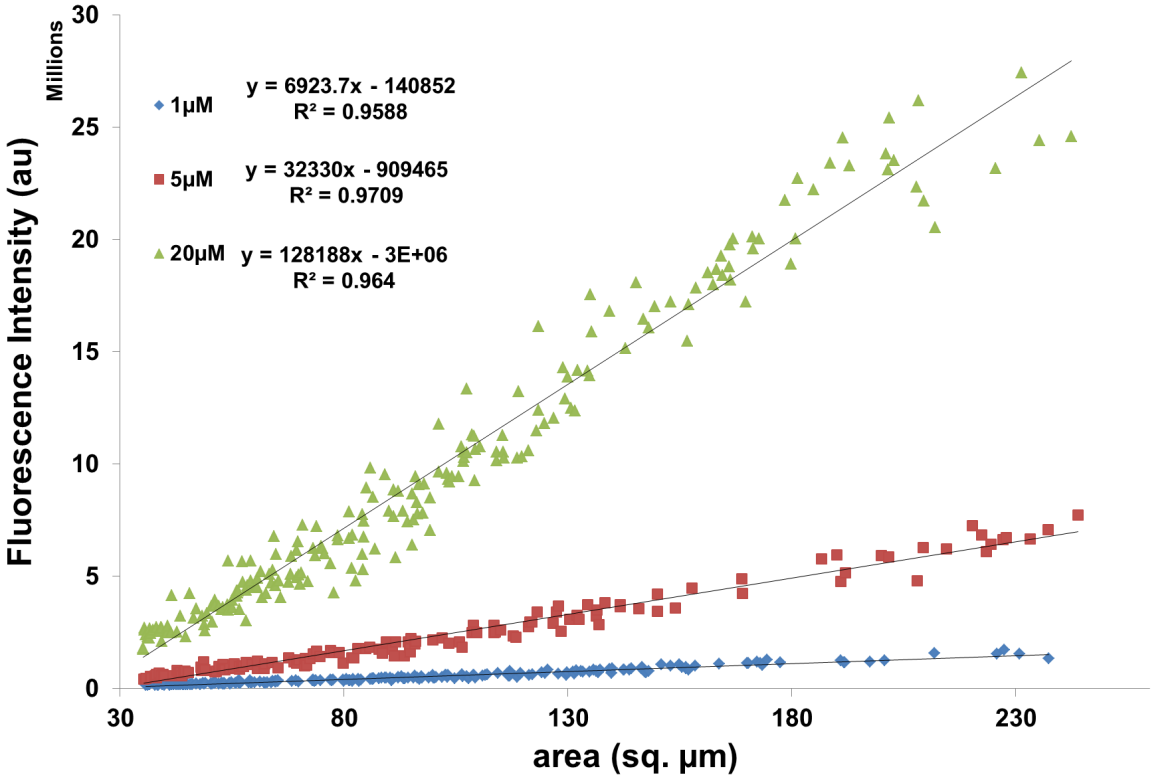

Figure 3.7 Intensity versus area curves for liposomes containing varying concentrations of 3 kDa TRITC-Dextran. Fit equations represent a linear fit.

To examine the encapsulation of larger molecules, I encapsulated various size TRITC-Dextran molecules, again at 1, 5, and 20 μM. Specifically, I looked at 3, 10, and 70 kDa dextran molecules. Figure 3.7 displays the encapsulation of 1, 5, and 20 μM of 3 kDa TRITC-Dextran. Similarly to UTP, the encapsulation of 3 kDa dextran scales linearly with the size of the liposome and with the concentration encapsulated.

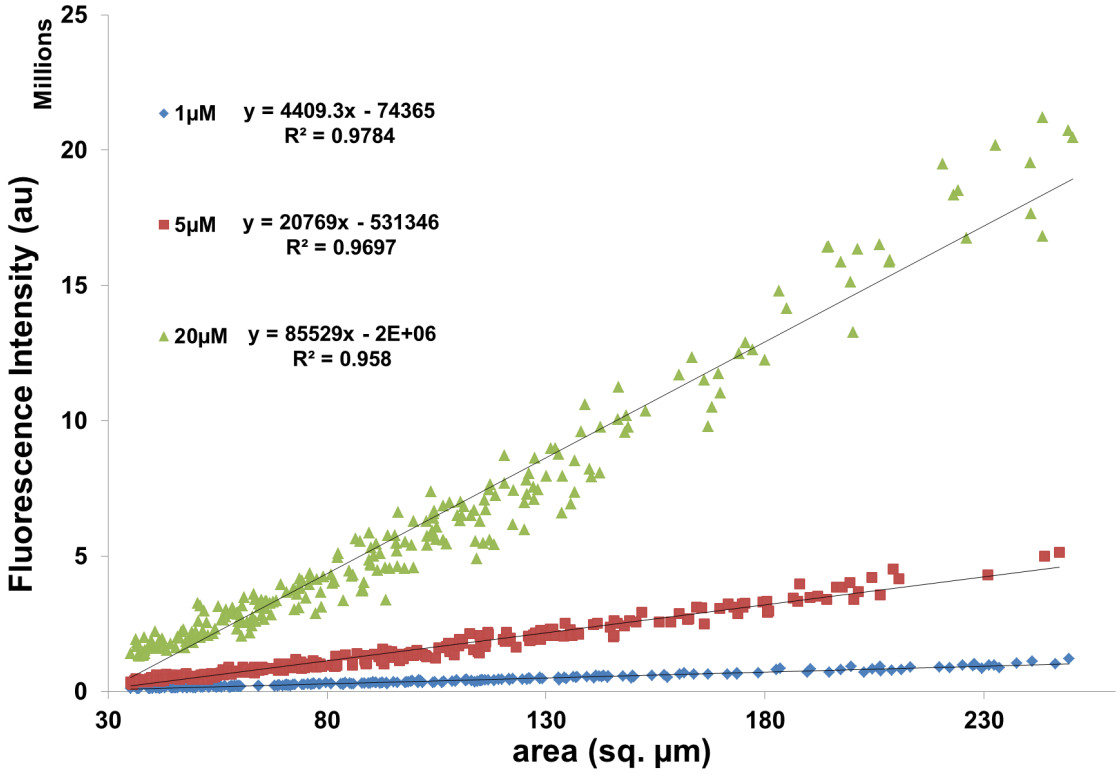

Figure 3.8 Intensity versus area curves for liposomes containing varying concentrations of 10 kDa TRITC-Dextran. Fit equations represent a linear fit.

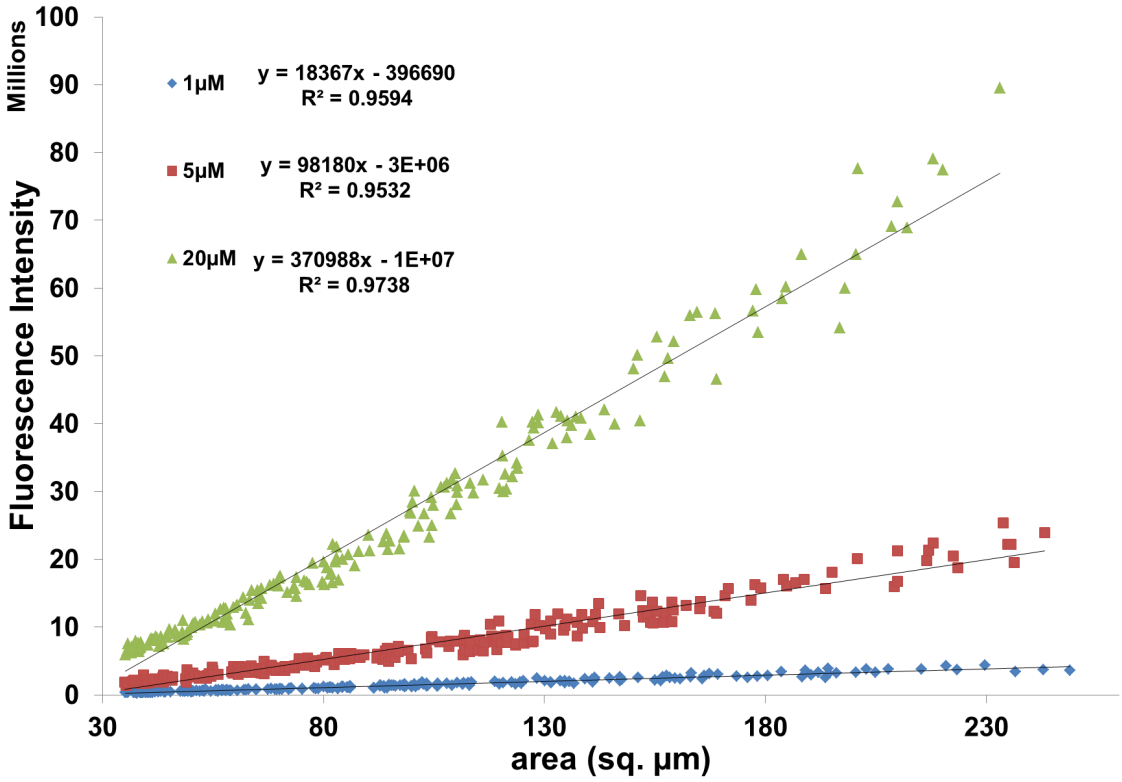

Figure 3.9 Intensity versus area curves for liposomes containing varying concentrations of 70 kDa TRITC-Dextran. Fit equations represent a linear fit.

Figures 3.8 and 3.9 show the encapsulation of 10 and 70 kDa TRITC-Dextran, respectively. Like with UTP and the 3 kDa polymer, the larger dextran polymers are distributed uniformly across the population of liposomes and the concentration in the liposome is directly proportional to the concentration in the reaction before encapsulation. These data further suggest that the emulsion transfer method is a suitable platform towards developing synthetic cells. TXTL reactions are sensitive to the concentrations of molecular components and it is thus imperative that the bulk reaction conditions can be transferred into liposomes to make any quantitative claims about the behavior of TXTL inside liposomes.

3.5 DNA Encapsulation and the Impact on Gene Expression

The data presented in section 3.4 suggests that the encapsulation of the TX and TL machinery, as well as the metabolic components, are uniformly distributed in liposomes prepared using the emulsion transfer method. Indeed, the concentration of these

components can be adjusted inside the liposomes simply by adjusting the concentration in the TXTL reaction that is being encapsulated. This is a powerful result, as the different cascades have different settings. However, these reaction cascades and circuits also rely on specific DNA stoichiometry between several different plasmids. The DNA concentration is also the most important component in terms of the protein output based on a TXTL input (e.g. the DNA is amplified by a factor of ~10000 for P70a-deGFP). For a synthetic cell that is programmed with DNA to encode a certain protein phenotype, then, we must have precise control over the concentration of DNA inside the liposome, both in terms of relative concentration between reactions and a uniform distribution between liposomes of different sizes. To measure this, I labeled plasmid DNA, P70a-deGFP specifically, and encapsulated it into PEG-modified liposomes at varying concentrations (Fig. 3.10). I again created total intensity versus area curves to investigate the relationship between concentration and area. Immediately apparent is the striking difference in concentration uniformity with respect to liposome area at DNA concentrations below 5 nM. While 1 or 2 nM [DNA] seems very low, this is the typical working concentration for most reactions, with many of the sigma factor plasmids being used at < 0.5 nM. However, at 5 and 20 nM, the R-squared values are again above 0.95, indicating the linear model explains over 95% of the variation in the data. The scaling between concentrations for the labeled DNA is also not as close between actual and expected values as the other components were. This suggests that the DNA concentration encapsulated in the liposomes cannot be assumed to be exactly the same as in TXTL reaction to which it originated. This is most likely due to the concentration of the DNA being 1000X smaller than that of the proteins or nucleotides in the reaction, as any small variations in the concentration of DNA is significantly amplified.

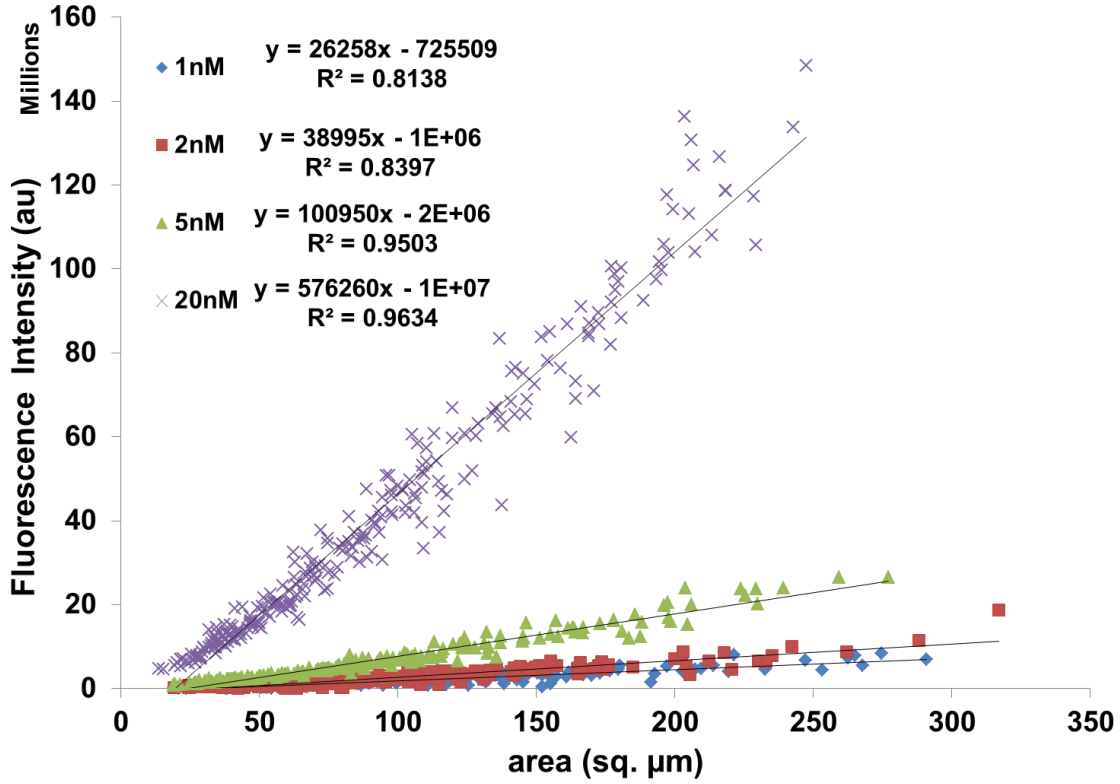

Figure 3.10 Intensity versus area curves for liposomes containing varying concentrations of fluorescently labeled P70a-deGFP plasmid DNA. Fit equations represent a linear fit.

Since the end goal of encapsulating TXTL reactions into liposomes is to program them to express functional proteins, I next looked at the protein output relative to the DNA input. In order to assess how multiple genes are expressed relative to their initial stoichiometry, I used mmCherry and deCFP, two reporter proteins with no spectral overlap (data not shown). Considering that a synthetic cell would likely need a large number of expressed proteins to function, these plasmids, both using the P70a promoter, were encapsulated separately and together at 1, 5, and 20 nM. Figure 3.11 shows the fluorescence intensity of both expressed deCFP (Fig. 3.11A) and mmCherry (Fig. 3.11B) against liposome area.

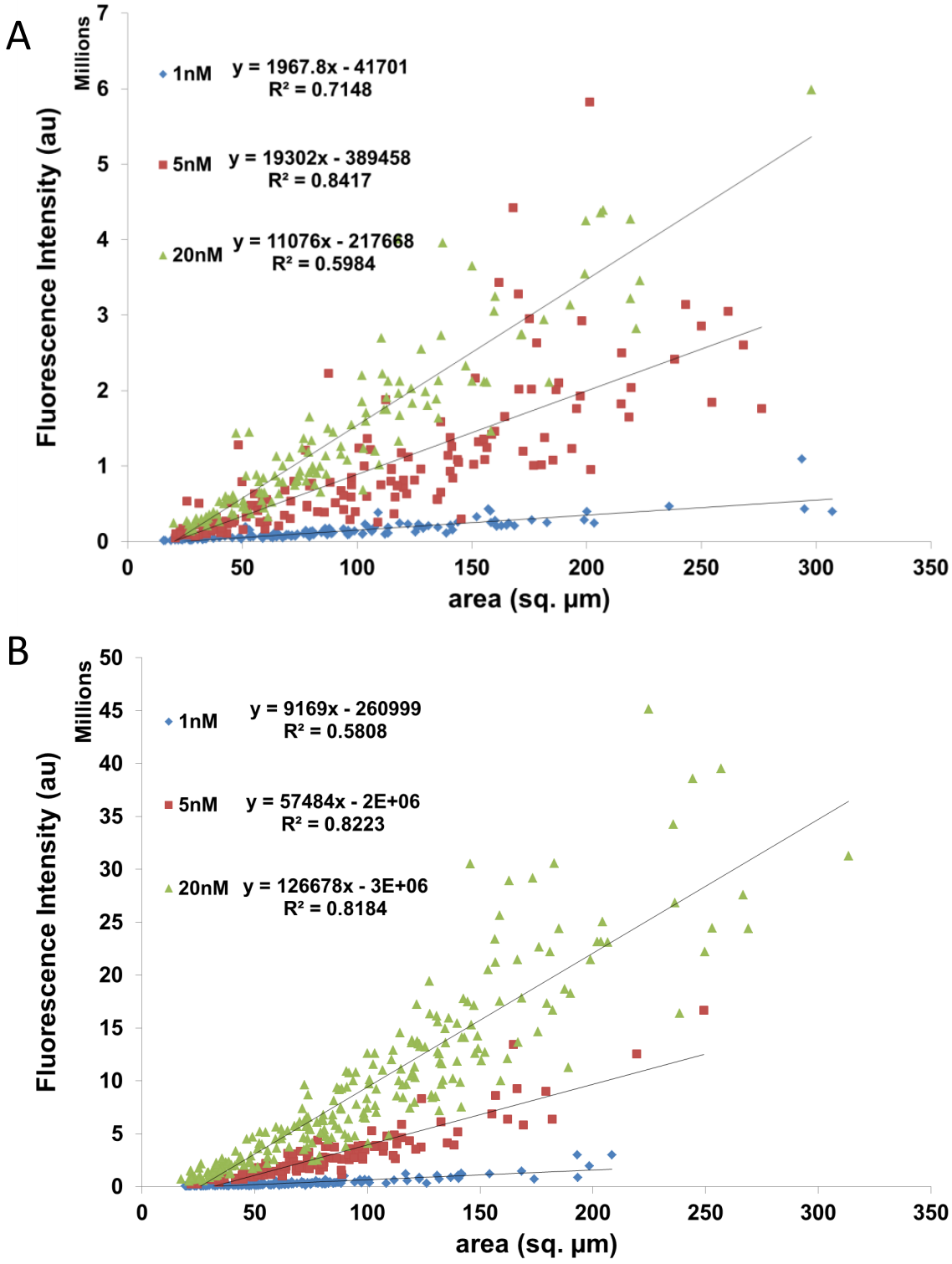

Figure 3.11 Intensity of expressed deCFP (A) and mmCherry (B) versus area curves for liposomes containing a TXTL reaction expressing either P70a-deCFP or P70a-mmCherry. Fit equations represent a linear fit.

All liposomes were prepared using the emulsion transfer method with a 19 : 1 mix of Egg PC : 16:0 PEG5000 PE. The first thing to note is that even at 20 nM of plasmid, the R-squared values are < 0.85, indicating that the expressed protein concentration is not uniformly distributed between liposomes of various areas, even though the encapsulation of the reaction components is. This can likely be explained by the fact that the protein expression output is a function of the encapsulation of all of the other components, each of which have some variance, however small, and thus the variance in the expression is greater. The data does indicate, though, that the protein expression becomes more uniform as the concentration of plasmid DNA increase, suggesting that the DNA encapsulation plays the biggest role in the variance. The leading coefficients do not scale with the plasmid concentration, though this makes sense, as the batch mode reactions do not scale linearly between 1 and 5 nM, 1 and 20 nM, or 5 and 20 nM. It is important to note here that both the encapsulation of P70a-mmCherry and P70a-deCFP lead to similar behavior between the fluorescence and liposome area. This suggests that the plasmids encapsulate in the same way, and that there is enough sequence similarity to compare their encapsulation. The absolute intensities of each reporter are arbitrary, so it is not important that mmCherry is roughly 10 times brighter than deCFP.

To understand how the protein expression of a two-plasmid system depends on DNA concentration, I co-encapsulated P70a-deCFP and P70-mmCherry, measuring the fluorescence intensities of each reporter via their respective filter on the microscope. Figure 3.12A shows the intensity versus area curves for the encapsulation of 1, 5 and 20 nM P70a-deCFP, while the same data set is shown for P70a-mmCherry in Figure 3.12B. Note that the plasmid concentrations were fixed against the other i.e. the 1 nM data means that 1 nM of each plasmid was encapsulated, for a total of 2 nM total DNA. In both plots, we notice that the R-squared values increase with increasing DNA concentration, suggesting the protein concentration is constant in relation to the liposome area as the DNA concentration is increased. However, looking at the data points and the leading coefficients, we see that the intensity and thus protein expression is weaker when 20 nM of each plasmid are encapsulated compared to when 5 nM of each are

encapsulated. This can be explained by considering the total DNA concentration, 40 nM. At such a high concentration, the translational machinery becomes saturated and we therefore waste resources on the production of mRNA that cannot be translated quickly enough.

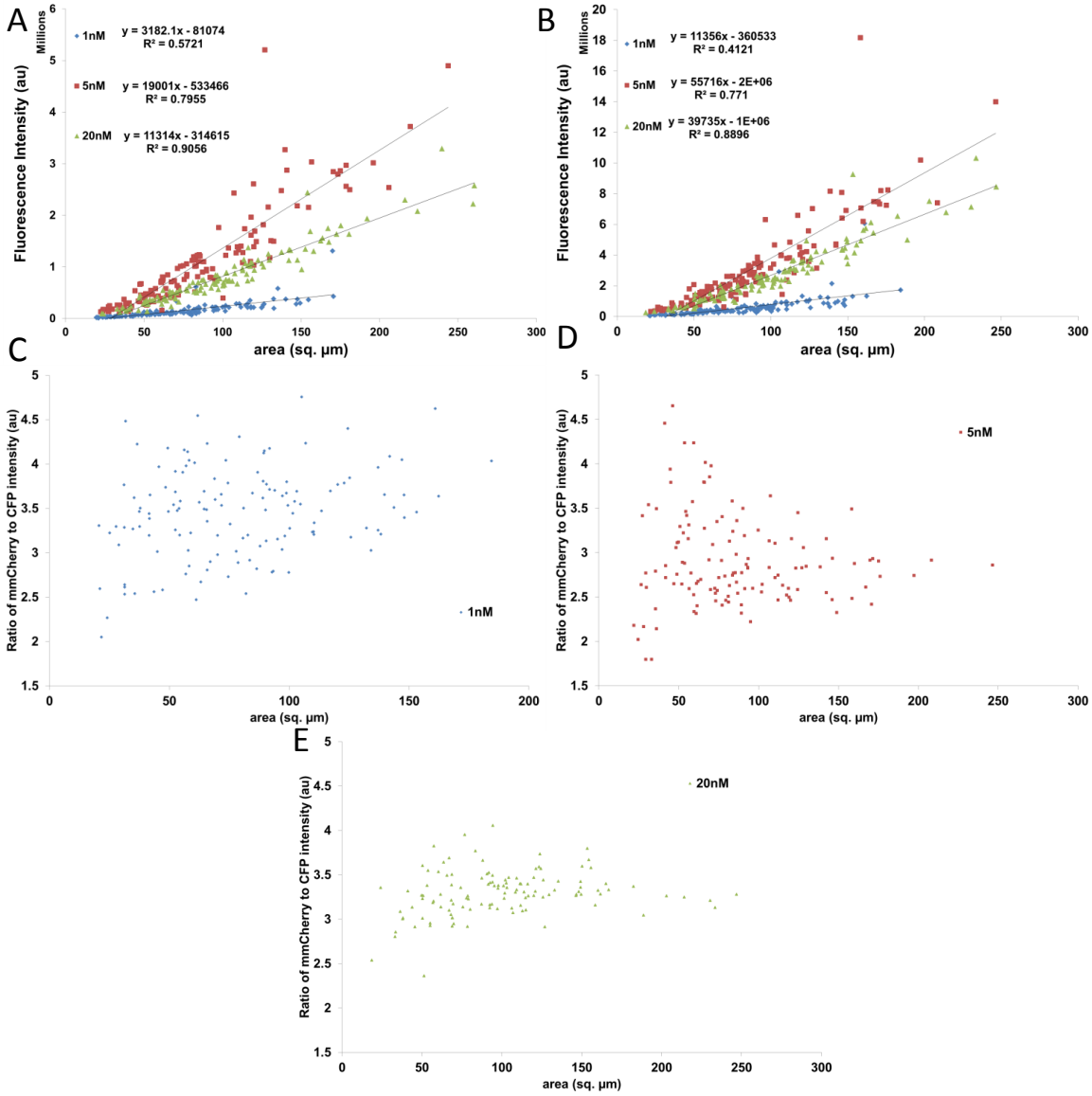

Figure 3.12 Intensity of expressed deCFP (A) and mmCherry (B) versus area curves for liposomes containing a TXTL reaction expressing both P70a-deCFP and P70a-mmCherry. Fit equations represent a linear fit. The ratios of mmCherry to deCFP intensity at a given area with 1, 5, and 20 nM plasmid DNA is plotted in C, D, and E, respectively.

Figure 3.12C-E shows the ratio of mmCherry intensity to deCFP intensity versus the liposome area for encapsulation of 1, 5, and 20 nM of each plasmid. This data gives a rough estimation of the protein stoichiometry given the DNA input. If all data points converge to a constant value, it would suggest that equal concentrations of mmCherry and deCFP are expressed in the reaction. As the DNA concentration is increased, the spread of data points converges towards the ratio of 3. The data also indicates that at smaller liposome volume, there is a higher amount of variance in the expression of one protein to the other. This would indicate that to express equal parts of the two plasmids, we must encapsulate so much DNA that we actually depress protein expression. This is obviously not an optimal solution for the purposes of a synthetic cell, as many proteins would need to be efficiently expressed, suggesting that a mix of plasmids expressing individual proteins is not an ideal solution.

To overcome this problem, I cloned two distinct plasmids. One of them, P70a-deCFP-UTR1-mmCherry, is a transcriptional fusion protein. This means that there is a single promoter site, but two distinct untranslated regions (UTR) and thus to ribosome binding sites. The other construct put each gene, deCFP and mmCherry, under the control of it's own promoter. This two-promoter plasmid was named P70a-deCFP-P70a-mmCherry. Ideally, each of these plasmids would offer equal stoichiometric proportions of deCFP and mmCherry when encapsulated with TXTL reactions in liposomes.

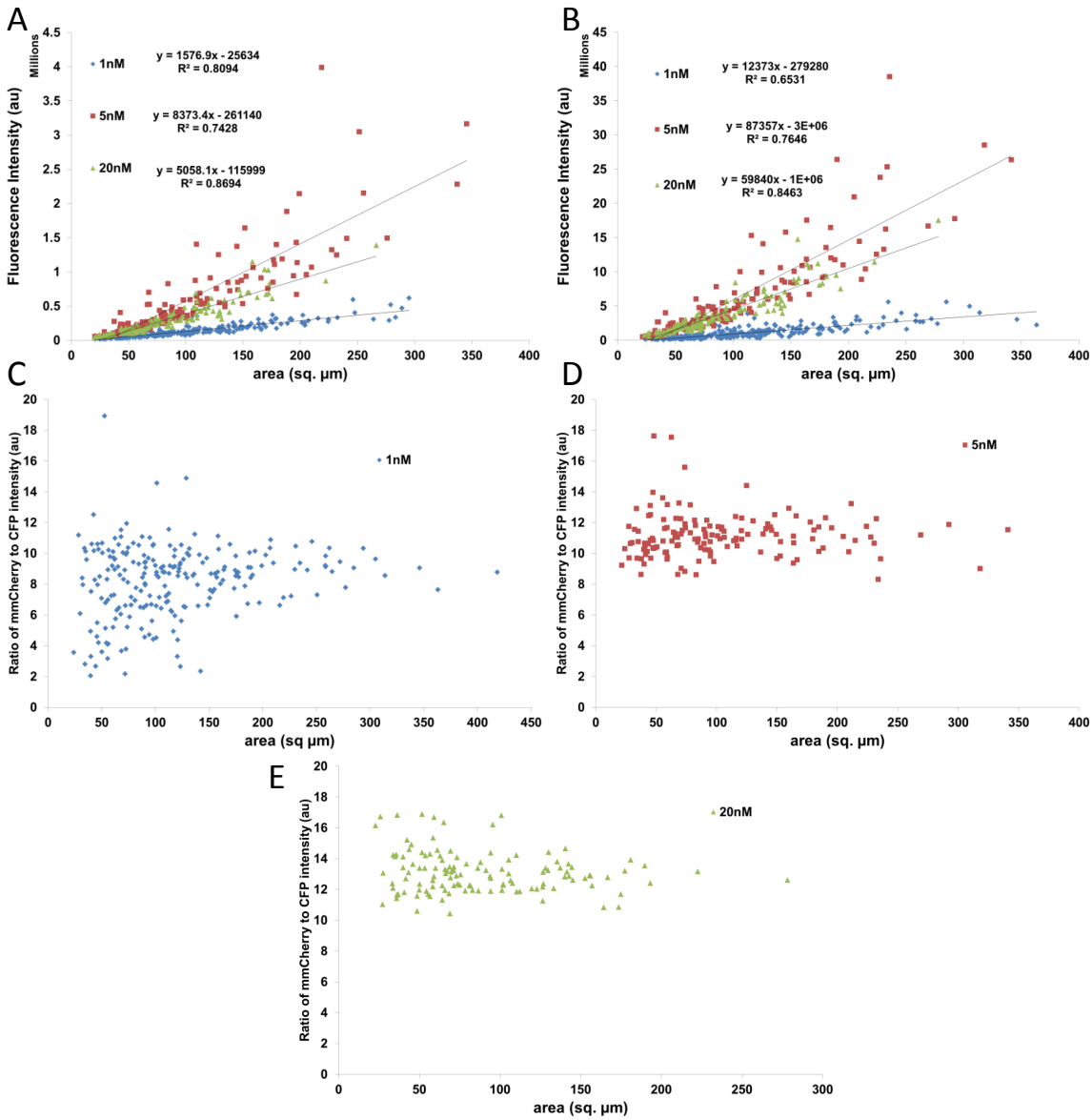

Figure 3.13 Intensity of expressed deCFP (A) and mmCherry (B) versus area curves for liposomes containing a TXTL reaction expressing P70a-deCFP-UTR1-mmCherry. Fit equations represent a linear fit. The ratios of mmCherry to deCFP intensity at a given area with 1, 5, and 20 nM plasmid DNA is plotted in C, D, and E, respectively.

Figure 3.13 shows the encapsulation data for the TX fusion plasmid expressing both mmCherry and deCFP. Figure 3.13A displays the deCFP intensity versus area curves, while Figure 3.13B shows the same plots for mmCherry. Similar to the two-plasmid experiments, these plots show an increasing concentration uniformity with respect to liposome area as the DNA concentration is increased. We also note a slight decrease in

the protein expression at 20 nM versus 5 nM, though it is less pronounced than in the two-plasmid experiments. However, looking at the ratio in concentrations of mmCherry to deCFP in Figure 3.13C-E, the TX fusion plasmid exhibits a noticeable decrease in the spread of liposomes around a constant value of 10-12, even at 1 nM. Again, the variance in smaller liposomes is significantly higher, even at 20 nM.

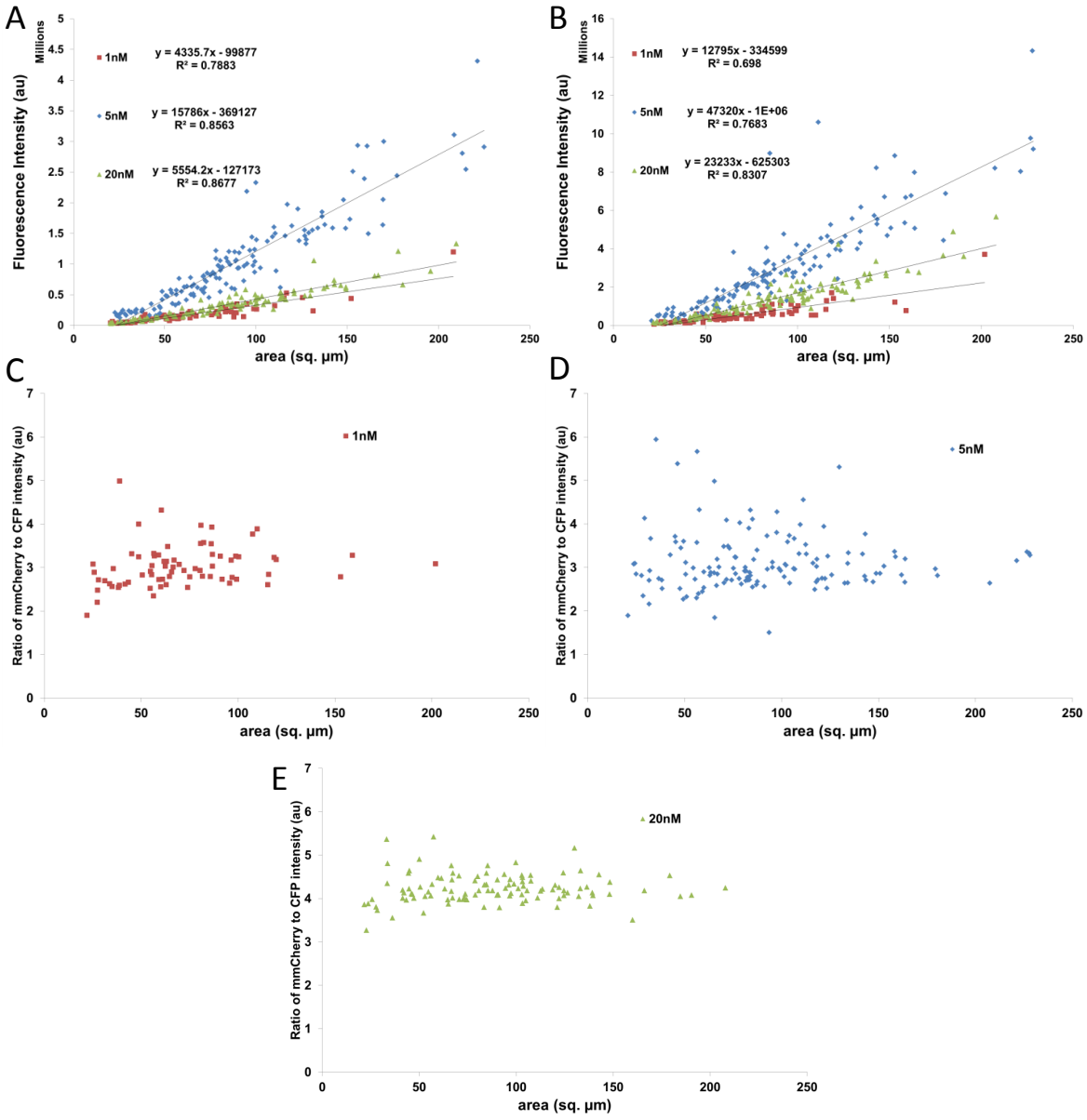

Figure 3.14 Intensity of expressed deCFP (A) and mmCherry (B) versus area curves for liposomes containing a TXTL reaction expressing P70a-deCFP-P70a-mmCherry. Fit equations represent a linear fit. The ratios of mmCherry to deCFP intensity at a given area with 1, 5, and 20 nM plasmid DNA is plotted in C, D, and E, respectively.

Figure 3.14 shows the encapsulation data for the two-promoter plasmid expressing both mmCherry and deCFP. Figure 3.14A displays the deCFP intensity versus area curves, while Figure 3.14B shows the same plots for mmCherry. Similar to the two-plasmid and TX fusion plasmid experiments, these plots show an increasing degree of uniformity in protein concentration with respect to liposome area as the DNA concentration is increased. The decrease in the protein expression at 20 nM versus 5 nM is higher than in both the two-plasmid system or in the TX fusion experiments. This is explained by the fact that the two-promoter plasmid continues to overexpress mRNA like the two-plasmid reactions, while there is also now potential that the binding of one of the promoter sites may inhibit the binding efficiency of the other promoter. As observed with the TX fusion plasmid, Figures 3.14C-E suggest that the concentrations of the two proteins in relation to one another are constant at lower concentrations, evidenced by the decrease in the spread of points around a ratio of 4.

Taken together, these data indicate that a synthetic cell system that requires precise protein stoichiometry would require genes to be under the control of a minimum number of operons. It is important to note that this applies only to the emulsion transfer method, and that swelling or microfluidic techniques could yield different results. Here, I have looked only at the co-encapsulation of two plasmids, though it is easy to extrapolate based upon the data that three or more plasmids would have even higher variance in their relative expression. Many of the genetic cascades used to express toxic genes, MscL, for example, require the production of a specific protein stoichiometry, indicating even primitive synthetic cells encapsulating something as simple as a σ28 cascade should be optimized with regards to DNA concentrations in both bulk and encapsulation reactions. Though it is possible to achieve uniform protein expression relative to liposome area by encapsulating > 10 nM DNA, multi-gene systems would likely see adverse effects on gene expression with such high concentrations of DNA.

Chapter 4

Synthetic Cell Cytoskeleton of Structure and Division

4.1 Reconstitution of the FtsZ Divisome

Cytokinesis is the process by which a single cell splits into two daughter cells. A macromolecular machine known as a divisome mediates this process in bacteria [89]. In *E. coli*, the divisome is a ring of protein subunits that work to contract the cell membrane known as a Z ring. The major cytoskeletal protein that forms this ring is FtsZ, a GTPase (383 aa, 40.2 kDa) [111]. FtsZ is composed of two independently folding subunits that polymerize head to tail by way of GTP [112]. In vivo, the concentration of FtsZ is between 4-10 μM. The protein was first imaged using immunoelectron microscopy in 1991 by Bi and Lutkenhaus; they provided evidence in was a cytoskeleton protein localized in a ring at the cell center [113], [114]. Nearly five years later, immunofluorescence light microscopy reveled FtsZ is present at nearly all cell centers, not only those undergoing division [115]. This discovery was confirmed using FtsZ labeled with GFP, also finding that the labeled division was functional as long as there remained three times as much wild type FtsZ than labeled FtsZ [116]. Using cells with a doubling time of 40 minutes, the Z ring appears 15% of the way through the cell cycle with constriction occurring at roughly 50% [117]. Though there is a high degree of variation between FtsZ in different strands of e. coil, the last 9-17 amino acids are highly conserved among bacteria assembling Z rings. This sequence is of particular importance as it the peptide sequence responsible for binding to the membrane via other proteins. The ring forms under the inner cell membrane at the cell center in cylindrical *E. coli* cells, with FtsZ being tethered by two membrane binding proteins, FtsA (420 aa, 48 kDa) and ZipA (328 aa, 36.3 kDa), which bind at the conserved C-terminal peptide. Though both proteins can be used to tether the ring simultaneously, only one or the other is needed for ring formation [118], [119]. ZipA is composed of a transmembrane anchor, a long, basic arm rich in proline and glutamine and a large, globular C-terminal domain. It is dispersed through the inner membrane until the onset of division when it is recruited to assemble the Z ring [120]. Unlike ZipA, FtsA is widely conserved in bacteria. This indicates FtsA

is the more essential of the two and indeed, with a gain of function mutation, FtsA can facilitate division without ZipA [121]–[123]. FtsZ has a structure similar to actin with a C-terminal peptide that forms an amphipathic helix that inserts into the lipid bilayer. It is maintained in *E. coli* at a 1:5 ratio in regards to FtsZ [124]. This ratio is critical for cell division in vivo.

To this point, FtsZ membrane studies in vitro have been performed using purified proteins. In 2013, Cabre et al studied the effect of FtsZ polymerization in the absence and presence of ZipA [125], [126]. FtsZ was encapsulated in unilamellar vesicles containing α-hemolysin pores. Upon the introduction of GTP into the exterior solution, FtsZ was observed to polymerize. With the same conditions but with ZipA in the membrane, the vesicles were seen to shrink and even collapse upon the introduction of GTP. However, the vesicles did not divide. A similar experiment was done by Osawa and Erickson using FtsA and a FtsZ mutant with a membrane targeting amphiphilic helix (mts) [127]. They first encapsulated a reaction solution containing FtsZ-YFP-mts and found contraction at the inner surface of the membrane in the form of Z rings. These were observed as outer protrusions on the membrane equator and fluorescent rings with a hollow center when viewed en face. Tubular vesicles, obtained by mixing the vesicle solution with agarose, also displayed Z rings contracting to a point below the resolution of light microscopy (<250 nm), but no division. Using wild type FtsZ and wild type FtsA, nothing useful was observed. This is consistent with the idea that wild type FtsA from *E. coli* is difficult to work with in vitro [128]. Using a mutant of wild type FtsA, FtsA*, more interesting results were obtained. FtsA* is the gain of function allele that bypasses the need for ZipA [129]. First, note that no significant structure was observed in the absence of GTP, consistent with previous experiments, and that no Z rings were seen without ATP as it is required for FtsA assembly [130]. However, in the presence of ATP, GTP, and with equimolar concentrations of FtsZ and FtsA*, Z rings, contraction, and complete division was observed in a small fraction of vesicles.

I cloned two genes from *E. coli* strain K12, FtsA and ZipA. I currently have five plasmids with which to construct a divisome, all under a Sigma 28 cascade: P28a-FtsZ, P28a-FtsZ-eGFP-mts, P28a-FtsZ-eGFP, P28a-FtsA, and P28a-ZipA. Using fluorescence

microscopy, I have encapsulated the plasmids in liposomes and observed them after overnight incubation and during their expression during kinetic experiments. Doing so, I have been able to further understand the relationship between the proteins in vitro using FtsZ tagged with eGFP as a proxy for FtsZ location. On it's own, FtsZ forms filaments in vitro when encapsulated. They are not organized in any appreciable direction and do not curve around the bilayer membrane. With the addition of FtsA, there is a phenotypic change in the liposome population. In a small percentage (<5%) of liposomes there is minor deformation, possibly due to Z-ring contraction. A similar effect is seen with FtsZ and ZipA coexpression. When FtsZ, FtsA and ZipA are all encapsulated together, there is again a higher degree of organization to the point where the deformation of individual liposomes is more common (5-20%).

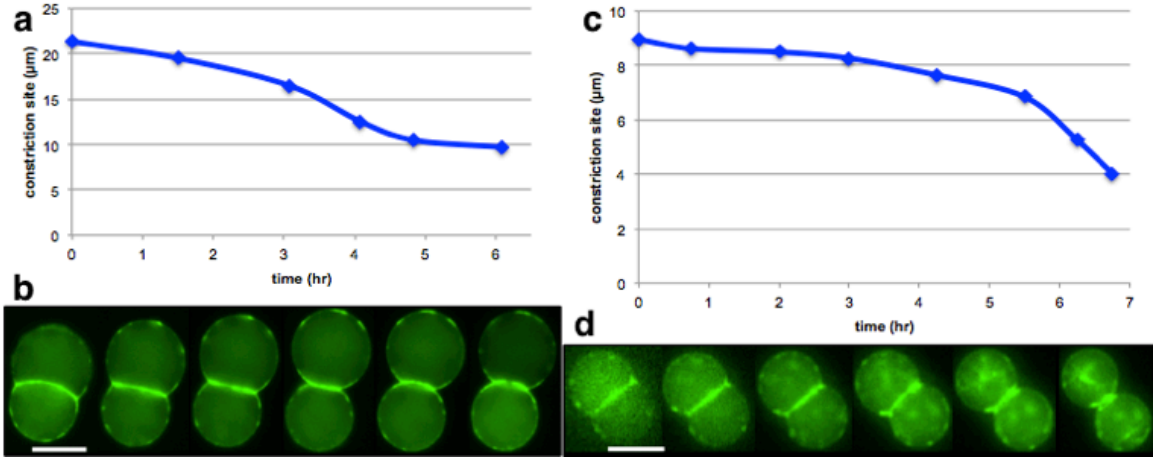

Figure 4.1 Two constriction events in initially fused liposomes containing FtsZ, FtsA, and ZipA. (a) Plot of the contour length of the constriction site versus time corresponding to (b). (b) Visualization of the liposome constricting at the point of fusion. (c) Plot of the contour length of the constriction site versus time corresponding to (d). (d) Visualization of the liposome constricting at the point of fusion. Scales bars correspond to 10 µm.

Most notably, with all three plasmids present, contraction is observed when two liposomes start out fused together (Fig. 4.1). This suggests that these contraction events need a point where symmetry is broken to overcome membrane tension and cause contraction.

However, this data proved to be inconclusive once a series of control experiments were carried. The constriction events exhibited by Fig. 4.1 was exciting, and we therefore

rushed to confirm that this constriction was indeed a result of an FtsZ constriction ring. I began by exploring different mixtures of FtsZ, FtsA, and ZipA, in an effort to see if ZipA, FtsA, or both was necessary for constriction. Experiments were performed by encapsulating TXTL reactions in liposomes programmed to express some combination of the three proteins of interest and tracking a sample of the population over time from the onset of encapsulation (t = 0 hr) to the endpoint of expression (t = 16 hr). I found with no FtsA or ZipA expressed, similar constriction events to those in Fig. 3.7 occurred. I then performed the same experiment while expressing deGFP alone, in the absence of any plasmids encoding for the divisome proteins, and observed the similar constriction events. Finally, I performed the experiment encapsulating a TXTL reaction with no DNA information and found that constriction occurred in liposomes as well (data not shown). At this point, I suspected that either the divisome proteins were proteins in the lysate or that when two liposomes begin as a single, compressed aggregate, it is energetically favorable for them to maximize the contact between the nonpolar head groups and the external solution. To test this, I encapsulated TXTL reactions with a diluted extract, both 50 and 25% of the typical extract volume corresponding to 15 and 7.5 µl of lysate, respectively. Fig. 3.8 shows brightfield microscopy images of liposomes containing a 50% (Fig. 4.2a) and 25% extract volume (Fig. 4.2b) taken upon encapsulation and after 18 hours of incubation.

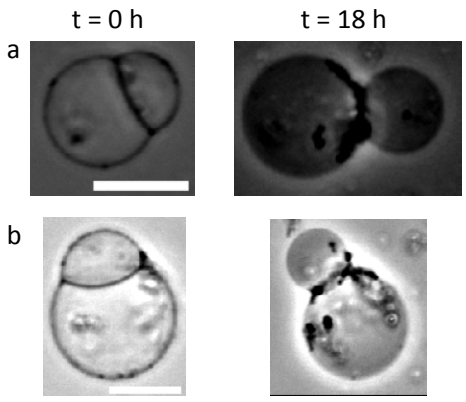

Figure 4.2 Observed constriction events in liposomes containing no plasmid DNA and 50 (a) or 25% (b) extract volume Scale bar: 10 µM

These data suggest that even with a decrease in the lysate concentration, there is still some force driving constriction. Further experiments were carried out in the absence of an active lysate and similar behavior as that in Figures 4.1 and 4.2 was observed (data not

shown). This indicates that these constriction events are entirely due to an entropic force acting on the aggregated liposomes.

It is possible that the liposomes need to be deformed to a different shape such that an FtsZ z-ring has the force necessary to cause constriction. *E. coli* is a rod-shaped bacterium, and the free energy required to collapse a cylinder is less than that of a sphere. I attempted to accomplish this via the incorporation of MreB, though, as I will describe in the next section, this was ultimately unsuccessful. A dividing synthetic cell remains an incredible challenge. Indeed, it is necessary as replication cannot take place without the initial division, and this does not consider the segregation of genetic material into potential daughter cells. However, TXTL does seem a viable platform to express the FtsZ divisome, as all of the proteins are well expressed in our system. This suggests that other methods of encapsulation, perhaps microfluidics to make a cylindrical object or a sonication technique that would yield smaller liposomes, would be beneficial. Likewise, the composition of the membrane could be altered to increase its fluidity and thus decrease its resistance to deformation. The emulsion transfer technique allows for such flexibility, though I did not utilize techniques to measure membrane rigidity.

4.2 Deformation of Liposomes in the Presence of MreB

Cellular shape and structure in *E. coli*, though extremely important for purposes of division and robustness, is not entirely understood. However, there has been a great deal of recent work shedding light on cytoskeletal proteins likely responsible for these critical functions [131], [132]. There are four proteins currently known to influence the shape of *E. coli*. MreB (347 aa, 37 kDa) is the main cytoskeleton protein, a prokaryotic actin homologue that assembles into helical filaments under the cell surface. In vivo, MreB helical and ring filament structures are formed by interacting with the membrane proteins MreC (367 aa, 39.5 kDa) and MreD (162 aa, 18.8 kDa) at the inner membrane [133], [134]. Even more recently, RodZ (337 aa, 36.1 kDa) was identified as an important transmembrane component of the cytoskeleton. Loss of RodZ leads to misassembly of MreB into non-spiral structures, and a consequent loss of cell shape [135], [136]. There is supporting evidence suggesting RodZ is responsible for cell length in regards to MreB cytoskeleton [137]. With the deletion of MreB components in vivo, not only are the

filaments absent, but the cells are often spherical and thus unable to divide using the FtsZ ring. They are also prone to lysing, suggesting the MreB cytoskeleton is necessary for cellular robustness. As these proteins have only recently been identified and isolated, the in vitro work regarding them is still young in its development. In vitro, MreB monomers from *E. coli* polymerize into thin and short nanofilaments of 100nm in length and 1nm in diameter. [138] MreB has been observed to aggregate with protein concentrations above 5 μM while polymerization rate and stability increases with lower salt concentration [139]. Most notably, Noireaux et al saw MreB cytoskeleton develop in liposomes in the presence of MreC, both expressed by a TX-TL system [140].

I began by cloning the genes corresponding to MreB, MreC, MreD, and RodZ into plasmids with robust gene expression. These genetic sequences were obtained from *E. coli* strain K12 via polymerase chain reaction. I then designed and cloned plasmids expressing MreB, MreC, and MreD fusion proteins. Upon beginning encapsulation experiments, I noticed filamentation and deformation when only expressing MreB (Fig. 3.9), with an increase in deformation proportional to the amount of MreB expressed. The filamentation of MreB was also evident and concentrated at the membrane. This was inconsistent with the literature, which indicates that MreB needs the other complimentary proteins to anchor to and interact with the membrane. I did not, however, observe any rod-shaped liposomes when MreB was expressed. I was also not able to obtain a significant change in the phenotype with any combination of MreB, MreC, MreD, or RodZ versus MreB alone. It is possible that MreB behaves differently in this specific TXTL environment as opposed in vivo or other in vitro done in other labs. It is also possible that there is a high concentration of MreC, MreD, or RodZ in the lysate and therefore, when MreB is overexpressed, there is enough of the sister proteins to see deformation. Given the potential issue of the energy barrier being to high for FtsZ to overcome for division, I attempted to encapsulate the FtsZ mix with the MreB mix. Given this combination, I did not see filamentation or deformation, likely due to the load on the system.

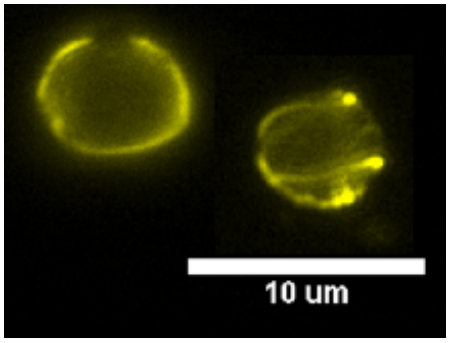

Figure 4.3 Liposomes containing MreB, MreC, MreD and RodZ. The fusion protein visualized is MreB-venus. The liposomes, separately, show examples of deformation of the liposome shape and filamentation of the MreB cytoskeleton.

4.3 DNA Nanotube Stability in TXTL for a Cytoskeleton Homologue

DNA nanotechnology is, like TXTL, a rapidly growing field that uses DNA not as a means to store and transfer genetic information, but to assemble structural motifs from the well understood properties of DNA folding and assembly [141]. It is of particular interest to my work as synthetic DNA can be designed to fold into nanoscale structures. These two-dimensional or three-dimensional structures can be designed for specific tasks, like drug delivery, intracellular scaffolding, or, most pertinent to my purposes, synthetic-cell design [142]–[146]. The diversity of DNA nanostructures is incredibly high and this versatility is certainly one of the benefits of working with the material, as highlighted in the literature [141]. During my PhD, I collaborated with researchers from UC Riverside's Mechanical Engineering department to engineer DNA nanotubes to be used in TXTL. DNA nanostructures are not generally compatible with living systems, and as such TXTL systems could be a useful platform for prototyping.

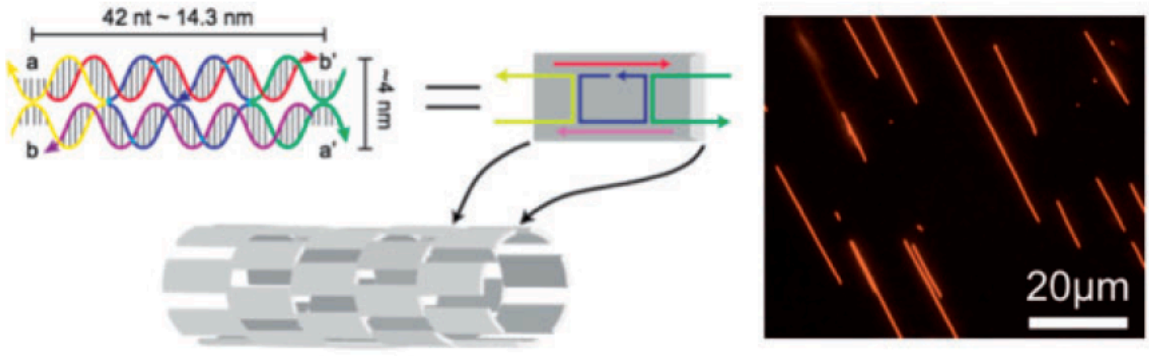

Figure 4.4 DNA nanotubes self-assemble from tiles composed of 5 ssDNA oligomers. At right, a representative microscopy image of nanotubes labeled with Cy 3 in TAE buffer. The DNA

nanotubes are adhered to the coverslip for optimal imaging. Reprinted from *Synthetic Biology*, Volume 3, Issue 1, 2018, ysy001 with permission from Oxford University Press.

We worked with synthetic-DNA nanotubes whose geometry and mechanical properties are close to actin filaments and microtubules [142]. These properties drove the majority of my interests as it suggests nanotubes could serve as an artificial cytoskeleton for synthetic cells, operating as scaffolds to localize or actively transport components and influence cell morphology. These structures can also be fluorescently tagged, making them easily observable via epifluorescence microscopy, allowing easy characterization (Fig 4.4). Using TXTL as a mimetic cytoplasm, we engineered DNA nanotubes to better withstand physiological conditions, including linear DNA degradation via the RecBCD complex found in *E. coli* [147], [148]. To study these structures we used both fluorescence anisotropy and epifluorescence microscopy on bulk TXTL reactions.

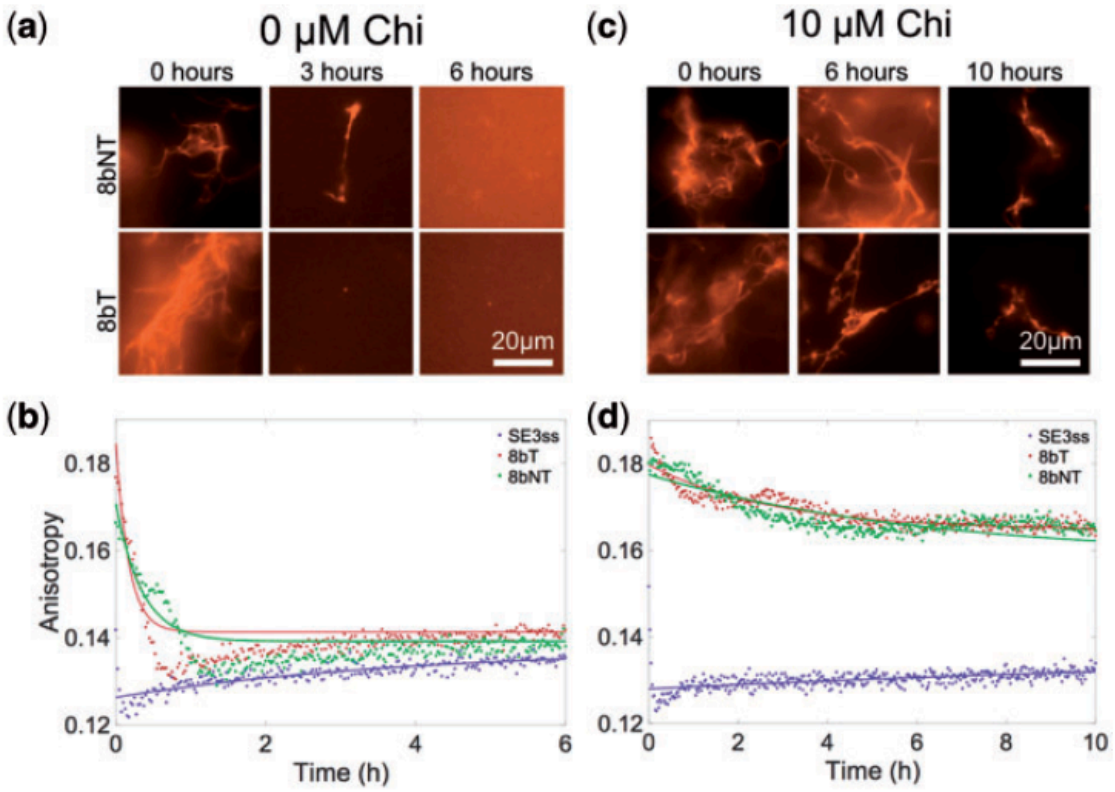

Figure 4.5 Fluorescence microscopy images (a and c) and fluorescence anisotropy measurements (b and d) for DNA nanotubes composed of 8bT and 8bNT tiles in 0 μM (a and b) and 10 μM (c and d) Chi6. Reprinted from *Synthetic Biology*, Volume 3, Issue 1, 2018, ysy001 with permission from Oxford University Press.

We investigated the potential of altering the oligonucleotide strands that make up the nanotubes to increase their resilience, and thus their lifetime, in the *E. coli* cell-free extract. The 8 base variants of DNA nanotubes degraded within hours upon addition into TXTL reactions (Fig. 4.5a). To monitor this degradation kinetically, we labeled the nanotubes with Cy3 (Ex/Em 540/590 nm) and used fluorescence anisotropy. This method uses fluorescence polarization to gain information about the rotational diffusion of molecules. Fluorescence anisotropy is calculated as $r = (I_{parallel} - I_{perpendicular})/(I_{total})$, where the parallel and perpendicular polarization are measured by the plate reader. Conceptually, larger molecules rotate more slowly and thus have higher anisotropy signals as the measured light will be more likely to be in a parallel polarization, as the excited dipole does not have time to rotate out of phase. Applying this logic to the DNA nanotubes, this means that their degradation will result in a decrease in the fluorescence anisotropy signal. I confirmed that in the buffer the nanotubes are most stable in, TAE, there is no significant change in anisotropy, assuming poly-T ssDNA is used to inhibit DNA adsorption (data not shown). Therefore, anisotropy data were fitted using an exponential decay model. The first nanotubes we tested were 8-base (8bT) sticky ended DNA nanotubes were designed with (8bT) and without (8bNT) short single stranded (toehold) domains on one of the sticky ends (Fig. 4.5). The degradation seen via fluorescence microscopy was verified via anisotropy. The anisotropy value decreases immediately, indicating the DNA nanotubes begin degrading within 5 minutes upon addition to a TXTL reaction (Fig. 4.5b). As expected, the nanotubes with no toehold region (8bNT) were more robust than those with the toehold domain as evidenced by the microscopy data. This is likely due to the toehold region giving RecBCD easier access to initiate degradation.

5-base (5bT) and 8-base (8bT) sticky ended DNA nanotubes were designed with (5bT, 8bT) and without (5bNT, 8bNT) short toehold domains on one of the sticky ends (Fig. 4.6a). This was done to understand how the length of the sticky ends affected nanotube stability, as well as the effect of the inclusion of additional binding regions. Increasing the sticky end length increases the melting temperature of the structures. Of

these four designs, both 8b nanotubes outlast the 5b nanotubes at room temperature and 29 °C. At room temperature, ~22 °C, the 8b tubes degrade in under 3 h (data not shown), significantly longer than the 5b tubes, which both degrade in under an hour. At 29 °C, degradation occurs even more readily, with the 8bNT nanotubes lasting under 3 hours and the rest of the variants degrading within an hour. Given what I knew about the Chi sequence's effect on DNA degradation in TXTL, we hypothesized that its inclusion would increase nanotube stability. At room temperature and with 10 µM Chi6, the 8b variants last up to 10 hours (Fig. 4.5c). Interestingly, the anisotropy data indicate that there might be aggregates present, not visible to microscopy, since the values for the 8b nanotubes do not converge in the presence or absence of Chi6 dsDNA

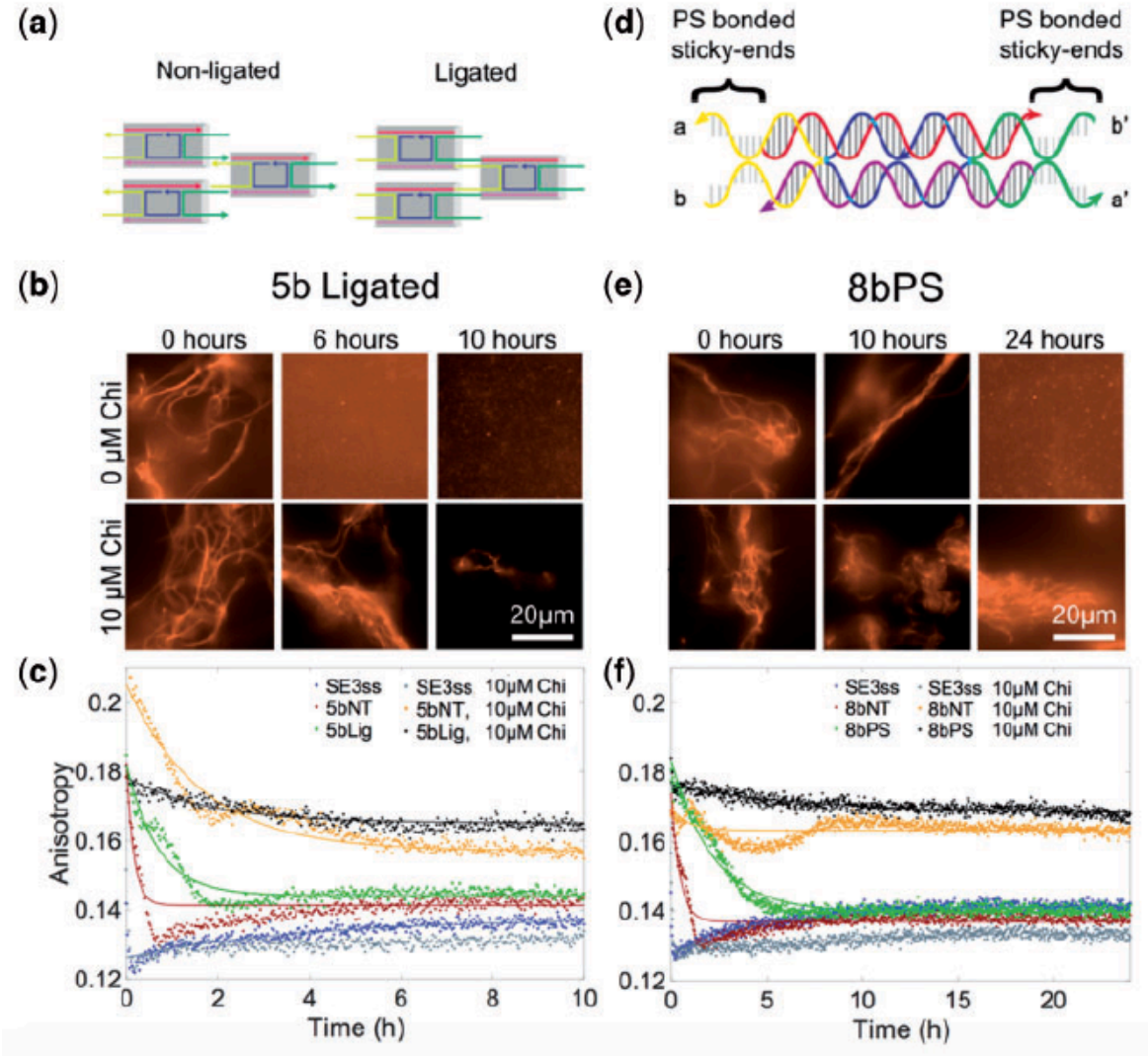

Figure 4.6 Enhancing DNA nanotube stability using ligation or phosphorothioation. (a) Cartoon of ligation. (b) Fluorescence microscopy images of 5b ligated tubes in TXTL at room temperature with 0 or 10 μM Chi6 dsDNA. (c) Fluorescence anisotropy assay of the 5bNT and 5bLig nanotubes with 0 and 10 μM Chi6 dsDNA. (d) Cartoon of phosphorothioation. (e) Fluorescence microscopy images of the 8bPS tubes in TXTL at room temperature with 0 or 10 μM Chi6 dsDNA. (f) Fluorescence anisotropy assay of the 8bNT and 8bPS nanotubes with 0 and 10 μM Chi6 dsDNA. Reprinted from *Synthetic Biology*, Volume 3, Issue 1, 2018, ysy001 with permission from Oxford University Press.

Next, we investigated the effect of chemical modifications to the tiles making up the nanotubes themselves. As robustness is known to improve under environmental stress in response to ligation, the tubes were ligated to seal breaks in the sugar-phosphate backbone (Fig. 4.6a) [149]. The data obtained from both microscopy experiments and fluorescence anisotropy measurements suggest that ligation does indeed improve nanotube robustness in TXTL (Fig. 4.6b, c). Another modification we made was to introduce phosphorothioate bonds in place of standard phosphodiester bonds, as some nucleases are inhibited by PS bonded DNA [150]. We chose to add PS bonds to the 8bNT nanotube design as these were the most robust in TXTL (Fig. 4.6d). The phosphorothioation of the bonds increased the nanotube lifetime by more than double, verified by both microscopy and anisotropy (Fig. 4.6e, f). The 8bPS nanotubes lasted over 10 hours without Chi6 dsDNA, and this lifetime increased to over 24 hours in the presence of the oligonucleotide.

To conclude, we find that DNA nanotubes degrade rapidly in a TXTL environment. This degradation is highly influenced by Chi6 dsDNA, with this oligo increasing the lifetime substantially. This suggests RecBCD is the major exonuclease present in the extract, which we suspected all along. DNA nanotube robustness can also be greatly improved by modifying the tiles that make up the nanotubes, with phosphorothioation having a greater effect than ligation. Increasing the length of the sticky ends also increased nanotube lifetime, and removing toehold overhangs enhanced this increase. This work demonstrates that TXTL is a viable experimental platform to test the robustness of DNA nanostructures in a mimetic cytoplasmic environment. This gives researchers the ability to engineer nanostructures with longer lifetimes and test their

characteristics in a semi-cellular environment. This work also validates TXTL as a tool to rapidly prototype DNA nanostructures in vitro.

Chapter 5

Engineering a Capable Membrane

5.1 Liposome Membrane Permeability Using TXTL

The main function of the membrane in a living cell or an idealized synthetic cell is that of a physical barrier between the cytoplasmic interior and the environment. Of course, the membranes of living cells have a plethora of other functions including cell adhesion, ion conductivity, and cell signaling. However, acting as a boundary provides the cell protection by controlling what exterior molecules or objects can interact with the cellular interior. For a synthetic cell driven via TXTL, the membrane carries the same importance, as TXTL is sensitive to the chemical conditions. Further, gene circuits can be activated or repressed using small molecules. Previously, it was established that Egg PC liposomes prepared using the emulsion transfer method are permeable to exterior melibiose [151]. I choose to investigate the permeability of the liposome membrane to external IPTG, a molecular mimic to allolactose that sequesters the repressor LacI. To do so, I encapsulated reactions programmed to express deGFP by way of the synthetic regulatory promoter, PL-LacO1. To repress this operator, I also encapsulated PL-TetO1-LacI to produce the repressor [70]. Therefore, deGFP would only be measured if IPTG was present to sequester LacI. In order to increase or decrease membrane permeability, I altered the composition of the lipid bilayer.

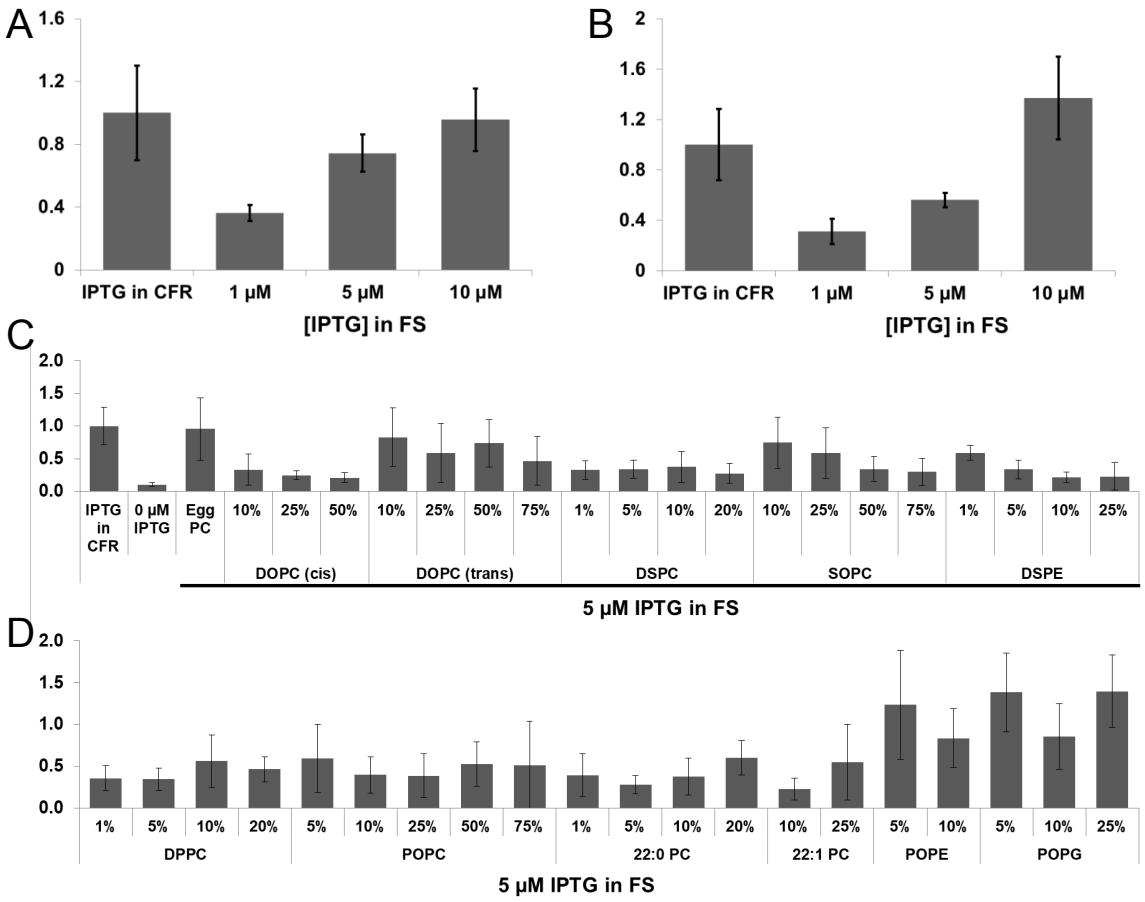

Figure 5.1 Membrane permeability to IPTG (A) Endpoint deGFP expression in Egg PC liposomes as a function of exterior IPTG concentration, normalized to the positive control where IPTG is encapsulated with the reaction. (B) Endpoint deGFP expression in 4:1 Egg PC:Cholesterol liposomes as a function of exterior IPTG concentration, normalized to the positive control where IPTG is encapsulated with the reaction. (C) and (D) Endpoint deGFP expression as a function of membrane composition normalized to the positive control where IPTG is encapsulated with the reaction. All liposomes contain 1 nM PL-LacO1-deGFP and 3 nM PL-TetO1-LacI.

Figure 5.1 displays the results of an extensive study into the permeability of liposomes to external IPTG with respect to IPTG concentration and lipid composition. The vertical axis in all plots represents the deGFP concentration normalized to the concentration in the positive control where IPTG is encapsulated along with the cell-free reaction (CFR). Thus, the case of IPTG in CFR is normalized to 1. All of the lipids were purchased from Avanti. Liposomes composed of purely Egg PC were permeable to external IPTG, with the activity of the circuit increasing as the concentration of IPTG

increase (Fig. 5.1A). As cholesterol is known to reduce membrane fluidity, I prepared liposomes composed of four parts Egg PC and one part cholesterol (4:1, or 20% cholesterol) [102]. Again, I observed an increase in deGFP in response to an increase in IPTG (Fig. 5.1B). Figure 5.1C and D show the deGFP expression when external IPTG is held at 5 μM and various lipids are mixed into Egg PC (e.g. 75% POPC represents liposomes prepared using 75% POPC and 25% Egg PC). While 0 μM IPTG represents the negative control, where no IPTG was in the internal or external solution, the circuit still produces roughly 10% as much deGFP as the positive control, simply due to the leaky nature of this cascade in TXTL (Fig. 5.1C). While IPTG was permeable to some degree in all cases, there are some mixtures to note. The cis and trans DOPC behave differently and unexpectedly based upon the orientation of the double bonds in their fatty acid chains. I expected the permeability to increase as the concentration of the cis DOPC increased, as the fatty acid chain would be more difficult to pack, creating more fluidity in the bilayer. However, I expected the trans DOPC to decrease permeability, as the trans bond would keep the chain straight, decreases the fluidity of the membrane. On the contrary, I observed the opposite in both cases (Fig. 5.1C). DSPC, SOPC, and DSPE all decreased the permeability of the membrane as they made up an increasing proportion of the bilayer, though none of them impeded the passage of IPTG to the level of the negative control (Fig. 5.1C). There was no significant effect on the permeability using DPPC, POPC, 22:0 PC, or 22:1 PC, at any concentration (Fig. 5.1D). POPG and POPE lipids did not decrease permeability in any way, likely due to the nature of the head groups (Fig. 5.1D). Since both PG and PE are charged, the polar heads would repel one another, causing potential gaps in the membrane.

It is not entirely clear why IPTG is permeable to liposomes composed of Egg PC prepared using the emulsion transfer method. It is possible that Egg PC is inherently permeable since it is contains a mixture of chain lengths. This could be explain the decrease in permeability observed in Fig. 3.22C when the proportion of a single, pure lipid increases. However, membranes in living cells are not homogenous and a sugar as large as IPTG would not be permeable to a live cell. There is also the possibility that the permeability is inherent to the encapsulation of a solution as complex as TXTL.

Molecules in the cellular interior may interact in some way with the bilayer to permeabilize it. Further, the interior and exterior solutions have roughly a 100 mOsm difference in osmotic pressure, and this could drive spontaneous fissures in the membrane to release this pressure.

5.2 α-hemolysin Function and Enhanced Gene Expression

Alpha-hemolysin (AH) is excreted by the bacterium Staphylococcus aureus as water-soluble monomers that oligomerize into a transmembrane heptamer, It forms a membrane pore, 1.4 nM wide at its narrowest point, allowing rapid diffusion of ions and small molecules roughly 3 kDa or smaller. It has been demonstrated that the presence of AH in membranes encapsulating cell free systems expression DNA programs allows the reaction to proceed for extended periods of time and reach higher yields [84]. Recently, similar experiments were performed with AH utilizing the new cell-free system [44]. AH was first expressed in a cell-free reaction. Then, we diluted this reaction 15-fold into a reaction containing the plasmid P70-deGFP and prepared liposomes. After 24 h of incubation, we measured a 2-fold increase of deGFP expression when AH was used, reaching 3.2 mg/ml in liposomes (Fig. 3.14). It is not clear why this is less than in batch semi-continuous cell-free reactions. The amount of reporter protein expressed is much larger than in previous, similar setups made with a T7-based cell-free system. The level of expression without AH in the external solution was comparable to batch mode reactions in test tubes (about 1.5-2 mg/ml of fluorescent deGFP). We monitored the kinetics of deGFP expression with and without AH and observed an extension of expression in the presence of the toxin.

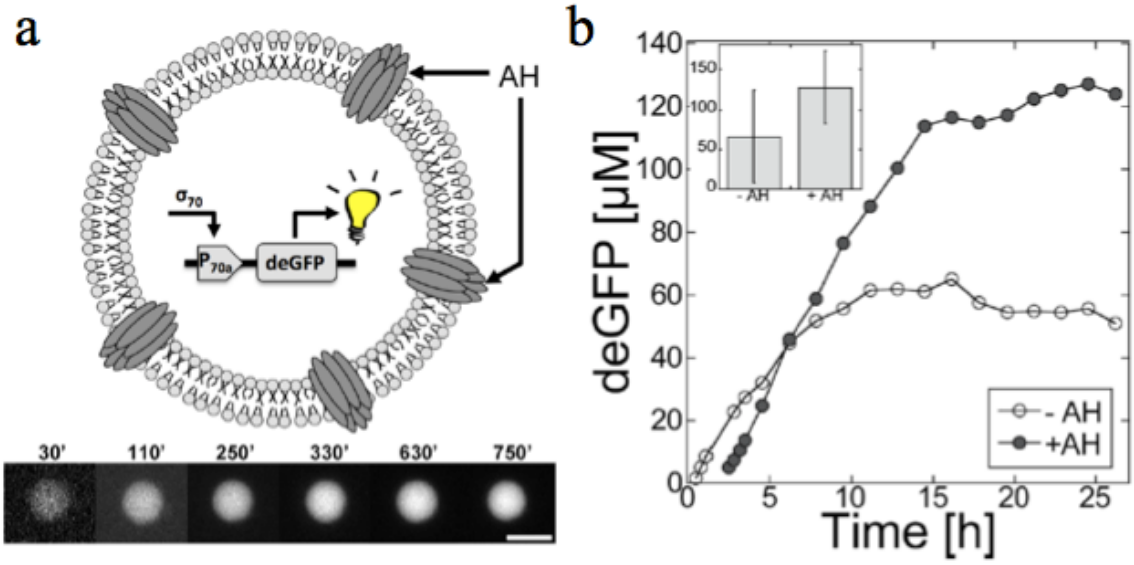

Figure 5.2 (a) Schematic showing a cell-free reaction (plasmid P70a-deGFP) inside a liposome. The toxin alpha-hemolysin (AH) was added to the encapsulated reaction. Below: a series of photos showing deGFP fluorescence intensity (time in minutes, scale bar: 10 μm), when AH was added to the reaction. (b) Kinetics of expression of deGFP (P70a-deGFP) inside liposomes with (liposome of diameter 11.5 μm and without AH (liposome of diameter 7.3 μm). Inset: statistics of deGFP fluorescence after 12 h of incubation with and without AH. The kinetics were rescaled to the average values of the histogram showed in the inset. The negative control with no plasmid did not show any signal (not shown). Reprinted with permission from *ACS Synth. Biol.*, **2016**, *5* (4), pp. 344–355. Copyright 2016 American Chemical Society.

This system was further characterized by monitoring the leak of UTP-fluorescein from liposomes, with and without adding AH in the internal solutions (Fig. 3.15). It takes a few hours to observe a complete leak of 5 μM of the fluorescent probe, while with no addition of AH no leak is observed.

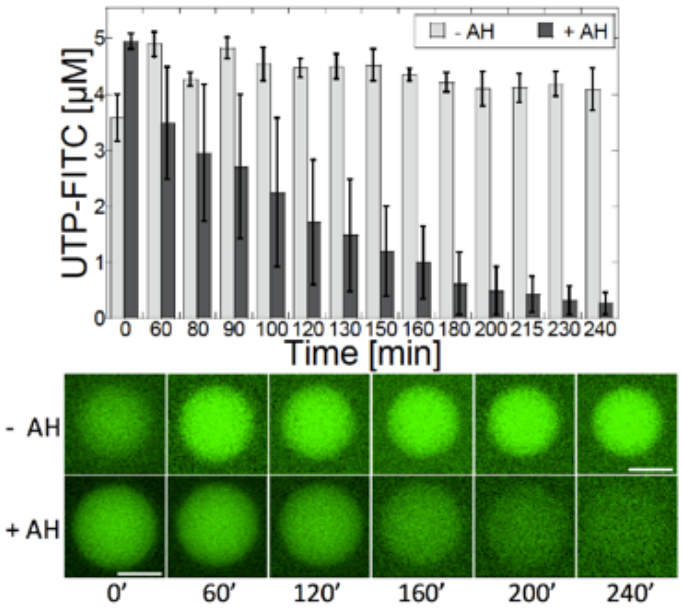

Figure 5.3 Leak of UTP-fluorescein from cell-sized liposomes through the pore forming protein alpha-hemolysin (AH). Top: kinetics of the leak with and without AH Error bars represent the standard deviation from six liposomes. Bottom: fluorescence images of liposomes at different times (minutes), with (8 µm diameter) and without (6 µm diameter) AH. Scale bars: 4 µm. Reprinted with permission from *ACS Synth. Biol.*, **2016**, *5* (4), pp. 344–355. Copyright 2016 American Chemical Society.

5.3 MscL as a Release of Osmotic Pressure

One of the greatest challenges to a minimal cell system is that of osmotic pressure. Recall from Equation 8 that the surface tension of a liposome is proportional the radius of the spherical object and also to the concentration difference of the various solutes in the solution. The reason this is such a challenge for a minimal cell system is due to the complexity of the reaction that must be encapsulated in order to express proteins from plasmid DNA. The entire TX TL cell free expression system must be encapsulated along with the DNA templates, salts, energy sources, substrates, and molecular crowding agents. Since membranes can be up to ten orders of magnitude more permeable to water than ions, any sort of imbalance leads to lysis.

An attempt to solve this problem is to match the exterior and interior conditions in an effort to match concentrations and thus osmotic pressure. However, consider the issue of a minimal cell dividing and assume a spherical liposome and the fact that the surface area must be conserved as lipids are not added to the membrane during division. Let R be the radius of the singular liposome and r be the radius of the two daughter cells after division.

(1) $A_i = 4\pi R^2 = 2(4\pi r^2) = A_f$

(2) $$r = \frac{R}{\sqrt{2}}$$

(3) $$V_i = \frac{4}{3}\pi R^3 \neq \frac{4}{3\sqrt{2}}\pi R^3 = V_f$$

(4) $$\frac{V_f}{V_i} = \frac{\sqrt{2}}{2}$$

Using these simple yet realistic assumptions, we find the radii and combined volume of the daughter cells decreases by ~30% upon division. Thus, the concentration difference and therefore pressure on the membrane increases by the same factor. This puts the membranes of the daughter cells under tremendous tension and is likely to cause lysis. There are two potential solutions to this problem. The first, conceptually simple yet difficult to implement, is to exactly match interior and exterior pressures by matching solute concentrations in those regions. There are several issues with the solution. The exterior solution does not contain the cell free extract in an effort to minimize protein expression outside the minimal cell as well as to create an environment that allows liposomes to form; if the solution they are centrifuged into is too dirty, liposome yield will be to low to be experimentally feasible. The exterior feeding solution also must maintain a range of specific PEG concentrations, as PEG will act to dissolve the lipid membranes.

The second solution and the realistic way around this problem is to implant in the membrane ion channels, specifically those that open when the membrane is under tension. Organisms detect sound, touch, gravity, and pressure through activation or inactivation of the mechanosensitive channels [87]. The most studied such protein is the mechanosensitive channel of large conductance, or MscL (136 aa, 15 kDa) [152]. A homopentamer, MscL serves as an emergency release valve in *E. coli*, directly sensing and responding to membrane tension [153]. In it's closed state, the pore retains the same degree of permeability, or lack thereof, as the membrane. However, under increased tension, it opens to a diameter of 25-30 Å and allows passage to molecules ~6.5 kDa or smaller in large unilamellar vesicles [154], [155]. The probability of opening increases with the pressure and also depends on the composition of the membrane. The activation

energy increase as lipid bilayer thickness increases [156]–[158] due to the orientation of the transmembrane helices [159], [160]. The effect of cholesterol on the activation energy is dependent upon the phospholipids that make up the bilayer. Cholesterol would serve to alter the membrane by reducing the bilayer fluidity, thus increasing the stiffness, and reduce the activity of MscL. In the case of phosphatidylcholine bilayers, cholesterol does not increase the bending modulus in concentrations as high as 40% [161]. As we hope to use it in a minimal cell as a release valve, cholesterol will not be used as regardless of the membrane composition. Fortunately, it is possible to decrease the activation energy of MscL using molecules incorporated into the bilayer. Lysolecithin (LPC) is a single-tailed lyso-lipid that reduces the activation energy of MscL [162] by 57% in concentrations of 5μM when distributed in the outer leaflet of the membrane [163].

In order to test the efficacy of using MscL as a pore responsive to osmotic pressure, I devised experiments looking at the leak of fluorescent molecules from liposomes expressing MscL [59]. Specifically, I investigated the leak of TRITC-Dextran molecules of 3, 10, and 70kDa, as well as GFP and BSA-TRITC, from liposomes whose membranes were under an osmotic pressure difference of ~100mOsm. To be sure this was an effect of MscL inserting into the membrane, I cloned a fusion gene, MscL-eGFP, under a P28a promoter. To grow MscL in *E. coli*, it is necessary to use a promoter associated with a sigma factor other than σ70, as the protein is toxic to the organism in large concentrations. Figure 5.4 shows the accumulation of MscL-eGFP at the membrane in an Egg PC liposome over the course of almost 3 hours. Since this is a σ28 cascade, meaning the expression of σ28 is required before MscL-eGFP can be expressed, there is delay in the appearance of significant amounts of MscL-eGFP until 80 minutes into the encapsulation.

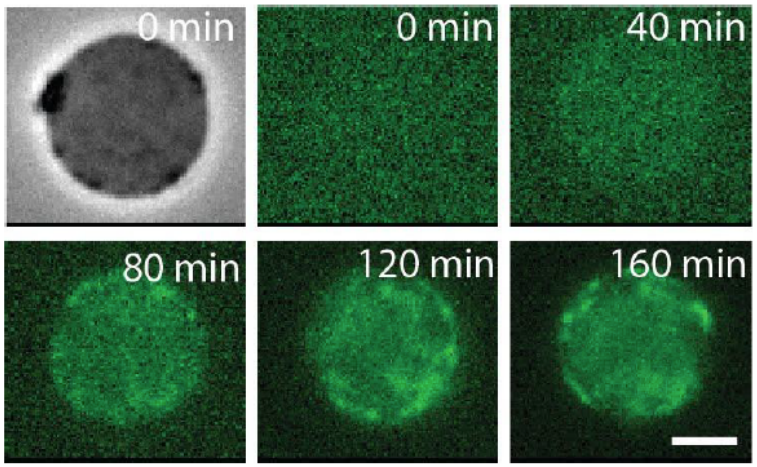

Figure 5.4 Fluorescence microscopy images of MscL-eGFP being expressed in a liposome. Scale bar: 5 µm. Reproduced from S. Majumder, J. Garamella, Y. Wang, M. DeNies, V. Noireaux and A. P. Liu, *Chem. Commun.*, 2017, **53**, 7349 with permission from the Royal Society of Chemistry.

For the leak experiments, plasmids encoding σ28 and MscL were encapsulated with 5 µM of the conjugated dyes. As the maximum diameter of MscL is ~2.4 nm, I began with the 3 kDa TRITC-Dextran as this size corresponds to a hydrodynamic radius of ~1 nM. 10 kDa and 70 kDa correspond to radii of ~2 and 5-6 nM, respectively. These numbers are approximate as the TXTL reaction is more complex than a simple aqueous solution.

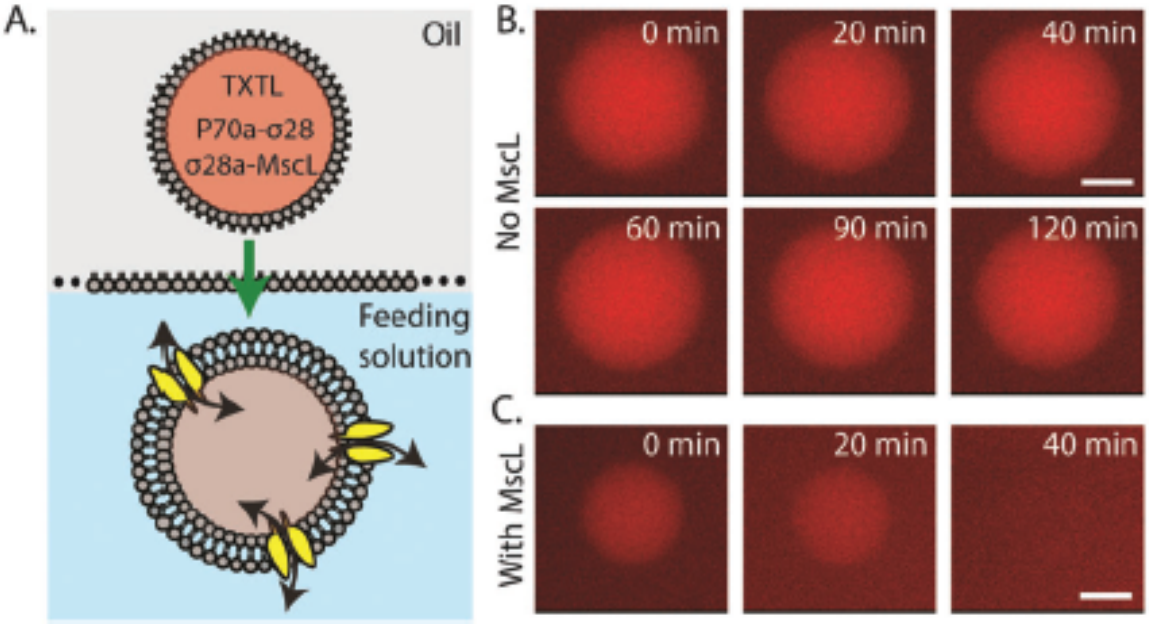

Figure 5.5 Measurement of the leak of 3 kDa TRITC-Dextran through MscL expressed in

liposomes. (A) Cartoon of the encapsulation scheme. (B) Fluorescence microscopy images of a liposomes containing 5 μM of 3 kDa TRITC-Dextran without expression MscL. (C) Fluorescence microscopy images of a liposomes containing 5 μM of 3 kDa TRITC-Dextran when MscL is expressed. Scale bar: 5 μm. Reproduced from S. Majumder, J. Garamella, Y. Wang, M. DeNies, V. Noireaux and A. P. Liu, *Chem. Commun.*, 2017, **53**, 7349 with permission from the Royal Society of Chemistry.

Figure 5.5 depicts the leakage of TRITC-dextran of 3kDa in the presence or absence of MscL. The general methodology of the experiment (Fig. 5.5A) is present, along with fluorescence microscopy images showing the leak, or lack thereof, of the dye (Fig. 5.5B-C). With no MscL present the presence of the dye persists for over two hours. When MscL is expressed, the dye is visibly dimmer after only 20 minutes, and completely gone after 40 minutes.

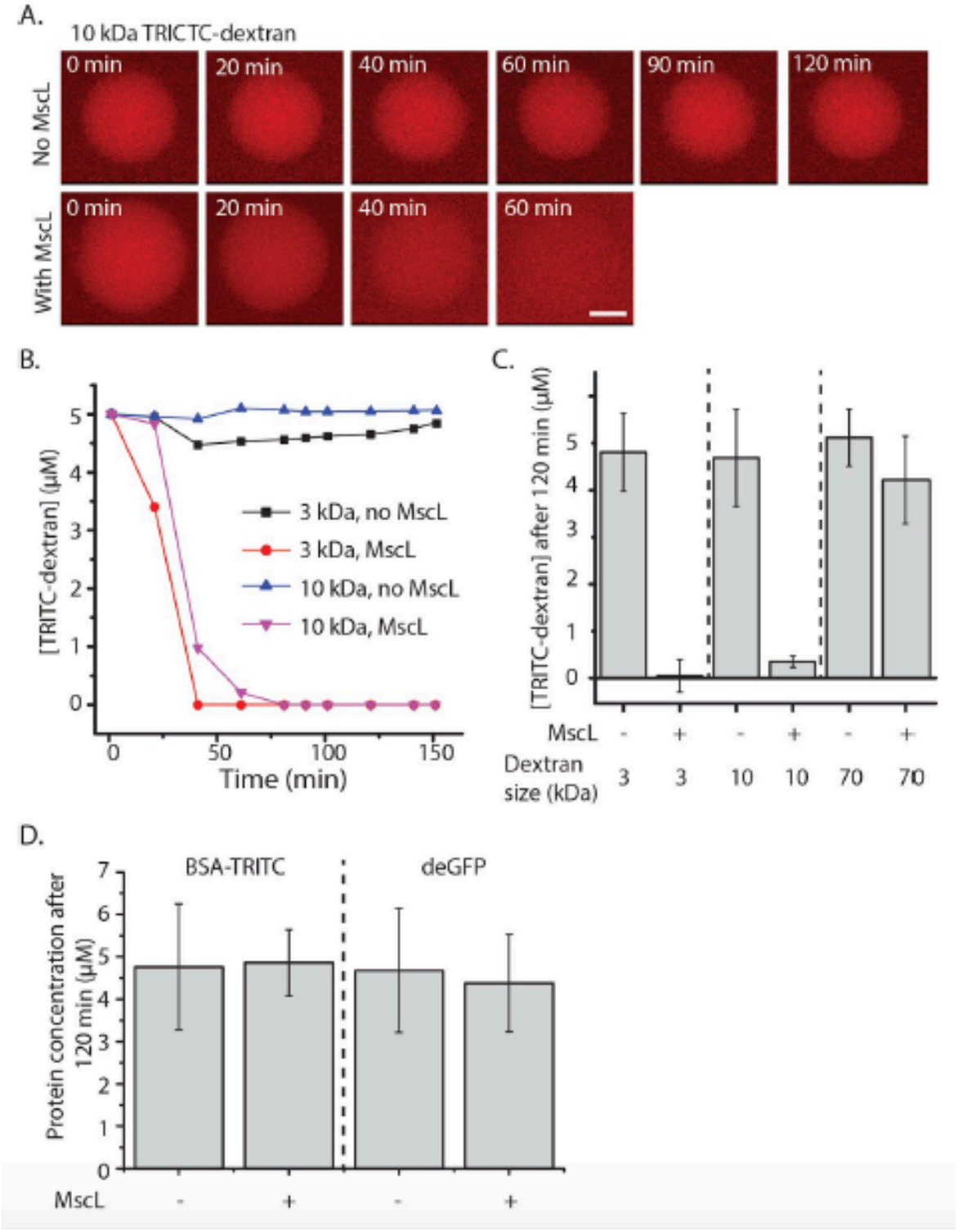

Figure 5.6 Functionality of MscL expressed using TXTL in liposomes. (A) Fluorescence microscopy images of the leak of 5 μM 10 kDa TRITC-Dextran in liposomes encoded to express MscL or express no proteins. (B) Kinetics of the leak of 3 and 10 kDa TRITC-Dextran in the

presence or absence of encoded MscL. (C) Concentration of 3, 10, and 70 kDa TRITC-Dextran after 120 minutes after encapsulation with and without plasmids encoding MscL. (D) The leak of BSA-TRITC and deGFP from liposomes after 2 hours in the presence or absence of plasmids encoding MscL. Scale bar: 5 μm. Reproduced from S. Majumder, J. Garamella, Y. Wang, M. DeNies, V. Noireaux and A. P. Liu, *Chem. Commun.*, 2017, **53**, 7349 with permission from the Royal Society of Chemistry.

I next explored the leak via MscL of the larger dextran polymers (Fig. 5.6). Fig. 5.6A displays fluorescence microscopy images of the leak of the 10 kDa conjugated polymer. Like with the 3 kDa dye, after 2 hours without MscL, there is no detectable leak. However, when MscL is expressed inside the liposome, the dextran is completely absent after 60 minutes. The microscopy images are supported by the analysis of the intensity presented in Figure 5.6B. While the 3 kDa leak is faster than 10 kDa, both are significantly faster than the experiments done without MscL. End point measurements were done after two hours, including for the leak of 70 kDa TRITC-Dextran through MscL expressed via a P28a cascade (Fig. 5.6C). The leak of the 70 kDa molecule is insignificant. This is to be expected as the polymer is larger than the pore, therefore the only way for the molecule to escape is via reputation, which would be a much slower process. Lastly, we analyzed the leak of both BSA (60 kDa) and GFP (27 kDa) to understand how larger proteins, both that we express and that we use in TXTL, would respond to the presence of MscL (Fig. 5.6D). We found the leak to be insignificant, suggesting MscL would be a viable pore to use in our experiments to use as a release of osmotic pressure. Given that the pore is active and open under an osmotic gradient, we conclude it can be used as a release valve of osmotic pressure.

5.4 A Synthetic Sensor

Using the knowledge of the functionality of MscL in TXTL, I next set out to construct a synthetic cell prototype capable of sensing its physical and chemical environment in collaboration with colleagues from the University of Michigan. Our experimental methodology was to use TXTL to produce proteins with biosensing or molecular transport properties inside phospholipid vesicles (Fig. 5.7A). Cell-free protein synthesis programmed by DNA inside liposomes links the information in the DNA to the phenotype exhibited by the synthetic cell prototype.

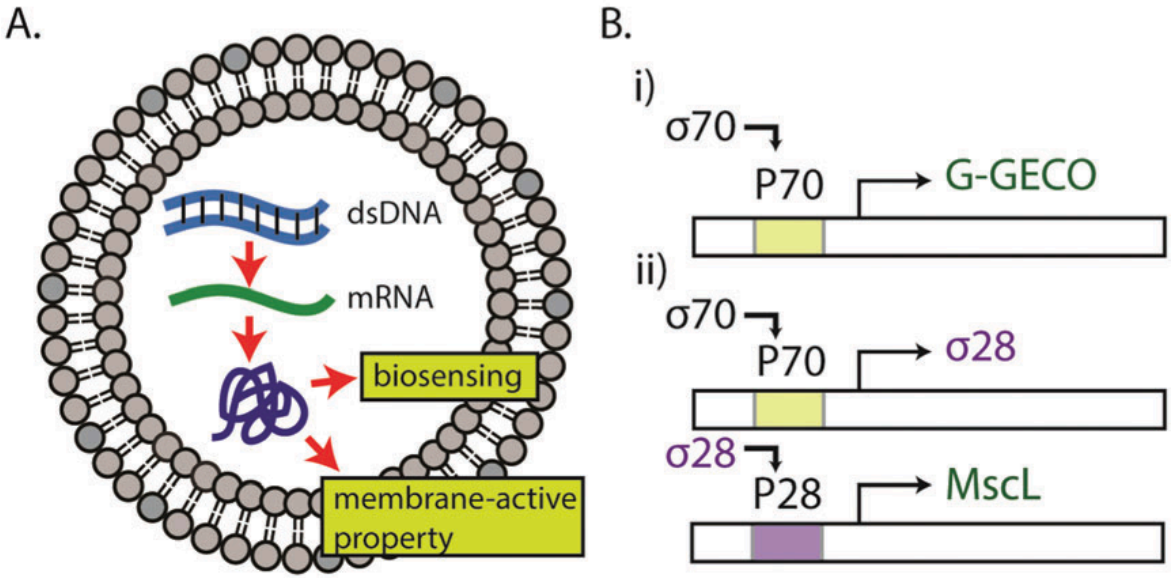

Figure 5.7 Schematics of (A) protein expression in liposomes and (B) gene circuits used to express G-GECO and MscL. Reproduced from S. Majumder, J. Garamella, Y. Wang, M. DeNies, V. Noireaux and A. P. Liu, *Chem. Commun.*, 2017, **53**, 7349 with permission from the Royal Society of Chemistry.

These biochemical reactions are similar to chemical reactions, in the sense that different genetic circuit schemes can lead to different reactions rates and outputs. For this set of experiments, we used multiple expression motifs. First and most simply, the endogenous *E. coli* core RNA polymerase drives constitutive expression via the P70a promoter as a holoenzyme of the RNAP and σ70. Then, we use the flagellar sigma factor, σ28, to drive expression using the P28a promoter (Fig. 5.7B).

We began by characterizing the behavior of the σ28 cascade in both bulk reactions and in liposomes. Bulk reactions were performed in 10 µl volumes in 96-well V-bottom plates and monitored on plate readers. Both the single step and the multistep cascade were compared. As expected, the multistep cascade has a delay in expression relative to the σ70 cascade due to the requirement that σ28 be expressed before the P28a promoter is active (Fig. 5.8A). The inset highlights this difference, showing the delay to be on the order of 15 minutes, or roughly the time to express the sigma factor. The bulk reaction persists until resources are depleted or toxic byproducts are produced which affect the biochemical nature of the reaction e.g. the pH. Both the single and multistep cascades have similar expression plateaus, as very little σ28 is required to drive the

reaction. The expression of these two circuit architectures in Egg PC liposomes generated using the emulsion transfer technique is shown in Fig. 5.8B. TXTL reactions of the same composition as the bulk reactions were encapsulated and incubated at 29 °C on a heated microscope stage. The expression delay for the multistep cascade is even more dramatic in the images. The first images are time-stamped at 15 minutes to account for the preparation time. Due to the initially low protein expression, the image exposure time was changed as the experiment went on so as not to saturate the CCD camera. These data are similar to the bulk reactions, with the expression plateauing after a similar period of time (data not shown). This data indicates the circuit cascade can be successfully encapsulated and the circuit behavior in the bulk persists upon encapsulation.

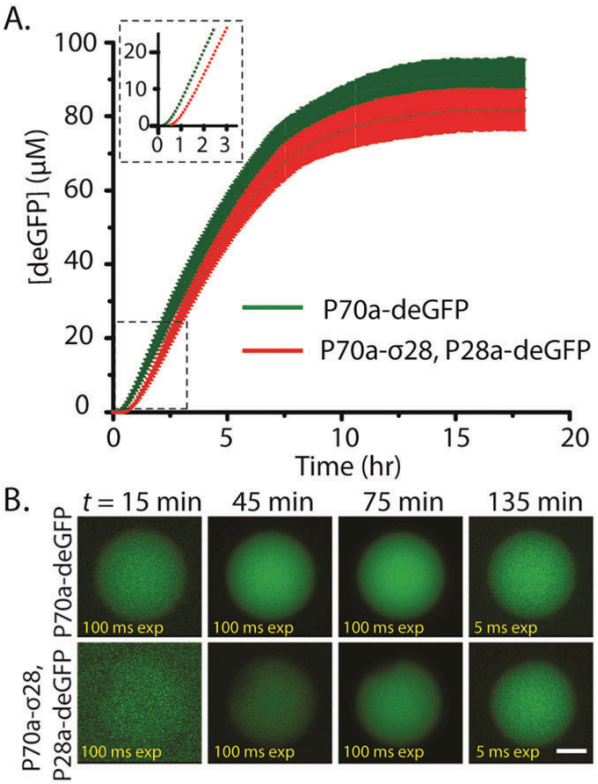

Figure 5.8 deGFP expression in bulk and liposomes via σ70 and σ28 cascades. (A) deGFP expression kinetics in bulk reactions. The inset shows the first 3 hours of the reaction. (B) deGFP expression via the single and two-step cascade in liposomes. Scale bar: 5 μm. Reproduced from S. Majumder, J. Garamella, Y. Wang, M. DeNies, V. Noireaux and A. P. Liu, *Chem. Commun.*, 2017, **53**, 7349 with permission from the Royal Society of Chemistry.

As I have previously shown MscL can be successfully recapitulated inside liposomes using a σ28 cascade, we used this circuit architecture to approach the next step in our experiment. We aimed to use MscL for the purposes of this sensor not only because we had knowledge of MscL inserting in the membrane of synthetic cells, but also for several other reasons. First, MscL can offer increased mechanical robustness by

alleviating osmotic pressure gradients. TXTL based synthetic cells also offer a simplified environment in which other MscL mutants can be tested. Third, the channel diameter is ideal in that it allows the passage of small molecules while retaining larger proteins, like those responsible for transcription and translation.

The next challenge we faced was finding a genetically-encoded reporter protein that we would be able to couple a mechanical input to biosensing. To do this, we cloned G-GECO under the control of the P70a promoter (P70a-G-GECO). G-GECO is a calcium ion (Ca2+) biosensor that is composed of a circularly permuted GFP fused to the calmodulin (CaM)-binding region of myosin light chain kinase M13 at its N-terminus and CaM at its C-terminus [164]. In the absence of Ca2+, G-GECO is dim, while it exhibits a calcium dependent fluorescence increase of ~23-26 fold when bound. We began by characterizing the behavior of G-GECO in TXTL by verifying it retained its Ca2+ sensing ability in plate reader assays (Fig. 5.9A). We found that when using G-GECO in TXTL, we needed to use a calcium chelator, EGTA, as there is background calcium of ~1 mM in the TXTL reaction.

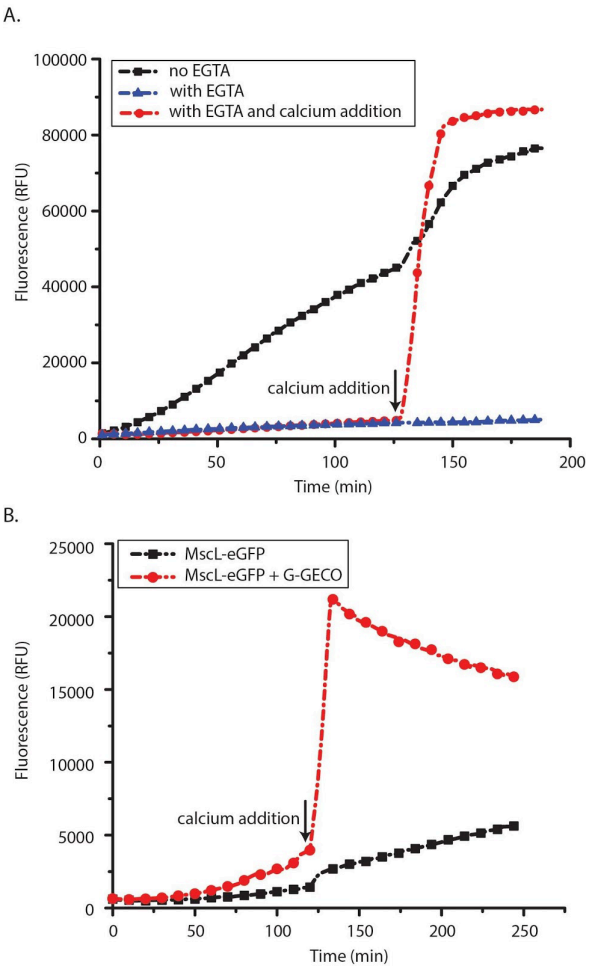

Figure 5.9 Bulk performance of G-GECO in TXTL reactions. (A) Fluorescence kinetics of G-GECO when expressed in a reaction with no EGTA, with EGTA, and with calcium added after 2 hours in a reaction containing EGTA. (B) Fluorescence kinetics of reactions expression MscL-eGFP in the presence of absence of G-GECO. Calcium is added after 2 hours in the reaction containing G-GECO. Reproduced from S. Majumder, J. Garamella, Y. Wang, M. DeNies, V. Noireaux and A. P. Liu, *Chem. Commun.*, 2017, **53**, 7349 with permission from the Royal Society of Chemistry.

Plate reader assays testing P70a-G-GECO were carried out under three different conditions: i) with no EGTA; ii) with 1 mM EGTA; and iii) with 1 mM EGTA and the addition of 2 mM calcium chloride added to the bulk reaction after 125 minutes. In the absence of EGTA, we observe a linear increase in the measured fluorescence intensity, corresponding to an increase in the expression of G-GECO, assuming the concentration of Ca2+ ions is so high in TXTL such that all G-GECO proteins are saturated. In the second condition, with EGTA added at the onset of the reaction, there is a negligible increase in fluorescence as all calcium ions are sequestered. Finally, we observe a dramatic increase in G-GECO fluorescence when calcium chloride is added after 125 minutes, indicating G-GECO is present in the reaction but not fluorescent. We tested similar conditions using P28a-MscL-eGFP and G-GECO to ensure that the presence of MscL would not interfere with the calcium sensor (Fig. 5.9B). Both reactions contained

EGTA, and in both calcium chloride was added after 120 minutes. Only in the reaction containing G-GECO was there a sharp increase in fluorescence. The small discontinuity in the reaction containing only MscL-eGFP is an experimental artifact from having to remove the plate from the reader, add the CaCl, and resume the measurement.

When creating our mechanosensitive-biosensing vesicles, we were not able to generate them using the emulsion transfer method as the membranes were found to be permeable to exterior calcium ions. Therefore, we utilized double emulsion template vesicles generated by droplet microfluidics [165], [166]. My colleagues had previously used this technique to successfully show that small molecules can enter encapsulated vesicles [167]. To ensure that these vesicles were not able to cross the phospholipid bilayer, we encapsulated and expressed G-GECO inside double emulsion template vesicles with an external calcium concentration of 10 mM. After three hours of incubation, no fluorescence was detected. However, in the presence of 1 μM A23187, a calcium ionophore, fluorescence was apparent after only ten minutes of incubation upon the addition of the ionophore. These data indicate that these vesicles are impermeable to calcium and that G-GECO fluorescence can be spiked with an influx of calcium ions (data not shown).

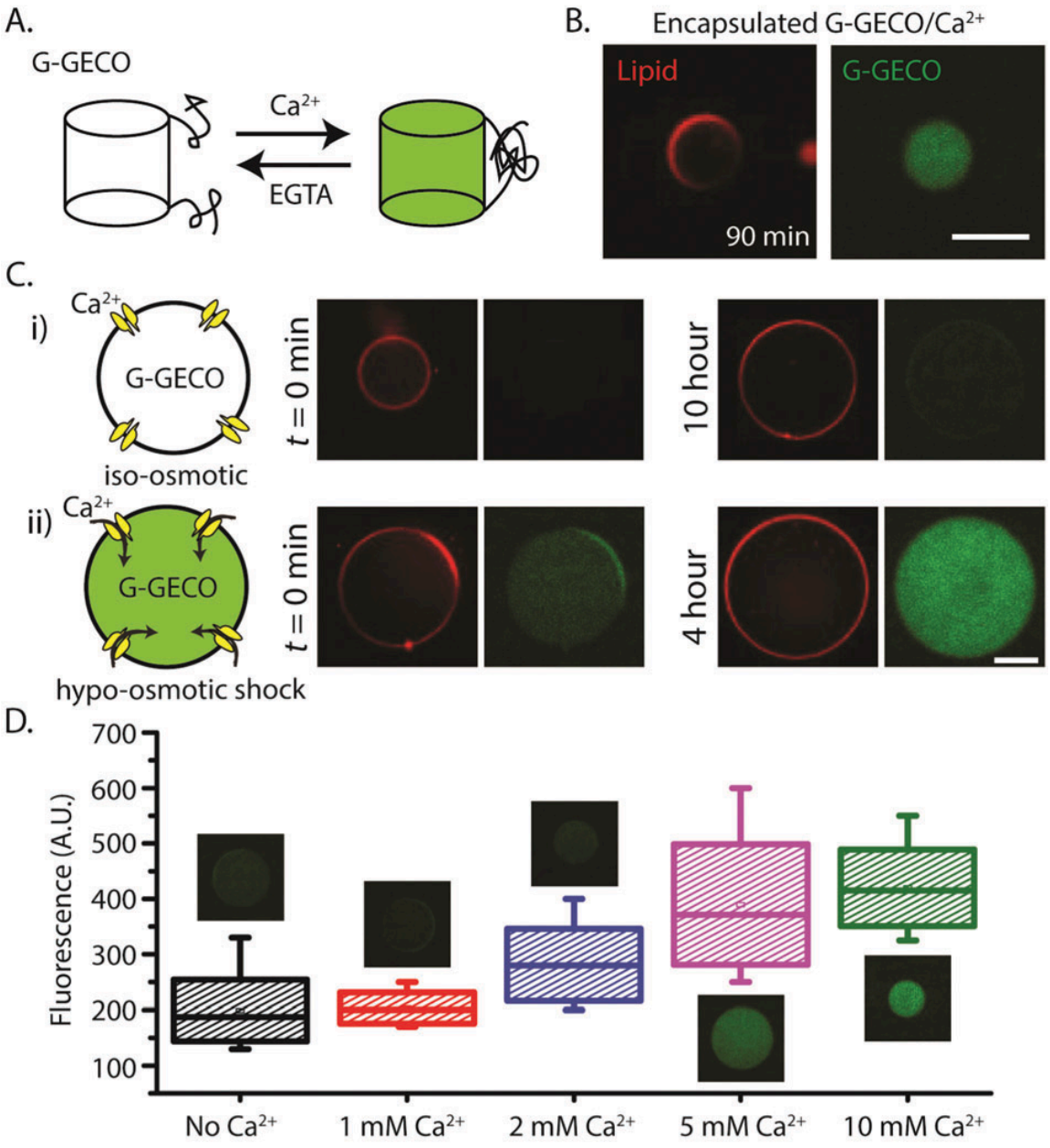

Figure 5.10 Mechanosensitive and biosensing synthetic cell prototype. (A) Schematic describing the reversal transformation between the two G-GECO protein confirmations in the presence of calcium or EGTA. (B) Fluorescence images of vesicles expressing G-GECO when calcium is encapsulated in the reaction. (C) G-GECO fluorescence when MscL and G-GECO are coexpressed under different osmotic conditions. (D) Box plot showing the relative fluorescence of G-GECO at varying calcium concentrations in hypo-osmotic conditions. Scale bar: 50 µm. Reproduced from S. Majumder, J. Garamella, Y. Wang, M. DeNies, V. Noireaux and A. P. Liu, *Chem. Commun.*, 2017, **53**, 7349 with permission from the Royal Society of Chemistry.

The effect on G-GECO of Ca2+ ions is shown in Figure 5.10A. When G-GECO was expressed inside these double emulsion template vesicles in the presence of 1.5 mM Ca2+, fluorescence was readily apparent after 90 minutes, again showing that G-GECO can be used to detect increased calcium concentration in an artificial cell (Fig. 5.10B).

In order to couple the mechanical input to sensing the external environment, G-GECO was co-expressed with MscL in TXTL for 2-3 hours before the entire reaction was encapsulated into double emulsion template vesicles. We used both iso-osmotic and hypo-osmotic solutions with an osmotic difference of 100 mOsm to incubate the vesicles. When the co-expressing vesicles were in the iso-osmotic solution, no fluorescence via G-GECO was observed even after 10 hours (Fig. 5.10C(i)). In hypo-osmotic conditions, with a difference in osmotic pressure of ~100 mOsm between the vesicle interior and exterior, there was a dramatic increase in G-GECO fluorescence as Ca2+ ions were able to enter into the synthetic cell prototypes via MscL (Fig. 5.10C(ii)). At the time of publication, this was, to our knowledge, the first demonstration of an AND-gate composed of a mechanical input and an external chemical input, leading to a specific fluorescence response. Furthermore, we demonstrated that the synthetic cell biosensor was able to quantitatively measure external calcium concentration in as short as 20 minutes (Fig. 5.10D).

To conclude, my colleagues and I have created a cell-sized synthetic cell prototype, programmed with DNA, capable of sensing osmotic pressure and external calcium concentration. In doing so, we characterized two genetic circuitries in TXTL that display different reaction kinetics that are sustained across scales in microliter bulk reactions down to femtoliter vesicles. This feat of bioengineering, being able to use mechanosensitivity to sense external molecules, allows for rapid sensing, as opposed to chemical inducers that influence reporter synthesis that were studied previously [31], [168]. Finally, we show that recapitulating TXTL for the purposes of synthetic cell engineering can be used to reconstitute cellular processes and functions [169].

5.5 An Adaptive Synthetic Cell

Much of my work during the course of my PhD has been in developing applications and technologies in TXTL in the pursuit of a synthetic cell. It was clear early on in my thesis

that MscL would be pivotal to this goal given its channel diameter and ability to respond to an external stimulus. Not only is the pore specific, in the sense that it is only open in the response to a mechanical stimulus, but also the size is larger enough such that it allows passage of relatively large small molecules while being impermeable to large, critical proteins. Further, it can be expressed in TXTL and is fully functional in liposomes, expressing from plasmid or linear DNA and inserting into the membrane. Indeed, this mechanosensitive behavior was coupled with a biosensing fluorophore, allowing for rapid sensing and once again showing the viability of TXTL as a prototyping platform for synthetic cells [59]. In this section, I will describe work done to advance our synthetic cell prototype beyond mere biosensing into a class of cell that is able to not only sense its environment, but also respond to it by altering gene expression to synthesize proteins responsible for cell morphology. Using the synthetic regulatory part LacO1, the mechanosensitivity of MscL is coupled to the influx of isopropyl β-D-1-thiogalactopyranoside (IPTG), which in turn sequesters the Lac repressor, allowing the σ70/RNAP holoenzyme to bind the constitutive LacO1 promoter and begin transcription. In doing so, I explored genetic circuits based around synthetic RNA aptamers in an effort to induce the expression of the *E. coli* cytoskeleton protein MreB.

Again collaborating with colleagues from the University of Michigan, Our overall methodology was to encapsulate TXTL reactions expressing a synergistic blend of proteins that would change the cytosolic environment in a quantifiable way in response to hypo-osmotic stimulus (Fig. 5.11).

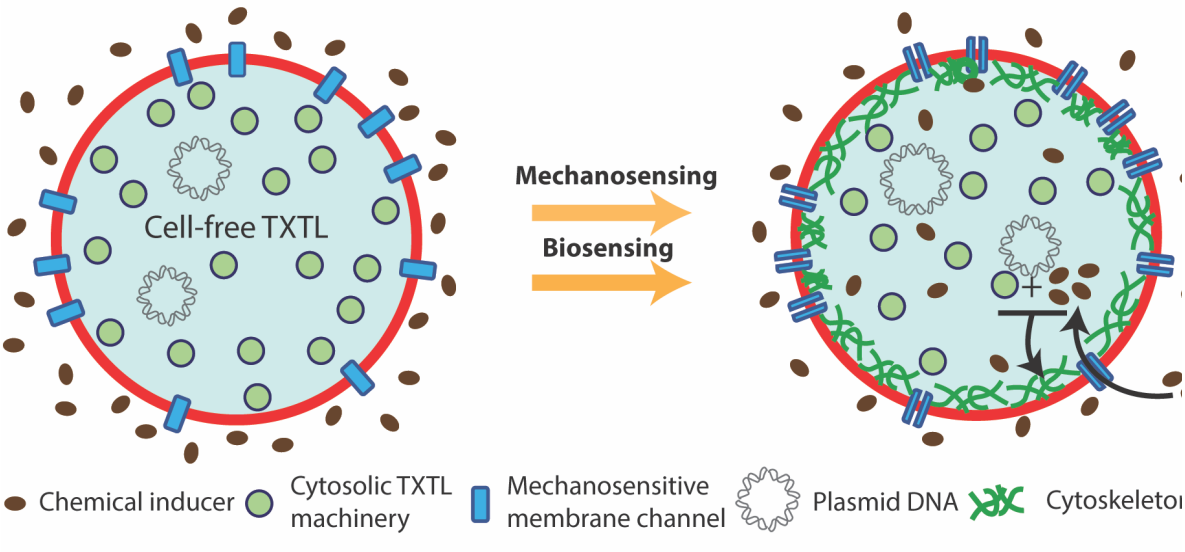

Figure 5.11 Schematic depicting the proposed synthetic cell's transition from its native state to an active state (development of cell-like cytoskeletal cortex) in response to mechanical and chemical stimuli.

The all *E. coli* TXTL system used throughout this thesis provided both the cytosolic environment and the machinery responsible for transcription and translation. The interior reaction solution would also be responsible for providing MscL, the avenue by which we intended to allow the passage of our small molecule. The exterior feeding solution contained the agonist that either changed the nature of interior mRNA or sequestered a repressor to influence gene expression. This change in gene expression would finally introduce the presence of MreB, which we used to simulate a synthetic cell cytoskeleton. Over the course of this experiment, we designed three iterations of our synthetic call prototype, all of which will be motivated and described.

Initially, our prototype was going to be based on a new class of RNA aptamers known as toehold switches (Fig. 5.12). These switches have recently been developed to have both a high dynamic range and be highly orthogonal [170], [171].

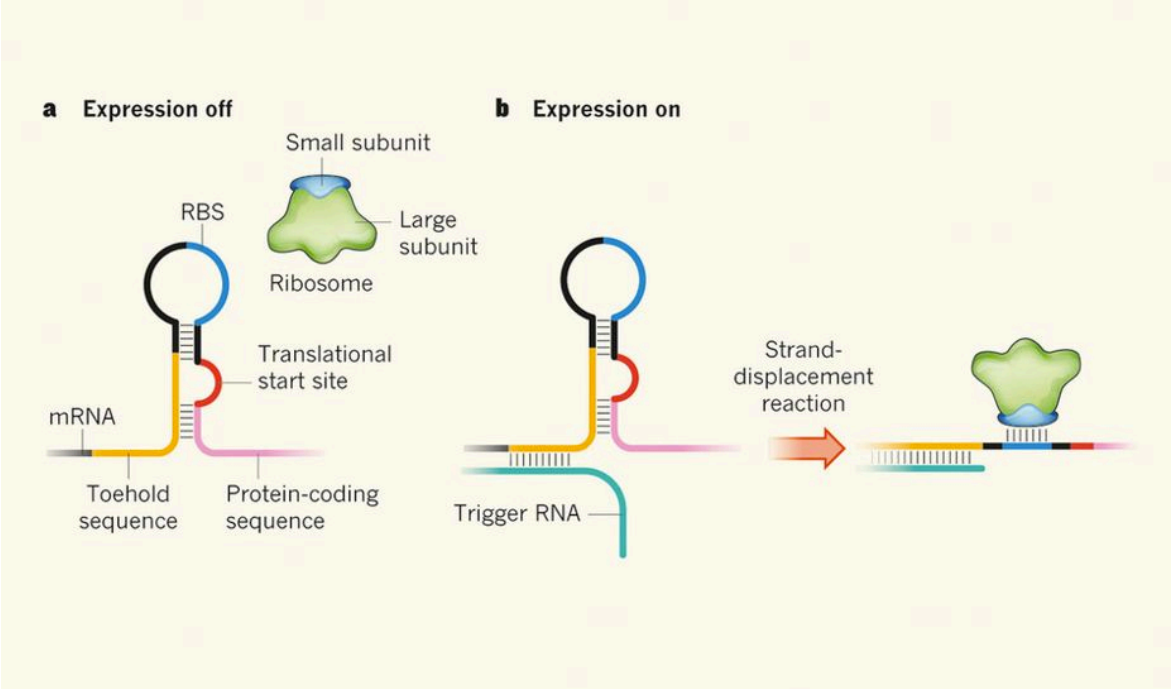

Figure 5.12 Schematic representation of the operation of toehold switches. Reprinted from **Nature**. 2014 Dec 18; 516 (7531): 333-4 with permission from Spring Nature[172].

Toehold switches rely on the unique secondary structures unique to RNA, specifically the affinity RNA has to form hairpins. In toehold switch circuits, the mRNA is transcribed but the ribosome binding site (RBS) is hidden in loop of an RNA hairpin, disallowing transcription. Upstream of the hairpin region is a "switch" region, which, when bound by a "trigger" transcript, opens up the hairpin and allows translation to proceed and the gene to be expressed. Incredibly, toehold switches can be regulated by arbitrary sequences, leaving their creation up to the creativity of the experimenter. This property also allows them to be used as both novel synthetic gene circuits and in practical medical applications [173].

Given the potential for the use of these switches in both synthetic biology and medicine writ large, we intended to base the first iteration of this synthetic cell on toehold switches. I began the experiments by cloning the a toehold switch cascade expressing deGFP using the switch/trigger pair designated as switch number 10 from Green et al.'s set of forward-engineered switches in Table S3 [171]. To characterize the toehold motif

in TXTL, I prepared plasmids putting the trigger sequence and the switch-deGFP sequence under the T7 promoter (Fig. 5.13a).

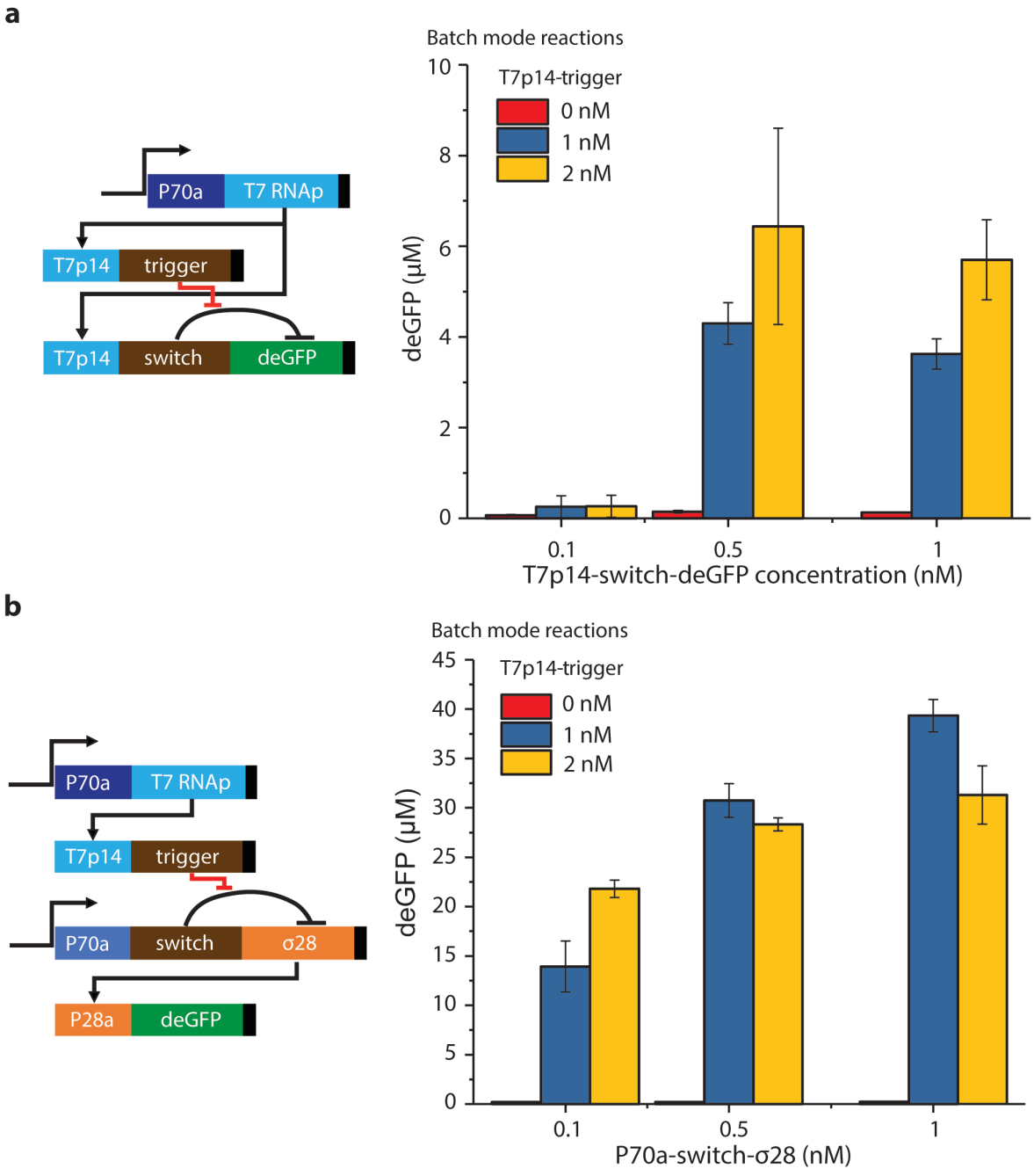

Figure 5.13 a) deGFP expression via the toehold switch cascade using the T7 promoter to express both switch and trigger sequences from plasmid DNA. **b**) deGFP expression via an amplified toehold switch cascade in which the P70a promoter is used to express switch-σ28, and deGFP is expressed via the P28a promoter. Concentrations of switch and trigger plasmids were

kept the same as a) and the concentration of P28a-deGFP plasmid was fixed at 5 nM.

I ranged the concentration of the reporter plasmid, T7p14-switch-deGFP, against the plasmid encoding the trigger, T7p14-trigger. When no trigger was present, we see there is negligible deGFP expression, indicating that the toehold retains its renowned regulation in TXTL with an ON/OFF ratio of ~80. While the T7 cascade is powerful in TXTL since it is based on such a strong promoter, here we only achieve endpoint expression of 6 μM as the concentrations of the trigger switch plasmids are increased. At this point, we decided to develop what I will refer to as a σ28 amplifier in order to increase the expression of the overall cascade (Fig. 5.13b). This was done by putting the transcription factor, σ28, under the control of the switch sequence. Therefore, even if a smaller amount of protein was produced by the switch plasmid, this result could be amplified using the endogenous machinery in *E. coli*. Indeed, as shown in Fig. 5.13b, we see that we are able to capture ~50% of the total protein synthesis of TXTL while once again retaining the tight regulation offered by the toehold system, with an ON/OFF ratio of 176. In this experiment, the trigger plasmid was ranged against the switch plasmid while the reporter plasmid, P28a-deGFP, was fixed at 5 nM. I decided on a σ28 amplifier against a T7 amplifier due to the relative ease of purchasing or purifying T7 RNA polymerase and using it in TXTL. Since we already had a T7p14-MscL, there would be a smaller load on TXTL if we simply added the RNA polymerase to the reaction without expressing it.

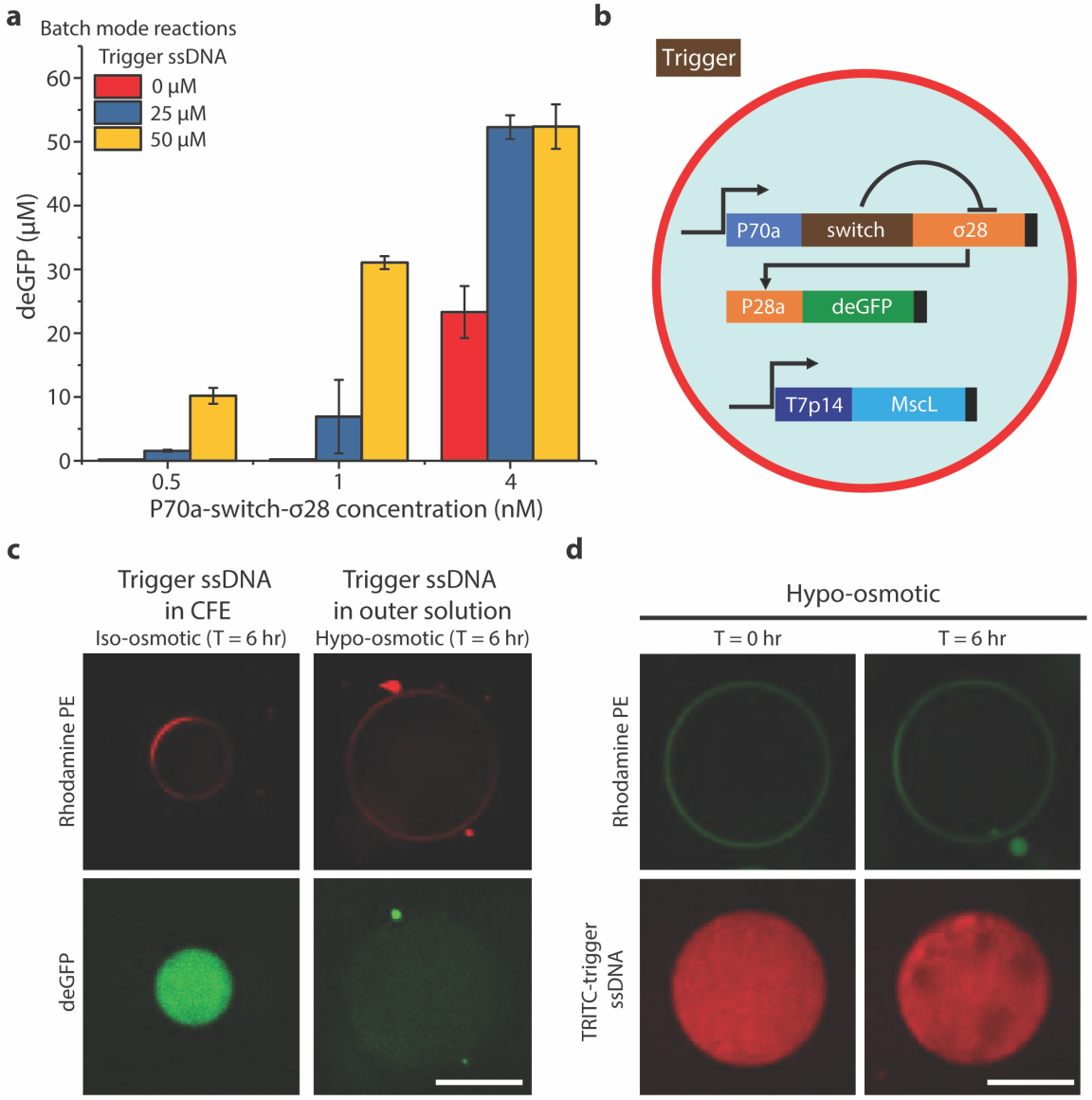

Figure 5.14 a) Plot showing the endpoint deGFP expression of the toehold switch cascade with different concentrations of switch plasmid and the trigger ssDNA in TXTL reactions performed in batch mode reactions. **b)** Schematic representing the first minimal cell model where the toehold switch cascade is encapsulated along with a TXTL reaction inside liposomes, orthogonally programmed to express MscL through the T7 promoter, which are then exposed to an outer solution containing the trigger ssDNA. **c)** Images of liposomes expressing deGFP with the trigger ssDNA inside (iso-osmotic conditions) or outside (hypo-osmotic conditions) the liposomes, respectively. **d)** Images of liposomes expressing MscL containing 50 µM TRITC-labeled trigger ssDNA that are exposed to a hypo-osmotic solution for 6 h. Scale bar: 50 µm.

Since the synthetic cell switch/trigger scheme would rely on the influx of the trigger from the exterior solution, which does not contain an active TXTL lysate for a multitude of reasons, I performed experiments to test whether or not the toehold switch could function with the addition of an oligonucleotide. This being a RNA aptamer, the trigger sequence is typically in the form of RNA. However, given the similarity of DNA to RNA and cost of DNA synthesis (on a per base basis from IDT, DNA costs $0.37 and RNA costs $7.50), we immediately tested the σ28 amplifier using a piece of single stranded DNA (ssDNA) (Fig. 5.14a). We again sought a stoichiometric regime where protein expression was simultaneously robust and well regulated. Ranging the ssDNA trigger against the σ28 encoding switch plasmid, we see that the toehold σ28 amplifier begins to leak in the absence of the trigger as we increase the concentration of the switch plasmid. However, ~50% of TXTL expression capacity is recapitulated using 50 μM trigger ssDNA and 1 nM P70s-switch-σ28 plasmid (P28a-deGFP was fixed at 5 nM). Fig. 5.14b depicts the first iteration of the synthetic cell based on a toehold switch. Inside, MscL is expressed using the T7 cascade while deGFP is expressed using the σ28 amplifier toehold switch. Ideally, the trigger ssDNA would influx into the cell in response to hypo-osmotic conditions. The positive control, where the trigger is encapsulated along with the TXTL in iso-osmotic conditions, results in a significant increase in fluorescence after six hours (Fig. 5.14c). However, under hypo-osmotic conditions where the trigger is in the external solution, there is not a noticeable change in fluorescence, indicating the trigger ssDNA does not pass through the 2.4 nM pore. Indeed, when a fluorescently labeled trigger sequence is encapsulated and MscL expressed, there is an insignificant change in fluorescence after six hours in hypo-osmotic conditions (Fig. 5.14d). This data suggests that the 30-nt trigger sequence is too large to pass through the pore, disallowing this iteration of our synthetic cell prototype and forcing us to look for alternatives.

Given my experience with the synthetic regulatory part, PL-LacO1, the second iteration of this synthetic cell prototype was based on the *lac* operon, one of the most studied genetic signaling pathways in bacteria [70]. This promoter is repressed by the *lac* repressor, LacI, which I cloned under the constitutive synthetic promoter PL-TetO1. The

reporter, deGFP, was then under the control of Pl-LacO1 while MscL expression was still moderated by the T7 promoter. TXTL reactions encoding the entire plasmid set were encapsulated, while IPTG was added to the feeding solution (Fig 5.15a).

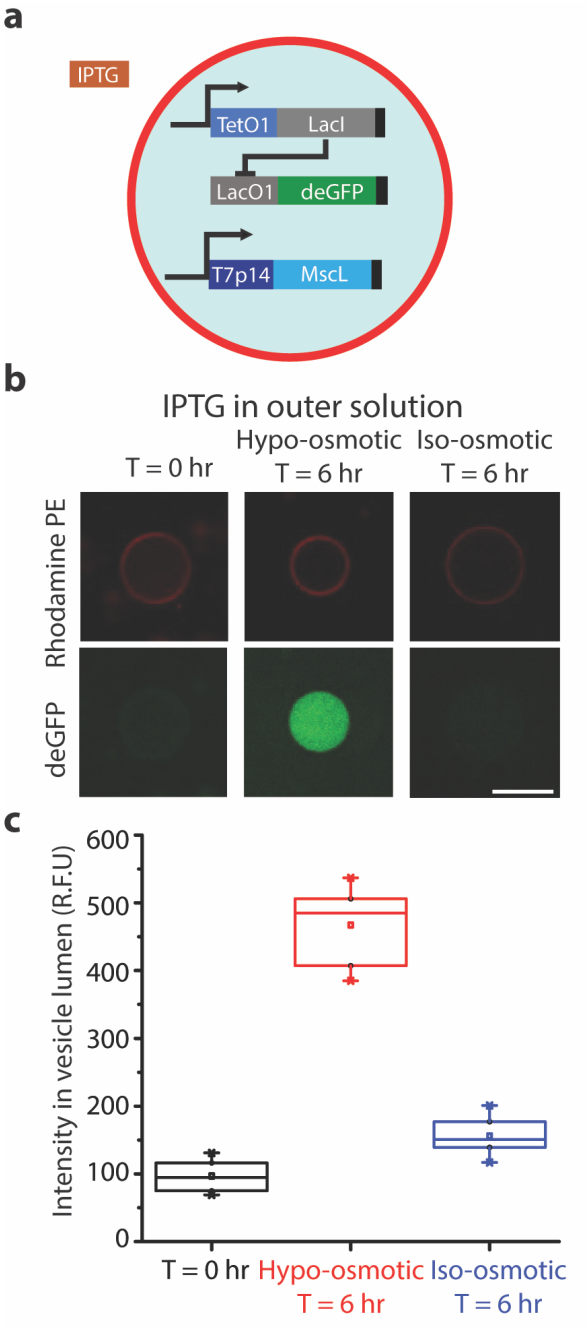

Figure 5.15 a) Schematic depicting the second model of the proposed synthetic cell co-expressing an inducible gene circuit and MscL constitutively. IPTG, the inducer, is in the outer solution. **b)** Fluorescence images showing expression of deGFP inside liposomes exposed to outer solutions with IPTG and different osmotic conditions at 0 and 6 h. **c)** Boxplot of deGFP fluorescence in the vesicle lumen under the different osmotic conditions. 10 liposomes were measured for each condition. Scale bar: 50 µm.

There was no fluorescence, and thus deGFP protein in solution, upon initial observation (Fig. 5.15b). After six hours of incubation, the fluorescence signal in the liposomes in

hypo-osmotic conditions increased by a factor of ~5, while liposomes in iso-osmotic conditions did not show a significant change in fluorescence (Fig. 5.15c). Figure 5.15 suggests IPTG is flowing into the synthetic cell prototype, specifically entering via MscL, which is opening in response to osmotic pressure differences. While this is a significant achievement in and of itself, this specific promoter is likely too weak for the purposes of MreB, as the cytoskeletal protein requires a critical concentration for polymerization [174]. Also, relative to the toehold switch we looked at previously, the regulation of this cascade is weak.

At this point, I built upon our work with the toehold σ28 amplifier and the knowledge that we can achieve an influx of IPTG during hypo-osmotic conditions by developing a PL-LacO1 σ28 amplifier. To do so, I cloned σ28 un the PL-LacO1 promoter and used the P28a promoter to express deGFP. In this way, LacI repressed the expression of σ28 and only a small amount of σ28 was necessary to achieve a large amount of deGFP expression.

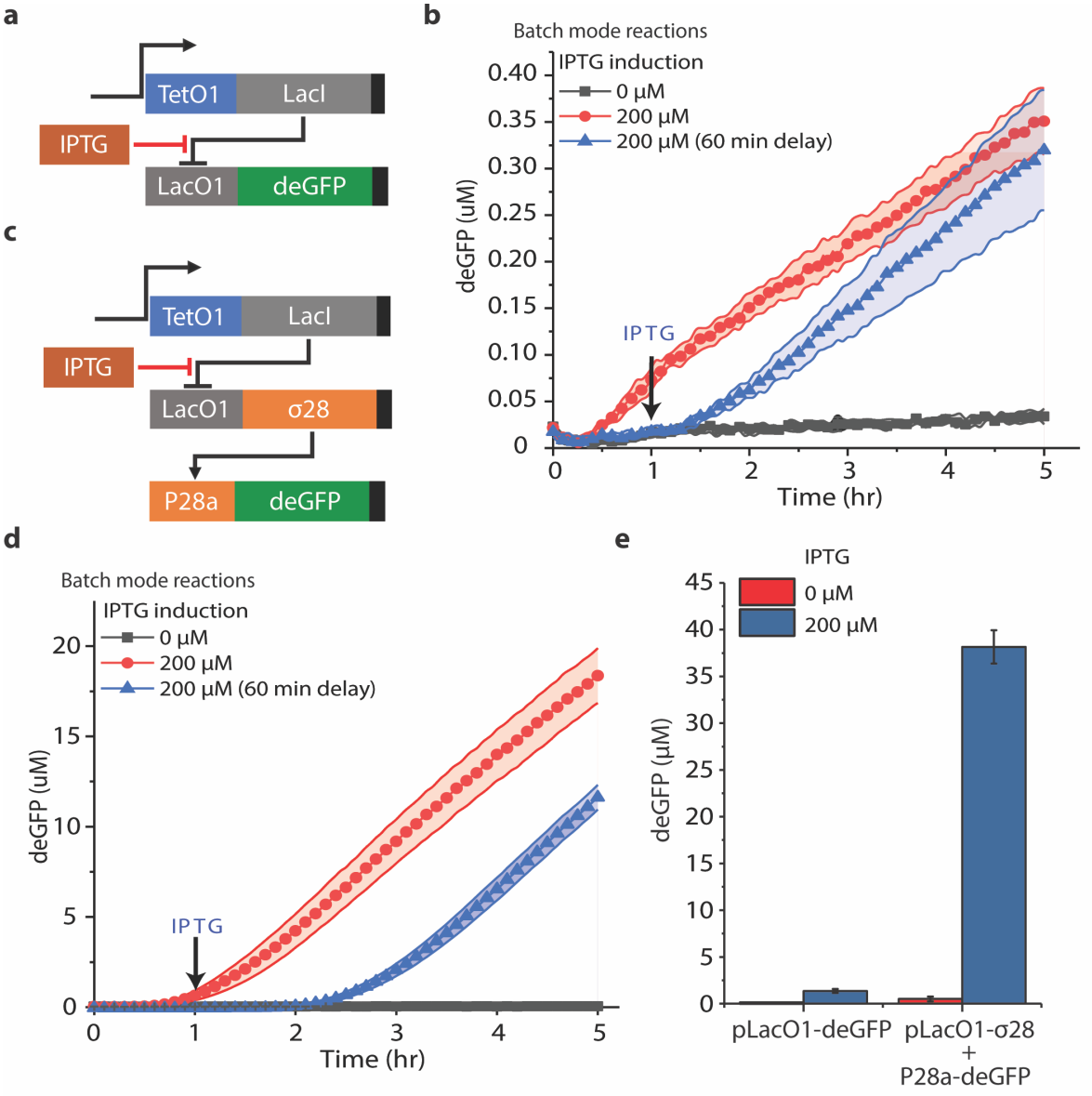

Figure 5.16 **a**) Schematic of the unamplified inducible gene circuit. **b**) Kinetics of deGFP expression in batch mode TXTL reactions using the circuit shown in a) with: no IPTG; induction at time T = 0 h; and delayed induction at time T = 1 h. **c**) Schematic of an amplified inducible circuit using the σ28 cascade. **d**) Kinetics of deGFP expression in batch mode TXTL reactions using the circuit shown in c) with: no IPTG; induction at time T = 0 h; and delayed induction at time T = 1 h. **e**) Plot of endpoint deGFP expression with and without IPTG induction after 14 h for the gene circuits shown in a) and c).

Figure 5.16 compares both the original PL-LacO1 cascade with the σ28-amplified version. In the simple cascade, GFP production increases linearly once detected after 30 minutes for over five hours when IPTG is a part of the initial TXTL reaction (Fig. 5.16a-

b). When IPTG is added after 60 minutes, deGFP is detected 30 minutes later and the synthesis is linear. In both cases, total protein concentration is low, reaching ~0.3 μM after 5 hours. The case where no IPTG is present shows minimal expression, above background fluorescence by a negligible amount. With the amplifier, the cascade behaves starkly different (Fig. 5.16c-d). The time needed to detect deGFP doubles to 60 minutes, unsurprisingly as the expression of σ28 is now required. When IPTG is added to the reaction after 60 minutes, the delay to produce synthesize is again 60 minutes after induction. Both the reaction where IPTG is present at the onset and the reaction that is induced show a linear increase in deGFP until 18 and 12 μM deGFP are expressed, respectively. The negative control again shows negligible protein production. Endpoint deGFP is shown in the final panel, Fig. 5.16e. Here, we see the enormous increase in protein production between the simple cascade (1.3 μM) and the amplifier (38.5 μM). Furthermore, the ON/OFF ratio for the classic circuit is 11, while the amplifier reaches an ON/OFF of 298, indicating the circuit offers a high degree of regulation.

The final iteration of our synthetic cell prototype now needed to move beyond showing a change in gene expression in response to hypo-osmotic conditions and the external chemical environment by changing its own cellular morphology. As our experimental output of this, we cloned a P28a-venus-MreB plasmid to place at the end of the σ28 amplifier in the place of P28a-deGFP. Thus, only when IPTG activated the amplified cascade would MreB be expressing, evidenced by being a fluorescent fusion protein. The experimental scheme for this third iteration is shown in Figure 5.17a. The T7 RNA polymerase required for the expression of MscL is added to the encapsulated reaction as a purified protein.

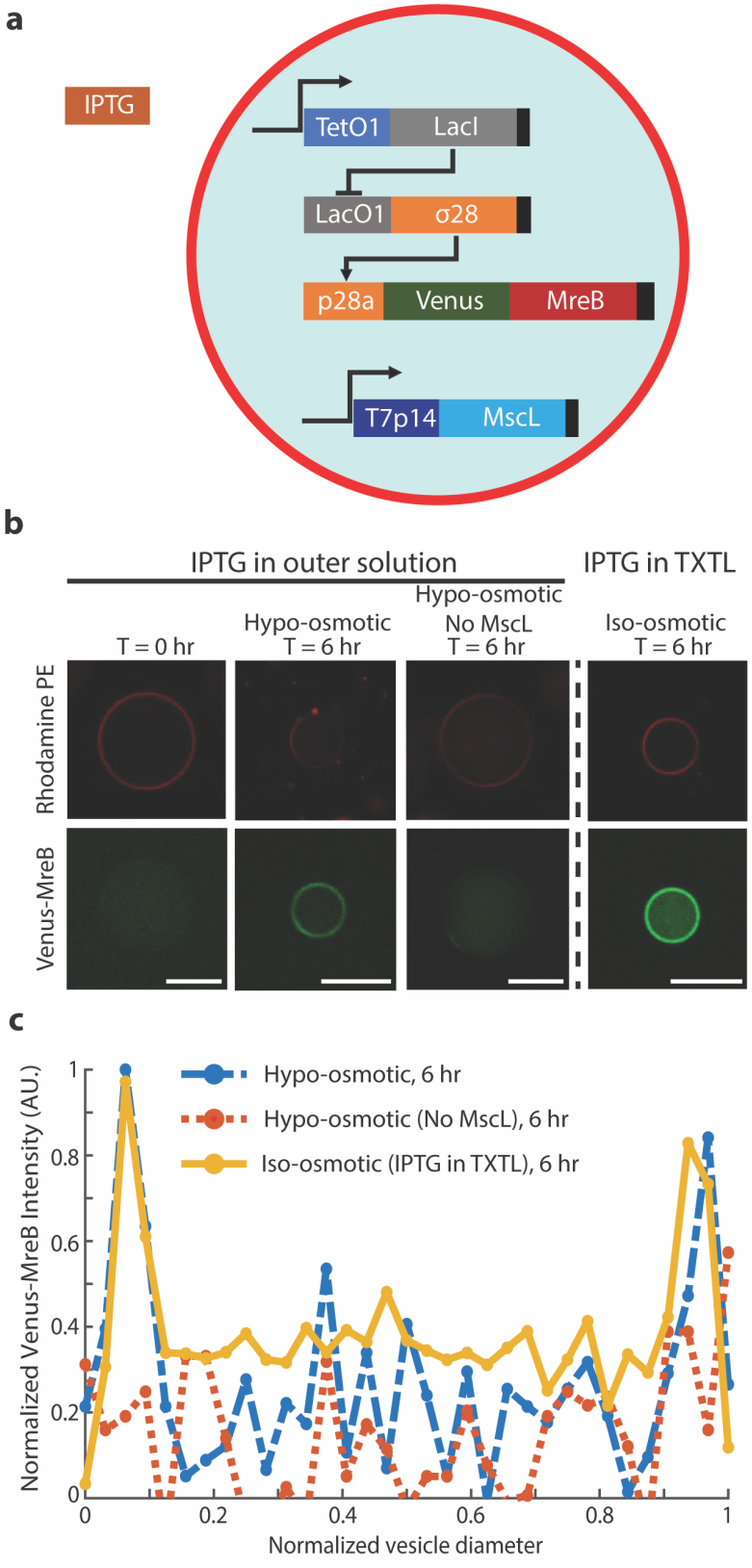

Figure 5.17 **a**) Schematic depicting the third proposed synthetic cell system co-expressing an amplified gene circuit encoding the gene for Venus-MreB and MscL constitutively. The liposomes were placed in a feeding solution containing 200 μM IPTG, except for the control experiment (IPTG inside liposomes). **b**) IPTG induction of synthetic cells in outer solutions containing IPTG and different osmotic conditions over a time duration of 6 h and a positive control experiment with IPTG inside the liposomes. **c**) Line scans of each liposome marked in b), normalized with respect to their diameters and individual maximum intensities. Scale bars: 50 μm.

The microscopy images show both a fluorescent lipid, used to label the membrane, in red and the fluorescence from the venus-MreB fusion in green. After 6 hours of incubation in hypo-osmotic solution containing IPTG, only the vesicles programmed to express MscL show an increase in the green channel, with this fluorescence being concentrated at the membrane (Fig. 5.17b). When IPTG is encapsulated in iso-osmotic solutions as a positive control, a similar concentration of fluorescence is seen at the membrane. Linescan traces were performed to further analyze the localization of the fluorescence caused by the venus-MreB (Fig. 5.17c). The traces from the positive control (solid yellow) and the hypo-osmotic+MscL (dashed blue) vesicles display a peak in fluorescence at the edges of the liposome, while the trace of the hypo-osmotic+blank (dotted orange) indicates an even distribution of fluorescence across the entire lumen. While these synthetic cells do not manifest MreB polymerization, this is likely due to their lifespan being on the order of 6 hours at which time peak expression for this type of complex reaction is not reached.

These data, taken as a whole, represent a minimal cell model that leverages TXTL to reconstitute inter-cellular and extra-cellular interactions towards the development of capabilities to respond to external time variant stimuli. Multiple proteins are expressed and separated both spatially and temporally. Similar orthogonal circuits to these described could be used to create a more complex synthetic cell, with multiple agonists than reconstitute a variety of inter-cellular processes. Indeed, even different pores could be used with different size cut-offs, which would add another level to the response mechanism of the prototype. These synthetic cell prototypes would allow researchers to better understand the dynamics of multi-protein interactions and step-by-step assembly architectures in order to probe the complex inner workings of real cells.

Chapter 6

Conclusion

Modern cell-free protein expression systems are diverse and robust, with the ability to produce recombinant protein at levels thousands of times greater than the platforms they grew out of. The current cell-free systems have evolved to meet the demands of biology, chemistry, physics, engineering, and medicine, broaching problems that are both fundamental and applicable. Over the course of my graduate career, I have helped optimize an all *E. coli* TXTL capable of producing over 2 mg/ml of recombinant protein in batch mode reactions. TXTL is able to utilize plasmid and linear DNA to carry out complex reactions and gene circuits, functioning in a wide range of conditions spanning nine orders of magnitude, from femtoliter (liposomes) to microliter volumes (bulk reactions). The entirety of the *E. coli* transcriptional and translational regulatory system is available in TXTL, including the full complement of sigma factors. Limiting the scope of this work to strictly test tube reactions, we could consider TXTL to be one of the most robust and versatile platforms capable of constructing complex biological systems through the execution of DNA programs composed of synthetic and natural bacterial regulatory parts. I have also demonstrated that TXTL can be used for applications beyond protein synthesis, for example as a mimetic cytoplasm. One of the major difficulties with translating DNA nanotechnology into living systems is the stability of these DNA structures, and in this thesis I showed that TXTL can be used to simulate an *E. coli* cytoplasm while introducing modifications to DNA nanotubes to improve their viability in real biological environments.

My initial interest in TXTL and biophysics writ large stems from their potential ability to address fundamental questions surrounding the origin of life. During the course of my thesis, TXTL was combined with the emulsion transfer method to investigate fundamental living systems by attempting to recapitulate synthetic cells *in vitro*. By developing these two techniques in tandem, I have created a robust platform for the construction of synthetic cells capable of self-reproduction. To carry out this construction, I used alpha-hemolysin to increase cell-free protein synthesis in liposomes while

executing larger (five and six) gene circuits, both necessities in order to recapitulate complex cellular functions. This synthetic cell prototyping platform allows for the variation of the composition of the bilayer membrane as well as the composition of the local cellular environment, simulated by the aqueous solution in which the synthetic cells reside. The lipid bilayer is the physical boundary hosting the molecular mechanisms to exchange nutrients and ions with the cellular exterior, making its complexion critical. By altering this, we can better understand how membrane proteins interact with various lipid combinations. It also allows for the creation of synthetic cells with bilayer compositions closer to that of the living systems that we are attempting to replicate. A synthetic cell platform that allows the modification of the external solution allows the study of how membrane proteins respond to different chemical environments, while also making it possible to create external solutions that mimic the conditions in which living cells reside.

This thesis also describes several synthetic cell prototypes made possible by the developed of the platform composed of a powerful TXTL and the emulsion transfer method. Liposomes were programmed with TXTL to express proteins that give them mechanosensitive and biosensing capabilities, creating the first biosensor of its kind. To do so, I used techniques that I optimized to encapsulate complex gene circuits as well as modify the environment of the synthetic cell. A synthetic cell prototype with mechanosensitive functions that is able to sense external small molecules using genetically-encoded biosensors allows for rapid, quantitative sensing, as opposed to relying on protein synthesis to measure a response. Similar synthetic cell prototypes were further engineered to reconstitute inter-cellular and extracellular interactions by enabling synthetic cells to respond to external, time-varying stimuli. Novel genetic circuits based on synthetic and inducible regulatory parts were combined with *E. coli* sigma factor cascades to enhance the dynamic range of the overall circuit in order to allow the synthetic cell prototypes to be adaptive to their environment, responding to an external chemical signal to alter their genetic expression programs and, in turn, change their cytoskeletal structure. Both of these prototypes recapitulate a primary feature of real cells, namely their ability to actively interact with their surroundings, particularly in stressed conditions.

Though much works remains to be done to realize the construction of a bottom-up minimal cell able to grow and evolve, the work described in this thesis presents a new toolbox for achieving this goal, as well as the foundation for synthetic cell prototypes capable of responding to their environment. This foundation can be readily expanded by leveraging orthogonal TXTL reactions to mediate simultaneous or sequential induction using circuits inducible to different molecules, providing modularity in the number of different systems that can be reconstituted in the same compartment. In creating ever more complex synthetic cells, we can begin to better approximate the complexities of real cells by learning the dynamics of multi-protein interactions or step-by-step assembly.

References

[1] R. A. Le Feuvre and N. S. Scrutton, "A living foundry for Synthetic Biological Materials: A synthetic biology roadmap to new advanced materials," *Synth. Syst. Biotechnol.*, vol. 3, no. 2, pp. 105–112, Jun. 2018.

[2] M. J. Smanski, H. Zhou, J. Claesen, B. Shen, M. A. Fischbach, and C. A. Voigt, "Synthetic biology to access and expand nature's chemical diversity," *Nat. Rev. Microbiol.*, vol. 14, no. 3, pp. 135–149, Mar. 2016.

[3] T. Chien, A. Doshi, and T. Danino, "Advances in bacterial cancer therapies using synthetic biology," *Curr. Opin. Syst. Biol.*, vol. 5, pp. 1–8, Oct. 2017.

[4] A. Madhavan, A. A. Jose, P. Binod, R. Sindhu, R. K. Sukumaran, A. Pandey, and G. E. Castro, "Synthetic Biology and Metabolic Engineering Approaches and Its Impact on Non-Conventional Yeast and Biofuel Production," *Front. Energy Res.*, vol. 5, p. 8, Apr. 2017.

[5] D. E. Cameron, C. J. Bashor, and J. J. Collins, "A brief history of synthetic biology," *Nat. Rev. Microbiol.*, vol. 12, no. 5, pp. 381–390, May 2014.

[6] J. MONOD and F. JACOB, "Teleonomic mechanisms in cellular metabolism, growth, and differentiation.," *Cold Spring Harb. Symp. Quant. Biol.*, vol. 26, pp. 389–401, 1961.

[7] F. Jacob and J. Monod, "On the Regulation of Gene Activity," *Cold Spring Harb. Symp. Quant. Biol.*, vol. 26, no. 0, pp. 193–211, Jan. 1961.

[8] F. Jacob and J. Monod, "Genetic regulatory mechanisms in the synthesis of proteins," *J. Mol. Biol.*, vol. 3, no. 3, pp. 318–356, Jun. 1961.

[9] S. Desiderio and S. Boyer, "Arber, Smith and Nathans: Nobel Laureates in medicine and physiology, 1978.," *Johns Hopkins Med. J.*, vol. 143, no. 5, pp. ix–x, Nov. 1978.

[10] Bio FAB Group, D. Baker, G. Church, J. Collins, D. Endy, J. Jacobson, J. Keasling, P. Modrich, C. Smolke, and R. Weiss, "Engineering life: building a fab for biology.," *Sci. Am.*, vol. 294, no. 6, pp. 44–51, Jun. 2006.

[11] P. E. M. Purnick and R. Weiss, "The second wave of synthetic biology: from modules to systems.," *Nat. Rev. Mol. Cell Biol.*, vol. 10, no. 6, pp. 410–22, Jun. 2009.

[12] M. B. Elowitz and S. Leibler, "A synthetic oscillatory network of transcriptional regulators.," *Nature*, vol. 403, no. 6767, pp. 335–8, Jan. 2000.

[13] T. S. Gardner, C. R. Cantor, and J. J. Collins, "Construction of a genetic toggle switch in Escherichia coli.," *Nature*, vol. 403, no. 6767, pp. 339–42, Jan. 2000.

[14] S. Basu, Y. Gerchman, C. H. Collins, F. H. Arnold, and R. Weiss, "A synthetic multicellular system for programmed pattern formation," *Nature*, vol. 434, no. 7037, pp. 1130–1134, Apr. 2005.

[15] N. J. Guido, X. Wang, D. Adalsteinsson, D. McMillen, J. Hasty, C. R. Cantor, T. C. Elston, and J. J. Collins, "A bottom-up approach to gene regulation.," *Nature*, vol. 439, no. 7078, pp. 856–60, Feb. 2006.

[16] A. Levskaya, A. A. Chevalier, J. J. Tabor, Z. B. Simpson, L. A. Lavery, M. Levy, E. A. Davidson, A. Scouras, A. D. Ellington, E. M. Marcotte, and C. A. Voigt, "Synthetic biology: engineering Escherichia coli to see light.," *Nature*, vol. 438, no.

7067, pp. 441–2, Nov. 2005.
[17] J. Stricker, S. Cookson, M. R. Bennett, W. H. Mather, L. S. Tsimring, and J. Hasty, "A fast, robust and tunable synthetic gene oscillator.," *Nature*, vol. 456, no. 7221, pp. 516–9, Nov. 2008.
[18] A. Tamsir, J. J. Tabor, and C. A. Voigt, "Robust multicellular computing using genetically encoded NOR gates and chemical 'wires'.," *Nature*, vol. 469, no. 7329, pp. 212–5, Jan. 2011.
[19] S. Chong, "Overview of cell-free protein synthesis: historic landmarks, commercial systems, and expanding applications.," *Curr. Protoc. Mol. Biol.*, vol. 108, p. 16.30.1-11, Oct. 2014.
[20] M. W. NIRENBERG and J. H. MATTHAEI, "The dependence of cell-free protein synthesis in E. coli upon naturally occurring or synthetic polyribonucleotides.," *Proc. Natl. Acad. Sci. U. S. A.*, vol. 47, pp. 1588–602, Oct. 1961.
[21] D. A. Chambers and G. Zubay, "The stimulatory effect of cyclic adenosine 3'5'-monophosphate on DNA-directed synthesis of beta-galactosidase in a cell-free system.," *Proc. Natl. Acad. Sci. U. S. A.*, vol. 63, no. 1, pp. 118–22, May 1969.
[22] G. Zubay, "In Vitro Synthesis of Protein in Microbial Systems," *Annu. Rev. Genet.*, vol. 7, no. 1, pp. 267–287, Dec. 1973.
[23] D. Craig, M. T. Howell, C. L. Gibbs, T. Hunt, and R. J. Jackson, "Plasmid cDNA-directed protein synthesis in a coupled eukaryotic in vitro transcription-translation system.," *Nucleic Acids Res.*, vol. 20, no. 19, pp. 4987–95, Oct. 1992.
[24] P. A. Krieg and D. A. Melton, "In vitro RNA synthesis with SP6 RNA polymerase.," *Methods Enzymol.*, vol. 155, pp. 397–415, 1987.
[25] D. E. Nevin and J. M. Pratt, "A coupled in vitro transcription-translation system for the exclusive synthesis of polypeptides expressed from the T7 promoter.," *FEBS Lett.*, vol. 291, no. 2, pp. 259–63, Oct. 1991.
[26] A. S. Spirin, V. I. Baranov, L. A. Ryabova, S. Y. Ovodov, and Y. B. Alakhov, "A continuous cell-free translation system capable of producing polypeptides in high yield.," *Science*, vol. 242, no. 4882, pp. 1162–4, Nov. 1988.
[27] L. A. Ryabova, Morozov IYu, and A. S. Spirin, "Continuous-flow cell-free translation, transcription-translation, and replication-translation systems.," *Methods Mol. Biol.*, vol. 77, pp. 179–93, 1998.
[28] V. A. Shirokov, A. Kommer, V. A. Kolb, and A. S. Spirin, "Continuous-exchange protein-synthesizing systems.," *Methods Mol. Biol.*, vol. 375, pp. 19–55, 2007.
[29] Y. Shimizu, A. Inoue, Y. Tomari, T. Suzuki, T. Yokogawa, K. Nishikawa, and T. Ueda, "Cell-free translation reconstituted with purified components.," *Nat. Biotechnol.*, vol. 19, no. 8, pp. 751–5, Aug. 2001.
[30] Y. Shimizu, T. Kanamori, and T. Ueda, "Protein synthesis by pure translation systems.," *Methods*, vol. 36, no. 3, pp. 299–304, Jul. 2005.
[31] J. Shin and V. Noireaux, "An E. coli cell-free expression toolbox: application to synthetic gene circuits and artificial cells.," *ACS Synth. Biol.*, vol. 1, no. 1, pp. 29–41, Jan. 2012.
[32] F. Caschera and V. Noireaux, "Synthesis of 2.3 mg/ml of protein with an all Escherichia coli cell-free transcription-translation system.," *Biochimie*, vol. 99, pp. 162–8, Apr. 2014.

[33] J. G. Perez, J. C. Stark, and M. C. Jewett, “Cell-Free Synthetic Biology: Engineering Beyond the Cell.,” *Cold Spring Harb. Perspect. Biol.*, vol. 8, no. 12, Dec. 2016.

[34] S. Mikami, T. Kobayashi, and H. Imataka, “Cell-free protein synthesis systems with extracts from cultured human cells.,” *Methods Mol. Biol.*, vol. 607, pp. 43–52, 2010.

[35] K. Madin, T. Sawasaki, T. Ogasawara, and Y. Endo, “A highly efficient and robust cell-free protein synthesis system prepared from wheat embryos: plants apparently contain a suicide system directed at ribosomes.,” *Proc. Natl. Acad. Sci. U. S. A.*, vol. 97, no. 2, pp. 559–64, Jan. 2000.

[36] R. J. Jackson and T. Hunt, “Preparation and use of nuclease-treated rabbit reticulocyte lysates for the translation of eukaryotic messenger RNA.,” *Methods Enzymol.*, vol. 96, pp. 50–74, 1983.

[37] C. W. Anderson, J. W. Straus, and B. S. Dudock, “Preparation of a cell-free protein-synthesizing system from wheat germ.,” *Methods Enzymol.*, vol. 101, pp. 635–44, 1983.

[38] K. Ishikawa, K. Sato, Y. Shima, I. Urabe, and T. Yomo, “Expression of a cascading genetic network within liposomes.,” *FEBS Lett.*, vol. 576, no. 3, pp. 387–90, Oct. 2004.

[39] V. Noireaux and A. Libchaber, “A vesicle bioreactor as a step toward an artificial cell assembly.,” *Proc. Natl. Acad. Sci. U. S. A.*, vol. 101, no. 51, pp. 17669–74, Dec. 2004.

[40] J. F. Zawada, G. Yin, A. R. Steiner, J. Yang, A. Naresh, S. M. Roy, D. S. Gold, H. G. Heinsohn, and C. J. Murray, “Microscale to manufacturing scale-up of cell-free cytokine production--a new approach for shortening protein production development timelines.,” *Biotechnol. Bioeng.*, vol. 108, no. 7, pp. 1570–8, Jul. 2011.

[41] T. Jaroentomeechai, J. C. Stark, A. Natarajan, C. J. Glasscock, L. E. Yates, K. J. Hsu, M. Mrksich, M. C. Jewett, and M. P. DeLisa, “Single-pot glycoprotein biosynthesis using a cell-free transcription-translation system enriched with glycosylation machinery.,” *Nat. Commun.*, vol. 9, no. 1, p. 2686, 2018.

[42] R. Marshall, C. S. Maxwell, S. P. Collins, T. Jacobsen, M. L. Luo, M. B. Begemann, B. N. Gray, E. January, A. Singer, Y. He, C. L. Beisel, and V. Noireaux, “Rapid and Scalable Characterization of CRISPR Technologies Using an E. coli Cell-Free Transcription-Translation System.,” *Mol. Cell*, vol. 69, no. 1, p. 146–157.e3, 2018.

[43] I. Dodevski, G. C. Markou, and C. A. Sarkar, “Conceptual and methodological advances in cell-free directed evolution.,” *Curr. Opin. Struct. Biol.*, vol. 33, pp. 1–7, Aug. 2015.

[44] J. Garamella, R. Marshall, M. Rustad, and V. Noireaux, “The All E. coli TX-TL Toolbox 2.0: A Platform for Cell-Free Synthetic Biology.,” *ACS Synth. Biol.*, vol. 5, no. 4, pp. 344–55, Apr. 2016.

[45] S. Periyasamy, A. Gray, and P. Kille, “The bottom–up approach to defining life: deciphering the functional organization of biological cells via multi-objective representation of biological complexity from molecules to cells,” *Front. Physiol.*,

vol. 4, 2013.
[46] F. Caschera and V. Noireaux, “Integration of biological parts toward the synthesis of a minimal cell.,” *Curr. Opin. Chem. Biol.*, vol. 22, pp. 85–91, Oct. 2014.
[47] S. L. MILLER, “A production of amino acids under possible primitive earth conditions.,” *Science*, vol. 117, no. 3046, pp. 528–9, May 1953.
[48] R. V Solé, “Evolution and self-assembly of protocells.,” *Int. J. Biochem. Cell Biol.*, vol. 41, no. 2, pp. 274–84, Feb. 2009.
[49] S. S. Mansy and J. W. Szostak, “Reconstructing the emergence of cellular life through the synthesis of model protocells.,” *Cold Spring Harb. Symp. Quant. Biol.*, vol. 74, pp. 47–54, 2009.
[50] D. A. Hammer and N. P. Kamat, “Towards an artificial cell.,” *FEBS Lett.*, vol. 586, no. 18, pp. 2882–90, Aug. 2012.
[51] N. P. Kamat, J. S. Katz, and D. A. Hammer, “Engineering Polymersome Protocells,” *J. Phys. Chem. Lett.*, vol. 2, no. 13, pp. 1612–1623, Jul. 2011.
[52] C. Xu, S. Hu, and X. Chen, “Artificial cells: from basic science to applications,” *Mater. Today (Kidlington).*, vol. 19, no. 9, p. 516, 2016.
[53] D. G. Gibson, J. I. Glass, C. Lartigue, V. N. Noskov, R.-Y. Chuang, M. A. Algire, G. A. Benders, M. G. Montague, L. Ma, M. M. Moodie, C. Merryman, S. Vashee, R. Krishnakumar, N. Assad-Garcia, C. Andrews-Pfannkoch, E. A. Denisova, L. Young, Z.-Q. Qi, T. H. Segall-Shapiro, C. H. Calvey, P. P. Parmar, C. A. Hutchison, H. O. Smith, and J. C. Venter, “Creation of a Bacterial Cell Controlled by a Chemically Synthesized Genome,” *Science (80-.).*, vol. 329, no. 5987, pp. 52–56, Jul. 2010.
[54] J. I. Glass, N. Assad-Garcia, N. Alperovich, S. Yooseph, M. R. Lewis, M. Maruf, C. A. Hutchison, H. O. Smith, J. C. Venter, and J. C. Venter, “Essential genes of a minimal bacterium.,” *Proc. Natl. Acad. Sci. U. S. A.*, vol. 103, no. 2, pp. 425–30, Jan. 2006.
[55] C. A. Hutchison, R.-Y. Chuang, V. N. Noskov, N. Assad-Garcia, T. J. Deerinck, M. H. Ellisman, J. Gill, K. Kannan, B. J. Karas, L. Ma, J. F. Pelletier, Z.-Q. Qi, R. A. Richter, E. A. Strychalski, L. Sun, Y. Suzuki, B. Tsvetanova, K. S. Wise, H. O. Smith, J. I. Glass, C. Merryman, D. G. Gibson, and J. C. Venter, “Design and synthesis of a minimal bacterial genome,” *Science (80-.).*, vol. 351, no. 6280, pp. aad6253-aad6253, Mar. 2016.
[56] R. Marshall, J. Garamella, V. Noireaux, and A. Pierson, “High-Throughput Microliter-Sized Cell-Free Transcription-Translation Reactions for Synthetic Biology Applications Using the Echo® 550 Liquid Handler,” 2018.
[57] J. Garamella, D. Garenne, and V. Noireaux, “TXTL-based approach to synthetic cells,” 2019, pp. 217–239.
[58] M. A. Klocke, J. Garamella, H. K. K. Subramanian, V. Noireaux, and E. Franco, “Engineering DNA nanotubes for resilience in an E. coli TXTL system,” *Synth. Biol.*, vol. 3, no. 1, Jan. 2018.
[59] S. Majumder, J. Garamella, Y.-L. Wang, M. DeNies, V. Noireaux, and A. P. Liu, “Cell-sized mechanosensitive and biosensing compartment programmed with DNA,” *Chem. Commun.*, vol. 53, no. 53, pp. 7349–7352, Jun. 2017.
[60] H. Maeda, N. Fujita, and A. Ishihama, “Competition among seven Escherichia coli

sigma subunits: relative binding affinities to the core RNA polymerase.," *Nucleic Acids Res.*, vol. 28, no. 18, pp. 3497–503, Sep. 2000.
[61] T. M. Gruber and C. A. Gross, "Multiple Sigma Subunits and the Partitioning of Bacterial Transcription Space," *Annu. Rev. Microbiol.*, vol. 57, no. 1, pp. 441–466, Oct. 2003.
[62] Z. Z. Sun, C. A. Hayes, J. Shin, F. Caschera, R. M. Murray, and V. Noireaux, "Protocols for Implementing an Escherichia coli Based TX-TL Cell-Free Expression System for Synthetic Biology," *J. Vis. Exp.*, no. 79, p. e50762, Sep. 2013.
[63] F. Caschera and V. Noireaux, "A cost-effective polyphosphate-based metabolism fuels an all E. coli cell-free expression system," *Metab. Eng.*, vol. 27, pp. 29–37, Jan. 2015.
[64] F. Caschera and V. Noireaux, "Preparation of amino acid mixtures for cell-free expression systems.," *Biotechniques*, vol. 58, no. 1, pp. 40–3, Jan. 2015.
[65] D. Collias, R. Marshall, S. P. Collins, C. L. Beisel, and V. Noireaux, "An educational module to explore CRISPR technologies with a cell-free transcription-translation system," *Synth. Biol.*, vol. 4, no. 1, Jan. 2019.
[66] T. D. Craggs, "Green fluorescent protein: structure, folding and chromophore maturation," *Chem. Soc. Rev.*, vol. 38, no. 10, p. 2865, Oct. 2009.
[67] E. Karzbrun, A. M. Tayar, V. Noireaux, and R. H. Bar-Ziv, "Programmable on-chip DNA compartments as artificial cells," *Science (80-.).*, vol. 345, no. 6198, pp. 829–832, Aug. 2014.
[68] R. Marshall, J. Garamella, V. Noireaux, and A. Pierson, "High-Throughput Microliter-Sized Cell-Free Transcription-Translation Reactions for Synthetic Biology Applications using the Echo 550 Liquid Handler," *Labcyte*, 2018. [Online]. Available: https://www.labcyte.com/content/applications/high-throughput-microliter-sized-cell-free-transcription-translation. [Accessed: 27-Mar-2019].
[69] T. Kigawa and S. Yokoyama, "A continuous cell-free protein synthesis system for coupled transcription-translation.," *J. Biochem.*, vol. 110, no. 2, pp. 166–8, Aug. 1991.
[70] R. Lutz and H. Bujard, "Independent and tight regulation of transcriptional units in Escherichia coli via the LacR/O, the TetR/O and AraC/I1-I2 regulatory elements.," *Nucleic Acids Res.*, vol. 25, no. 6, pp. 1203–10, Mar. 1997.
[71] K. Sitaraman, D. Esposito, G. Klarmann, S. F. Le Grice, J. L. Hartley, and D. K. Chatterjee, "A novel cell-free protein synthesis system," *J. Biotechnol.*, vol. 110, no. 3, pp. 257–263, Jun. 2004.
[72] M. Spies, I. Amitani, R. J. Baskin, and S. C. Kowalczykowski, "RecBCD enzyme switches lead motor subunits in response to chi recognition.," *Cell*, vol. 131, no. 4, pp. 694–705, Nov. 2007.
[73] N. Michel-Reydellet, K. Woodrow, and J. Swartz, "Increasing PCR Fragment Stability and Protein Yields in a Cell-Free System with Genetically Modified <i>Escherichia coli </i>Extracts," *J. Mol. Microbiol. Biotechnol.*, vol. 9, no. 1, pp. 26–34, 2005.
[74] G. R. Smith, "How RecBCD Enzyme and Chi Promote DNA Break Repair and

Recombination: a Molecular Biologist's View," *Microbiol. Mol. Biol. Rev.*, vol. 76, no. 2, pp. 217–228, Jun. 2012.
[75] F. W. Studier and B. A. Moffatt, "Use of bacteriophage T7 RNA polymerase to direct selective high-level expression of cloned genes.," *J. Mol. Biol.*, vol. 189, no. 1, pp. 113–30, May 1986.
[76] D. J. Studholme and M. Buck, "The biology of enhancer-dependent transcriptional regulation in bacteria: insights from genome sequences," *FEMS Microbiol. Lett.*, vol. 186, no. 1, pp. 1–9, May 2000.
[77] T. A. Baker and R. T. Sauer, "ClpXP, an ATP-powered unfolding and protein-degradation machine.," *Biochim. Biophys. Acta*, vol. 1823, no. 1, pp. 15–28, Jan. 2012.
[78] J. M. Flynn, S. B. Neher, Y. I. Kim, R. T. Sauer, and T. A. Baker, "Proteomic discovery of cellular substrates of the ClpXP protease reveals five classes of ClpX-recognition signals.," *Mol. Cell*, vol. 11, no. 3, pp. 671–83, Mar. 2003.
[79] J. Shin and V. Noireaux, "Study of messenger RNA inactivation and protein degradation in an Escherichia coli cell-free expression system," *J. Biol. Eng.*, vol. 4, no. 1, p. 9, Jul. 2010.
[80] J. Ouellet, "RNA Fluorescence with Light-Up Aptamers.," *Front. Chem.*, vol. 4, p. 29, 2016.
[81] J. Shin and V. Noireaux, "Efficient cell-free expression with the endogenous E. Coli RNA polymerase and sigma factor 70," *J. Biol. Eng.*, vol. 4, no. 1, p. 8, Jun. 2010.
[82] B. T. Bajar, E. S. Wang, S. Zhang, M. Z. Lin, and J. Chu, "A Guide to Fluorescent Protein FRET Pairs.," *Sensors (Basel).*, vol. 16, no. 9, Sep. 2016.
[83] C. Depry and J. Zhang, "Using FRET-based reporters to visualize subcellular dynamics of protein kinase A activity.," *Methods Mol. Biol.*, vol. 756, pp. 285–94, 2011.
[84] Y. T. Maeda, T. Nakadai, J. Shin, K. Uryu, V. Noireaux, and A. Libchaber, "Assembly of MreB filaments on liposome membranes: A synthetic biology approach," *ACS Synth. Biol.*, vol. 1, pp. 53–59, 2012.
[85] A. S. Spirin, "High-throughput cell-free systems for synthesis of functionally active proteins," *Trends Biotechnol.*, vol. 22, no. 10, pp. 538–545, Oct. 2004.
[86] D. Deamer, "A giant step towards artificial life?," *Trends Biotechnol.*, vol. 23, no. 7, pp. 336–338, Jul. 2005.
[87] V. Noireaux and A. Libchaber, "A vesicle bioreactor as a step toward an artificial cell assembly.," *Proc. Natl. Acad. Sci. U. S. A.*, vol. 101, no. 51, pp. 17669–74, Dec. 2004.
[88] Y. Kuruma, P. Stano, T. Ueda, and P. L. Luisi, "A synthetic biology approach to the construction of membrane proteins in semi-synthetic minimal cells," *Biochim. Biophys. Acta - Biomembr.*, vol. 1788, no. 2, pp. 567–574, Feb. 2009.
[89] P. Walde, K. Cosentino, H. Engel, and P. Stano, "Giant vesicles: preparations and applications.," *Chembiochem*, vol. 11, no. 7, pp. 848–65, May 2010.
[90] J. P. Reeves and R. M. Dowben, "Formation and properties of thin-walled phospholipid vesicles.," *J. Cell. Physiol.*, vol. 73, no. 1, pp. 49–60, Feb. 1969.
[91] M. I. Angelova and D. S. Dimitrov, "Liposome electroformation," *Faraday*

Discuss. Chem. Soc., vol. 81, p. 303, Jan. 1986.

[92] E. K. Sackmann, A. L. Fulton, and D. J. Beebe, "The present and future role of microfluidics in biomedical research," *Nature*, vol. 507, no. 7491, pp. 181–189, Mar. 2014.

[93] S. Pautot, B. J. Frisken, and D. A. Weitz, "Engineering asymmetric vesicles.," *Proc. Natl. Acad. Sci. U. S. A.*, vol. 100, no. 19, pp. 10718–21, Sep. 2003.

[94] E. Hand, "The planetary police.," *Nature*, vol. 459, no. 7245, pp. 308–9, May 2009.

[95] P. H. Rampelotto, "Extremophiles and extreme environments.," *Life (Basel, Switzerland)*, vol. 3, no. 3, pp. 482–5, Aug. 2013.

[96] R. Mehta, P. Singhal, H. Singh, D. Damle, and A. K. Sharma, "Insight into thermophiles and their wide-spectrum applications.," *3 Biotech*, vol. 6, no. 1, p. 81, Jun. 2016.

[97] P. Gabani and O. V Singh, "Radiation-resistant extremophiles and their potential in biotechnology and therapeutics.," *Appl. Microbiol. Biotechnol.*, vol. 97, no. 3, pp. 993–1004, Feb. 2013.

[98] O. Ces and X. Mulet, "Physical coupling between lipids and proteins: a paradigm for cellular control," *Signal Transduct.*, vol. 6, no. 2, pp. 112–132, Apr. 2006.

[99] C. Sohlenkamp and O. Geiger, "Bacterial membrane lipids: diversity in structures and pathways," *FEMS Microbiol. Rev.*, vol. 40, no. 1, pp. 133–159, Jan. 2016.

[100] T. Nomura, C. G. Cranfield, E. Deplazes, D. M. Owen, A. Macmillan, A. R. Battle, M. Constantine, M. Sokabe, and B. Martinac, "Differential effects of lipids and lyso-lipids on the mechanosensitivity of the mechanosensitive channels MscL and MscS," *Proc. Natl. Acad. Sci.*, vol. 109, no. 22, pp. 8770–8775, May 2012.

[101] M. Wikström, A. A. Kelly, A. Georgiev, H. M. Eriksson, M. R. Klement, M. Bogdanov, W. Dowhan, and A. Wieslander, "Lipid-engineered Escherichia coli membranes reveal critical lipid headgroup size for protein function.," *J. Biol. Chem.*, vol. 284, no. 2, pp. 954–65, Jan. 2009.

[102] R. A. Cooper, "Influence of increased membrane cholesterol on membrane fluidity and cell function in human red blood cells," *J. Supramol. Struct.*, vol. 8, no. 4, pp. 413–430, 1978.

[103] K. C. Dee, D. A. Puleo, and R. Bizios, *An introduction to tissue-biomaterial interactions*. Wiley-Liss, 2002.

[104] T. Harayama and H. Riezman, "Understanding the diversity of membrane lipid composition," *Nat. Rev. Mol. Cell Biol.*, vol. 19, no. 5, pp. 281–296, Feb. 2018.

[105] P. Charles, V. Stubbs, C. Soto, B. Martin, B. White, and C. Taitt, "Reduction of Non-Specific Protein Adsorption Using Poly(ethylene) Glycol (PEG) Modified Polyacrylate Hydrogels In Immunoassays for Staphylococcal Enterotoxin B Detection," *Sensors*, vol. 9, no. 1, pp. 645–655, Jan. 2009.

[106] X.-F. XIAO, X.-Q. JIANG, and L.-J. ZHOU, "Surface Modification of Poly Ethylene Glycol to Resist Nonspecific Adsorption of Proteins," *Chinese J. Anal. Chem.*, vol. 41, no. 3, pp. 445–453, Mar. 2013.

[107] J. S. Suk, Q. Xu, N. Kim, J. Hanes, and L. M. Ensign, "PEGylation as a strategy for improving nanoparticle-based drug and gene delivery," *Adv. Drug Deliv. Rev.*, vol. 99, no. Pt A, pp. 28–51, Apr. 2016.

[108] D. B. Knowles, A. S. LaCroix, N. F. Deines, I. Shkel, and M. T. Record,

"Separation of preferential interaction and excluded volume effects on DNA duplex and hairpin stability," *Proc. Natl. Acad. Sci.*, vol. 108, no. 31, pp. 12699–12704, Aug. 2011.
[109] S. G. M. Ong, L. C. Ming, K. S. Lee, and K. H. Yuen, "Influence of the Encapsulation Efficiency and Size of Liposome on the Oral Bioavailability of Griseofulvin-Loaded Liposomes.," *Pharmaceutics*, vol. 8, no. 3, p. 25, Aug. 2016.
[110] T. Nii and F. Ishii, "Encapsulation efficiency of water-soluble and insoluble drugs in liposomes prepared by the microencapsulation vesicle method.," *Int. J. Pharm.*, vol. 298, no. 1, pp. 198–205, Jul. 2005.
[111] D. W. Adams and J. Errington, "Bacterial cell division: assembly, maintenance and disassembly of the Z ring.," *Nat. Rev. Microbiol.*, vol. 7, no. 9, pp. 642–53, Sep. 2009.
[112] H. P. Erickson, D. E. Anderson, and M. Osawa, "FtsZ in bacterial cytokinesis: cytoskeleton and force generator all in one.," *Microbiol. Mol. Biol. Rev.*, vol. 74, no. 4, pp. 504–528, 2010.
[113] A. Mukherjee and J. Lutkenhaus, "Guanine nucleotide-dependent assembly of FtsZ into filaments.," *J. Bacteriol.*, vol. 176, no. 9, pp. 2754–8, May 1994.
[114] H. P. Erickson, D. W. Taylor, K. A. Taylor, and D. Bramhill, "Bacterial cell division protein FtsZ assembles into protofilament sheets and minirings, structural homologs of tubulin polymers.," *Proc. Natl. Acad. Sci. U. S. A.*, vol. 93, no. 1, pp. 519–23, Jan. 1996.
[115] E. Bi and J. Lutkenhaus, "FtsZ ring structure associated with division in Escherichia coli," *Nature*, vol. 354, no. 6349, pp. 161–164, Nov. 1991.
[116] P. A. Levin and R. Losick, "Transcription factor Spo0A switches the localization of the cell division protein FtsZ from a medial to a bipolar pattern in Bacillus subtilis.," *Genes Dev.*, vol. 10, no. 4, pp. 478–88, Feb. 1996.
[117] X. Ma, D. W. Ehrhardt, and W. Margolin, "Colocalization of cell division proteins FtsZ and FtsA to cytoskeletal structures in living Escherichia coli cells by using green fluorescent protein.," *Proc. Natl. Acad. Sci. U. S. A.*, vol. 93, no. 23, pp. 12998–3003, Nov. 1996.
[118] M. E. G. Aarsman, A. Piette, C. Fraipont, T. M. F. Vinkenvleugel, M. Nguyen-Distèche, and T. den Blaauwen, "Maturation of the Escherichia coli divisome occurs in two steps," *Mol. Microbiol.*, vol. 55, no. 6, pp. 1631–1645, Mar. 2005.
[119] T. Den Blaauwen, N. Buddelmeijer, M. E. Aarsman, C. M. Hameete, and N. Nanninga, "Timing of FtsZ assembly in Escherichia coli.," *J. Bacteriol.*, vol. 181, no. 17, pp. 5167–75, Sep. 1999.
[120] S. Pichoff and J. Lutkenhaus, "Unique and overlapping roles for ZipA and FtsA in septal ring assembly in Escherichia coli.," *EMBO J.*, vol. 21, no. 4, pp. 685–93, Feb. 2002.
[121] C. A. Hale and P. A. de Boer, "Direct binding of FtsZ to ZipA, an essential component of the septal ring structure that mediates cell division in E. coli.," *Cell*, vol. 88, no. 2, pp. 175–85, Jan. 1997.
[122] C. A. Hale and P. A. de Boer, "Recruitment of ZipA to the septal ring of Escherichia coli is dependent on FtsZ and independent of FtsA.," *J. Bacteriol.*, vol. 181, no. 1, pp. 167–76, Jan. 1999.

[123] Z. Liu, A. Mukherjee, and J. Lutkenhaus, “Recruitment of ZipA to the division site by interaction with FtsZ.,” *Mol. Microbiol.*, vol. 31, no. 6, pp. 1853–61, Mar. 1999.
[124] C. S. Bernard, M. Sadasivam, D. Shiomi, and W. Margolin, “An altered FtsA can compensate for the loss of essential cell division protein FtsN in Escherichia coli.,” *Mol. Microbiol.*, vol. 64, no. 5, pp. 1289–305, Jun. 2007.
[125] S. Rueda, M. Vicente, and J. Mingorance, “Concentration and assembly of the division ring proteins FtsZ, FtsA, and ZipA during the Escherichia coli cell cycle.,” *J. Bacteriol.*, vol. 185, no. 11, pp. 3344–51, Jun. 2003.
[126] A. Feucht, I. Lucet, M. D. Yudkin, and J. Errington, “Cytological and biochemical characterization of the FtsA cell division protein of Bacillus subtilis.,” *Mol. Microbiol.*, vol. 40, no. 1, pp. 115–25, Apr. 2001.
[127] E. J. Cabré, A. Sánchez-Gorostiaga, P. Carrara, N. Ropero, M. Casanova, P. Palacios, P. Stano, M. Jiménez, G. Rivas, and M. Vicente, “Bacterial division proteins FtsZ and ZipA induce vesicle shrinkage and cell membrane invagination,” *J. Biol. Chem.*, vol. 288, pp. 26625–26634, 2013.
[128] M. Osawa and H. P. Erickson, “Liposome division by a simple bacterial division machinery.,” *Proc. Natl. Acad. Sci. U. S. A.*, vol. 110, no. 27, pp. 11000–4, 2013.
[129] A. Martos, B. Monterroso, S. Zorrilla, B. Reija, C. Alfonso, J. Mingorance, G. Rivas, and M. Jiménez, “Isolation, characterization and lipid-binding properties of the recalcitrant FtsA division protein from Escherichia coli.,” *PLoS One*, vol. 7, no. 6, p. e39829, Jan. 2012.
[130] B. Geissler, D. Elraheb, and W. Margolin, “A gain-of-function mutation in ftsA bypasses the requirement for the essential cell division gene zipA in Escherichia coli.,” *Proc. Natl. Acad. Sci. U. S. A.*, vol. 100, no. 7, pp. 4197–202, Apr. 2003.
[131] B. Lara, A. I. Rico, S. Petruzzelli, A. Santona, J. Dumas, J. Biton, M. Vicente, J. Mingorance, and O. Massidda, “Cell division in cocci: localization and properties of the Streptococcus pneumoniae FtsA protein.,” *Mol. Microbiol.*, vol. 55, no. 3, pp. 699–711, Feb. 2005.
[132] P. Szwedziak, Q. Wang, S. M. Freund, and J. Löwe, “FtsA forms actin-like protofilaments,” *EMBO J.*, vol. 31, no. 10, pp. 2249–2260, May 2012.
[133] L. J. Jones, R. Carballido-López, and J. Errington, “Control of cell shape in bacteria: helical, actin-like filaments in Bacillus subtilis.,” *Cell*, vol. 104, no. 6, pp. 913–22, Mar. 2001.
[134] T. Kruse, J. Møller-Jensen, A. Løbner-Olesen, and K. Gerdes, “Dysfunctional MreB inhibits chromosome segregation in Escherichia coli.,” *EMBO J.*, vol. 22, no. 19, pp. 5283–92, Oct. 2003.
[135] T. Kruse, J. Bork-Jensen, and K. Gerdes, “The morphogenetic MreBCD proteins of Escherichia coli form an essential membrane-bound complex.,” *Mol. Microbiol.*, vol. 55, no. 1, pp. 78–89, Jan. 2005.
[136] F. van den Ent, M. Leaver, F. Bendezu, J. Errington, P. de Boer, and J. Löwe, “Dimeric structure of the cell shape protein MreC and its functional implications.,” *Mol. Microbiol.*, vol. 62, no. 6, pp. 1631–42, Dec. 2006.
[137] F. O. Bendezú, C. A. Hale, T. G. Bernhardt, and P. A. J. de Boer, “RodZ (YfgA) is required for proper assembly of the MreB actin cytoskeleton and cell shape in E. coli.,” *EMBO J.*, vol. 28, no. 3, pp. 193–204, Feb. 2009.

[138] D. Shiomi, H. Mori, and H. Niki, “Genetic mechanism regulating bacterial cell shape and metabolism.,” *Commun. Integr. Biol.*, vol. 2, no. 3, pp. 219–20, May 2009.
[139] R. Madabhushi and K. J. Marians, “Actin homolog MreB affects chromosome segregation by regulating topoisomerase IV in Escherichia coli.,” *Mol. Cell*, vol. 33, no. 2, pp. 171–80, Jan. 2009.
[140] P. Nurse and K. J. Marians, “Purification and characterization of Escherichia coli MreB protein.,” *J. Biol. Chem.*, vol. 288, no. 5, pp. 3469–75, Feb. 2013.
[141] N. C. Seeman and H. F. Sleiman, “DNA nanotechnology,” *Nat. Rev. Mater.*, vol. 3, no. 1, p. 17068, Nov. 2017.
[142] P. W. K. Rothemund, A. Ekani-Nkodo, N. Papadakis, A. Kumar, D. K. Fygenson, and E. Winfree, “Design and Characterization of Programmable DNA Nanotubes,” *J. Am. Chem. Soc.*, vol. 126, no. 50, pp. 16344–16352, Dec. 2004.
[143] P. W. K. Rothemund, “Folding DNA to create nanoscale shapes and patterns,” *Nature*, vol. 440, no. 7082, pp. 297–302, Mar. 2006.
[144] S. H. Park, P. Yin, Y. Liu, J. H. Reif, T. H. LaBean, and H. Yan, “Programmable DNA Self-Assemblies for Nanoscale Organization of Ligands and Proteins,” *Nano Lett.*, vol. 5, no. 4, pp. 729–733, Apr. 2005.
[145] M. Langecker, V. Arnaut, T. G. Martin, J. List, S. Renner, M. Mayer, H. Dietz, and F. C. Simmel, “Synthetic Lipid Membrane Channels Formed by Designed DNA Nanostructures,” *Science (80-.).*, vol. 338, no. 6109, pp. 932–936, Nov. 2012.
[146] S. M. Douglas, I. Bachelet, and G. M. Church, “A Logic-Gated Nanorobot for Targeted Transport of Molecular Payloads,” *Science (80-.).*, vol. 335, no. 6070, pp. 831–834, Feb. 2012.
[147] R. Marshall, C. S. Maxwell, S. P. Collins, C. L. Beisel, and V. Noireaux, “Short DNA containing χ sites enhances DNA stability and gene expression in E. coli cell-free transcription-translation systems.,” *Biotechnol. Bioeng.*, vol. 114, no. 9, pp. 2137–2141, 2017.
[148] Z. Z. Sun, E. Yeung, C. A. Hayes, V. Noireaux, and R. M. Murray, “Linear DNA for Rapid Prototyping of Synthetic Biological Circuits in an Escherichia coli Based TX-TL Cell-Free System,” *ACS Synth. Biol.*, vol. 3, no. 6, pp. 387–397, Jun. 2014.
[149] P. O’Neill, P. W. K. Rothemund, A. Kumar, and D. K. Fygenson, “Sturdier DNA Nanotubes via Ligation,” *Nano Lett.*, vol. 6, no. 7, pp. 1379–1383, Jul. 2006.
[150] C. A. Stein, C. Subasinghe, K. Shinozuka, and J. S. Cohen, “Physicochemical properties of phosphorothioate oligodeoxynucleotides.,” *Nucleic Acids Res.*, vol. 16, no. 8, pp. 3209–21, Apr. 1988.
[151] F. Caschera and V. Noireaux, “Compartmentalization of an all- *E. coli* Cell-Free Expression System for the Construction of a Minimal Cell,” *Artif. Life*, vol. 22, no. 2, pp. 185–195, May 2016.
[152] O. P. Hamill and B. Martinac, “Molecular basis of mechanotransduction in living cells.,” *Physiol. Rev.*, vol. 81, no. 2, pp. 685–740, Apr. 2001.
[153] S. I. Sukharev, P. Blount, B. Martinac, and C. Kung, “Mechanosensitive channels of Escherichia coli: the MscL gene, protein, and activities.,” *Annu. Rev. Physiol.*, vol. 59, pp. 633–57, Jan. 1997.

[154] N. Levina, S. Tötemeyer, N. R. Stokes, P. Louis, M. A. Jones, and I. R. Booth, "Protection of Escherichia coli cells against extreme turgor by activation of MscS and MscL mechanosensitive channels: identification of genes required for MscS activity.," *EMBO J.*, vol. 18, no. 7, pp. 1730–7, Apr. 1999.
[155] P. Moe and P. Blount, "Assessment of potential stimuli for mechano-dependent gating of MscL: effects of pressure, tension, and lipid headgroups.," *Biochemistry*, vol. 44, no. 36, pp. 12239–44, Sep. 2005.
[156] Y. Wang, Y. Liu, H. A. Deberg, T. Nomura, M. T. Hoffman, P. R. Rohde, K. Schulten, B. Martinac, and P. R. Selvin, "Single molecule FRET reveals pore size and opening mechanism of a mechano-sensitive ion channel.," *Elife*, vol. 3, p. e01834, Jan. 2014.
[157] C. C. Cruickshank, R. F. Minchin, a C. Le Dain, and B. Martinac, "Estimation of the pore size of the large-conductance mechanosensitive ion channel of Escherichia coli.," *Biophys. J.*, vol. 73, no. October, pp. 1925–1931, 1997.
[158] G. van den Bogaart, V. Krasnikov, and B. Poolman, "Dual-color fluorescence-burst analysis to probe protein efflux through the mechanosensitive channel MscL.," *Biophys. J.*, vol. 92, no. 4, pp. 1233–40, Feb. 2007.
[159] E. Perozo, A. Kloda, D. M. Cortes, and B. Martinac, "Physical principles underlying the transduction of bilayer deformation forces during mechanosensitive channel gating.," *Nat. Struct. Biol.*, vol. 9, no. 9, pp. 696–703, Sep. 2002.
[160] T. Nomura, C. G. Cranfield, E. Deplazes, D. M. Owen, A. Macmillan, A. R. Battle, M. Constantine, M. Sokabe, and B. Martinac, "Differential effects of lipids and lyso-lipids on the mechanosensitivity of the mechanosensitive channels MscL and MscS.," *Proc. Natl. Acad. Sci. U. S. A.*, vol. 109, no. 22, pp. 8770–5, May 2012.
[161] E. Perozo, D. M. Cortes, P. Sompornpisut, A. Kloda, and B. Martinac, "Open channel structure of MscL and the gating mechanism of mechanosensitive channels," *Nature*, vol. 418, no. 6901, pp. 942–948, Aug. 2002.
[162] J. Pan, S. Tristram-Nagle, and J. F. Nagle, "Effect of cholesterol on structural and mechanical properties of membranes depends on lipid chain saturation," *Phys. Rev. E*, vol. 80, no. 2, p. 021931, Aug. 2009.
[163] B. Martinac, J. Adler, and C. Kung, "Mechanosensitive ion channels of E. coli activated by amphipaths.," *Nature*, vol. 348, no. 6298, pp. 261–3, Nov. 1990.
[164] S. Su, S. C. Phua, R. DeRose, S. Chiba, K. Narita, P. N. Kalugin, T. Katada, K. Kontani, S. Takeda, and T. Inoue, "Genetically encoded calcium indicator illuminates calcium dynamics in primary cilia," *Nat. Methods*, vol. 10, no. 11, pp. 1105–1107, Nov. 2013.
[165] A. S. Utada, E. Lorenceau, D. R. Link, P. D. Kaplan, H. A. Stone, and D. A. Weitz, "Monodisperse Double Emulsions Generated from a Microcapillary Device," *Science (80-.).*, vol. 308, no. 5721, pp. 537–541, Apr. 2005.
[166] K. K. Y. Ho, V. L. Murray, and A. P. Liu, "Engineering artificial cells by combining HeLa-based cell-free expression and ultrathin double emulsion template," in *Methods in cell biology*, vol. 128, 2015, pp. 303–318.
[167] F. Caschera, J. W. Lee, K. K. Y. Ho, A. P. Liu, and M. C. Jewett, "Cell-free compartmentalized protein synthesis inside double emulsion templated liposomes with in vitro synthesized and assembled ribosomes," *Chem. Commun.*, vol. 52, no.

31, pp. 5467–5469, Apr. 2016.
[168] P. Siuti, J. Yazbek, and T. K. Lu, “Synthetic circuits integrating logic and memory in living cells,” *Nat. Biotechnol.*, vol. 31, no. 5, pp. 448–452, May 2013.
[169] A. P. Liu and D. A. Fletcher, “Biology under construction: in vitro reconstitution of cellular function,” *Nat. Rev. Mol. Cell Biol.*, vol. 10, no. 9, pp. 644–650, Sep. 2009.
[170] S. Ausländer and M. Fussenegger, “Toehold gene switches make big footprints,” *Nature*, vol. 516, no. 7531, pp. 333–334, Dec. 2014.
[171] A. A. Green, P. A. Silver, J. J. Collins, and P. Yin, “Toehold Switches: De-Novo-Designed Regulators of Gene Expression,” *Cell*, vol. 159, no. 4, pp. 925–939, Nov. 2014.
[172] S. Ausländer and M. Fussenegger, “Toehold gene switches make big footprints,” *Nature*, vol. 516, no. 7531, pp. 333–334, Dec. 2014.
[173] K. Pardee, A. A. Green, M. K. Takahashi, D. Braff, G. Lambert, J. W. Lee, T. Ferrante, D. Ma, N. Donghia, M. Fan, N. M. Daringer, I. Bosch, D. M. Dudley, D. H. O’Connor, L. Gehrke, and J. J. Collins, “Rapid, Low-Cost Detection of Zika Virus Using Programmable Biomolecular Components,” *Cell*, vol. 165, no. 5, pp. 1255–1266, May 2016.
[174] P. Nurse and K. J. Marians, “Purification and Characterization of Escherichia coli MreB Protein,” *J. Biol. Chem.*, vol. 288, no. 5, pp. 3469–3475, Feb. 2013.